Politecnico di Torino

Master of science in Energy and Nuclear engineering

Master Thesis

Application of the SERPENT2 code to neutronic analyses of the MYRRHA core: a sensitivity approach

at SCK CEN in Mol, Belgium

Supervisor:
Prof. Gianni Coppa

Candidate:
Heddy Barale

Mentors:
Dr. Augusto Hernandez Solis (SCKCEN)
Dr. Luca Fiorito (SCKCEN)

Academic Year 2019/2020

Abstract

In 80 years of nuclear reactor history two types of reactors were constructed, one leading to energy production and the other one for scientific research. At the moment, the operational nuclear reactors are represented by 440 nuclear power plants and 220 research reactors; therefore, it can be easily deducted the high relevance that the scientific community reserves for research reactors. In the early days of the nuclear history, research reactors were used to product fissile nuclides for weapon applications. Nowadays, they have several utilities in the medical field as the production of radio-nuclides for cancer treatments and in the industrial field for the recycling of nuclear waste and material testing applications.

The Multipurpose hYbrid Research Reactor for High-tech Applications (MYRRHA) designed at SCK•CEN in Belgium is one of the promising projects in this area. This reactor is committed to fulfill the criteria of the future GEN-IV reactor type for what concerns safety, proliferation resistance and sustainability. The innovative features of such reactor are the reprocessed mixed oxide fuel (MOX) with high enrichment, the lead-bismuth eutectic (LBE) as coolant and spallation target, and the possibility to operate as critical reactor as well as a subcritical system driven by a spallation neutron source based on a proton accelerator; operational mode known as Accelerator Driven System (ADS).

In this thesis, all the analyses were performed on the MYRRHA version 1.6 while operating under critical mode. Such neutronic analysis aims to address answers to some of the safety requirements of the reactor under critical operation. The Monte Carlo code chosen for the evaluation of such safety parameters corresponded to SERPENT2, a modern code with several interesting features. This code was applied in particular for several void injection analyses due to the hypothetical occurrence of different accidental scenarios leading to distinct reactivity effects. In addition, sensitivity calculations were conducted to prove the SERPENT2 capabilities and to assess which neutron induced reaction (and from which nuclide) has the greatest effect on different parameters as, for instance, the effective multiplication factor and the kinetic parameters of the core.

The simulations highlight a reactivity enhancement due to the void presence, an increase affected either by the volume of the void and the spatial location of the injection, or both. In order to understand the physics behind the reactivity increase, local and global analyses were performed. Regarding local analyses such as flux and reaction rates, different tallies for different nuclides were performed. On the other hand, global analyses came as sensitivity calculations, in which the nominal condition and the void injection condition leading to the highest reactivity increase were also studied.

Another feature of this work was to provide a comparison between the SERPENT2 results for several MYRRHA neutronic observables with respect to the well-established MCNP code. In the end, the nature of all the aforementioned calculations based on SERPENT2 can be used to compare previous safety studies carried out with other codes, as well as to form a basis for future ones.

Acknowledgments

Firstly, I would like to express my sincere gratitude to my supervisor Prof. Gianni Coppa for his continuous support, encouragement and patience.

I wish to express my deepest gratitude to my mentors Augusto and Luca, who provided me the opportunity to join the NSP team at SCK CEN as an intern. Without your precious support it would have been impossible to conduct this thesis. I tried to learn as much as possible from you and it is mostly thanks to you that I decided to undertake a scientific path through the doctoral program after this Master's degree. I would like to extend my thankfulness to the entire SCK CEN organization for enabling me to live and to carry out this research study there.

I am extremely grateful to my parents for educating and preparing me for my future. Special thanks are and will always be dedicated to my mom, for every kind of support she gave to me... And of course to the one who is much more than just a sister.

Last but not least, I would like to thank my entire family and friends for all their different but in a certain way similar moral supports.

Contents

List of Figures

List of Tables

Chapter 1

Introduction

This Master's thesis is an analysis performed on the Multipurpose hYbrid Research Reactor for High-tech Applications (MYRRHA) designed at SCK•CEN in Belgium. It is a lead-bismuth eutectic (LBE) cooled research reactor with the possibility to run at critical and subcritical mode as Accelerator Driven System (ADS) [1].

Fast reactors with closed fuel cycle are the future of the nuclear power technology, for the simple reason that they can extract more energy (60-70 times higher) than thermal reactors that utilize natural uranium and reduce the volume and toxicity of the final waste [2]. Even if the Sodium cooled Fast Reactor (SFR) was the European reference choice for what concern GEN-IV reactor with fast spectrum [3], recent developments [4] [5] show that the Lead cooled Fast Reactor (LFR) have become more than a first alternative technology.

Nuclear research reactors, as well as nuclear power plants, have strictly safety requirements to consider during the design and to fulfill in operation. In this thesis, key neutronic safety parameters have been evaluated with the SERPENT2 Monte Carlo code, sometimes with different methodologies, and compared to the ones obtained with well validated codes such as the Monte Carlo N-Particle (MCNP) [6].

Since nuclear data are evaluated experimentally, they are not exact and exhibit a degree of uncertainty. It can be said that the design of a new reactor concept always leads to the discovery of shortcomings in nuclear data. For this reason, a sensitivity approach has been used in order to determine the effects of nuclear data perturbation on several response functions like the ones corresponding to safety parameters. Such purpose aimed at either ranking the reactions and the nuclides more relevant to the reactor, or to estimate the uncertainties in the reactor parameters due to the nuclear data uncertainties.

In this first introduction Chapter some basic information about the MYRRHA reactor and the modeling of reactor core with Monte Carlo and deterministic codes are briefly presented.

1.1 Monte Carlo method

The Monte Carlo approach, or stochastic approach, makes use of probabilities to describe and solve problems relative to different fields. Today this method is widely used for various tasks in physics, mathematics, economics and engineering. In the past, one of its first applications was in the modeling of complicated particle transport problem. In fact, this calculation technique was first called "Monte Carlo" by Los Alamos scientists in the late 1940s, when the method was used to solve particle transport problem for the nuclear weapons project [7].

This method is based on the sequence of random numbers to obtain sample values of well-suited complicated problems. It is characterized as a brute-force calculation technique, because the stochastic calculations are performed several times in order to estimate the associated statistical errors. In this Section, the use of this approach is investigated when it is applied to the neutron particle transport in the reactor physics field governing phenomena.

The Monte Carlo method, when applied to particle transport simulation problems, follows a precise calculation routine. In principle, the code has to simulate the life of a single photon, neutron or any other particle from its initial emission up to the eventual escape from the domain or eventually collision-absorption in another nucleus. The frequency of the interactions and their outcomes occurred during the life of the particles are randomly sampled and simulated according to the interaction laws derived from particle physics [8]. Thus, it can be said that the cumulative information related to the life of each particle when the code repeats the calculation several times (cycles), is a detailed simulation of the particle transport process inside the domain.

The first drawback of the Monte Carlo method is the tremendous cost in computational time, due to the simulation of all of these particle's paths, called random walks. The second main drawback is the high memory requirement that is needed to collect all the information about the consequence of these collisions, such as the particle energy and its direction after the interaction. For these difficulties, from the beginning of the reactor physics field, another method became the dominant approach in particle transport calculations, the deterministic method, based on the concept of a collective density function known as neutron flux [9].

In both calculations, Monte Carlo and deterministic, the nuclear interaction data are a required input derived from experimental measurements and supplemented by mathematical models collected into large data libraries. In Monte Carlo based codes, these data are processed and then used in the tabular point-wise format in order to preserve the continuous energy dependence of the reactions. On the other hand, deterministic codes require pre-processed data into a group-wise format and successively a homogenization that further reduce the data level of detail at the scale-level, in order to use them efficiently in reactor calculations. Moreover, another advantage of Monte Carlo codes is the possibility to model very complex geometry; on the contrary, using deterministic codes brings another level of approximation, the homogenization of the geometry into a mesh of macroscopic regions called nodes [10].

For these reasons, the simplicity and the potential to produce very accurate results are the main advantages of Monte Carlo codes with respect to deterministic ones. The link between these exceptional capabilities and the fast computers development in the last decades, led to the implementation of several Monte Carlo codes, with different features, such as criticality safety analyses, validation of deterministic reactor physics codes, dosimetry calculations and medical applications [9]. Since neither today nor in the near future Monte Carlo methods would offer a practical and computationally inexpensive way to solve routine neutron transport problems for reactor applications, deterministic codes are still today the widely used for this purpose. Therefore, the most interesting actual and future applications of Monte Carlo methods are developed in correspondence of the shortcomings of deterministic codes, such as burnup calculations, sensitivity calculations and group constant generation [11].

In the end, it can derived that the high accuracy of Monte Carlo codes can be used for validating deterministic ones and its simple implementation can be useful to treat problems that cannot be treated by the latter. Nevertheless, the achievements of the Monte Carlo codes in the past years opened new possibilities in reactor simulation, as the the implementation of hybrid deterministic-Monte Carlo based algorithms for the acceleration convergence of the fission source [12].

1.2 MYRRHA

The Multipurpose hYbrid Research Reactor for High-tech Applications (MYRRHA) project is a new reactor designed at SCK•CEN in Mol, Belgium. It has been designed to operate in subcritical mode, as an Accelerator Driven System (ADS), but also in critical mode, as a fast lead-bismuth cooled reactor. The MYRRHA project is a multipurpose nuclear facility, which endeavor to demonstrate ADS technology and waste transmutation. It will also address structural and material studies for other type of reactors such as future Gen-IV fast reactor concepts and fusion reactors [13]. This pool-type reactor uses MOX-fuel and lead-bismuth eutectic (LBE), the latter serving as both coolant and spallation target [14]. Another feature of MYRRHA will be the production of radionuclides for medical and industrial applications, such as ^{99}Mo [15].

As Fig. 1.1 shows, a pool type configuration has been selected in order to exploit the major advantages such as making the reactor easily accessible and to have the whole primary cooling system under normal pressure, avoiding as much as possible the high temperatures and great pressures typical of nuclear power plants [16].

Due to its applications, MYRRHA has been designed in order to satisfy different requirements, as a high fast flux in the order of 10e15 [neutrons/(cm^2 s)] at hot spot around the central channel. On the other hand, the design is also affected by neutronic and thermo-hydraulic constraints as, for instance, LBE velocities less than 2 m/s and maximum acceptable cladding temperature of 466 °C [18].

The ADS technology is receiving more attentions in nuclear research due to some remarkable features. For example, the ADS is able to tolerate more presence of minor actinides than other systems. In fact, ADS makes possible to design cores with Americium fraction as reactor fuel, even if it may challenge safety

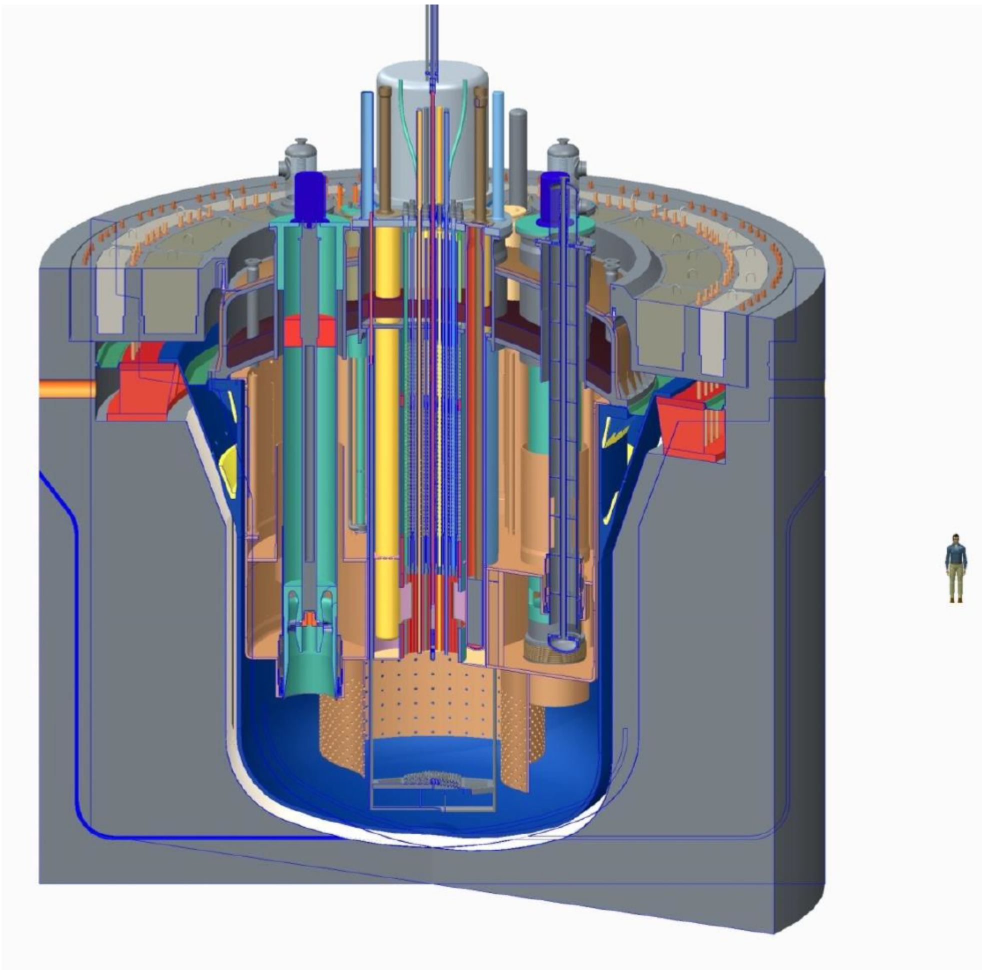

Figure 1.1: MYRRHA 1.6 reactor systems design[17].

neutronic parameters, such as a reduction of the Doppler constant, an increase of coolant temperature coefficient and the reduction of the effective delayed neutron fraction [19]. In ADS mode, 600 MeV high-energy protons create neutrons in the spallation LBE window target needed to maintain the fission chain reaction in the subcritical reactor configuration. Therefore, ADS is an attractive option to study high-level waste transmutation and recycling.

One of the MYRRHA future tasks is to integrate-replace the old BR2 reactor, that currently produces nuclides for nuclear medicine, especially radio-isotopes for cancer treatments [20]. In addition, it will be able to produce new theranostic radio-isotopes for diagnostic examinations and more targeted therapeutic treatments. MYRRHA will also be useful for industrial applications, such as for development of innovative fuels and materials for future Gen-IV fast reactor concepts. Moreover, MYRRHA will also enhance the knowledge of materials for fusion reactors, since compared to the current research reactors, it will reach irradiations conditions close to fusion applications.

MYRRHA is defined as a new reactor concept also for the particular choice of LBE as coolant. Since 1950s, heavy-metal coolant such as LBE has been investigated for fast reactors. However, other liquid-metal coolants were chosen, leading to sodium cooled reactors. Favorable features of lead based coolant are e.g. the lower reactivity feedback coefficient in case of voiding, better shielding properties against high energy neutrons and gamma rays, and a high boiling point temperature [21]. On the contrary, the main drawbacks of such coolants like Pb based LBE are the corrosion [22] and the production of alpha particles due to neutron capture in ^{209}Bi that leads to ^{210}Po, which is a highly radiotoxic alpha emitter due to its nature decay mode [23].

Regarding the project, since 1998 the MYRRHA design has been improved. As first phase, in 2016 the construction of the 100 MeV accelerator for research reasons was started. Then, it is foreseen that in 2026 the 600 MeV accelerator and the reactor will be constructed, representing the second and the third phase. Finally, the start of the operations of the reactor and full ADS is planned for 2033 [24].

Even if MYRRHA is designed to run a lot of experiments in a sub-critical mode of operation, there are important safety parameters that must be taken into account related to the criticality operations. For this reason, all the calculations presented in this thesis were conducted on the version 1.6 of MYRRHA while operating under critical mode.

Chapter 2

Theoretical background and Tools

In this Chapter, a brief recap of the theoretical tools needed to understand the results, the physics behind and the code methodology are presented. These go from the equation that governs the reactor physics field and all main parameters related to the core, to the neutronic code used for the present study. Finally, the theory behind the sensitivity calculations and different methods to perform such calculations are highlighted.

2.1 Neutron Transport equation

Neutrons can be defined as a classic object, and they are defined by the phase space, corresponding to the location $\bar{r}$, the energy E, the direction of travel $\bar{\Omega}$ and the time t. The neutron population is described by the angular neutron population, $N(\bar{r}, E, \bar{\Omega}, t)$, that defines the density of neutrons in a volume dr about r, with energy dE about E, traveling in direction $d\Omega$ about Ω and time dt about t. Therefore the angular flux ϕ can be defined as the product of the angular density and the neutron speed v:

$$\phi(\bar{r}, E, \bar{\Omega}, t) = N(\bar{r}, E, \bar{\Omega}, t)\, v \tag{2.1}$$

successively, the angular flux can be integrated over all directions, leading to the scalar flux.

$$\phi(\bar{r}, E, t) = \oint \phi(\bar{r}, E, \bar{\Omega}, t)\, d\bar{\Omega} \tag{2.2}$$

Any type of reaction rate (e.g. capture, fission, scattering, etc.) over a well defined volume in space is proportional to the neutron flux (if integrated over all directions, then it would just be directly proportional to the scalar flux). These type of quantities can be computed (or "tallied") by Monte Carlo-based codes via different estimators, just by scoring certain type of collisions over a defined space-domain, by scoring the total track-length, etc.

In order to introduce the neutron transport equation (or Boltzmann equation), some assumptions are introduced: collisions are point-like and instantaneous; due to their sufficiently low density, it can be assumed that neutron-neutron collision is unlikely to happen; in a first approximation,delayed neutron contributions are omitted for the sake of simplicity (the contribution of delayed neutron in the equation is discussed in Section 2.1.2). The neutron transport equation simply represents the balance between gain and loss of neutrons, therefore the change on neutron density per time step in a certain volume can be formulated as follows:

$$\frac{dN}{dt} = Gain - Loss \tag{2.3}$$

thus, the integral differential form of the neutron transport equation in terms of angular flux can be expressed as:

$$\begin{aligned}
\frac{1}{v(E)}\frac{\partial \phi(\bar{r}, E, \bar{\Omega}, t)}{\partial t} \;+\; \nabla(\Omega\, \phi(\bar{r}, E, \bar{\Omega}, t)) \;+\; \Sigma_{tr}(\bar{r}, E)\, \phi(\bar{r}, E, \bar{\Omega}, t) \;= \\
= S(\bar{r}, E, \bar{\Omega}, t) + \oint d\Omega' \int dE'\, \bar{\nu}\, \Sigma_f(\bar{r}, E')\, \phi(\bar{r}, E', \bar{\Omega}', t)\, \frac{\chi(\bar{r}, E)}{4\pi} + \\
+ \oint d\Omega' \int dE'\, \Sigma_s(\bar{r}, E')\, \phi(\bar{r}, E', \bar{\Omega}', t)\, f_s(\bar{r}, E' \mapsto E, \bar{\Omega}' \mapsto \bar{\Omega})
\end{aligned} \tag{2.4}$$

where the first term represents the time rate of change of neutrons in the system. The second terms describes the movement of neutrons in or out of the volume of space of interest, represented as the divergence of the neutron current, usually called streaming term. The third term accounts for all neutrons that have a collision in that phase space leading to the particle loss in the phase space. The first term on the right hand side is a generic source of neutrons. The second term on the right hand side is in-scattering, these are neutrons that enter this area of phase space as a result of scattering interactions in another. The last term on the right hand side is the production of neutrons in this phase space due to fission.

In Eq. 2.13, the symbol Σ represents the macroscopic cross section, which is related to the probability per unit path that a certain collision happens and it can be calculated such as:

$$\Sigma = N\,\sigma \quad [1/cm] \tag{2.5}$$

where N is the atomic density of the nuclide, and σ is the microscopic cross section, or nuclear cross section, defined in [barn] units (equal to 10^{-24} [cm]). This type of unit can be defined in terms of "characteristic area", where a large area means a higher probability of interaction. During the years, a huge amount of experiments have been conducted to evaluate nuclear cross sections σ for different nuclides, interactions and incoming neutron energies. Nowadays, all these results can be found in libraries as point wise data; however, most Monte Carlo codes do not directly use raw nuclear data coming from the major nuclear data libraries around the world. Instead, other processing codes are employed to do some treatments in the microscopic data (i.e. arrangement in well-structured energy meshes, construction of continuous-energy resonances from resonant parameters, adding temperature dependence, etc.) and, in the end, arrange such data in a certain format that codes can easily read; further discussions are presented in [11].

The other nuclear data appearing in Eq. 2.13 is ν, which is the number of neutrons emitted per fission event. This parameter depends on the energy of the incoming neutron and the nuclide in which fission occurs. In general, ν tends to increase with the energy of the incident neutron. The expression $\bar{\nu}$ simply indicates the statistical average.

The last nuclear data introduced in Eq. 2.13 is χ, the fission spectrum, the probability that a neutron is emitted with a particular energy after a fission process and it only depends on the nuclide and the outgoing neutron energy. It describes the outcomes of the fission process. It does not depend on the direction, because the 4π accounts for it since fission is an isotropic event.

The remaining symbol not yet discussed, is f_s, the probability density function for scattering. It represents the likelihood that a particle would out-go in a certain energy and direction, based on its incoming energy and direction. f_s is a complex function that can be approximated with series of Legendre's polynomial [25].

For what concerns nuclear data, they can be consulted at the Nuclear Energy Agency website (OECD-NEA) in the 'Data Bank' section. It is possible to access to different data libraries, of different countries or representative institutions. As a first conclusion derived from this discussion, nuclear data (either being experimentally evaluated or drawn from computational calculations) are affected by uncertainties. Therefore, the sensitivity analysis (explained in Section 2.3) has been conducted for this reason.

In the following, some parameters of interest are introduced.

2.1.1 Effective multiplication factor k_{eff}

The effective multiplication factor k_{eff} is the average number of neutrons from one fission that may cause another fission. It is the characteristic parameter of a nuclear reactor and it can be defined in several ways. It can be expressed in terms of neutron balance:

$$k_{eff} = \frac{\text{Neutron production}}{\text{Neutron loss}} = \frac{\mathbf{P}}{\mathbf{L}} \tag{2.6}$$

The production operator $\mathbf{P}$ is equal to the fission operator $\mathbf{F}$ in absence of an external source, while the loss operator $\mathbf{L}$ is the sum of the leakage and the capture rate. The effective multiplication factor can be derived from the solution of the eigenvalue criticality source problem:

$$(\mathbf{L} - \mathbf{S})\phi = \frac{1}{k_{eff}}\mathbf{F}\phi \tag{2.7}$$

Where $\mathbf{S}$ is the scattering operator.

With the hypotheses of a non-leaking system (an infinite medium) and considering that all neutrons have the same energy, it is possible to define from diffusion theory [26] the k_∞ approximation in one energy group:

$$k_\infty = \frac{\bar{\nu}\Sigma_f}{\Sigma_a} \tag{2.8}$$

where $\bar{\nu}$ is the average number of neutrons release per fission reaction, Σ_f and Σ_a are respectively the fission and absorption macroscopic cross sections. This first raw approximation of k_{eff} is useful to understand what are its dependences and the behavior if one of the nuclear data is perturbed like, for example, when we are dealing with sensitivity analysis.

A more precise definition of k_∞ can be derived assuming two energy groups, the thermal one accounting for neutrons with energy < 1 eV and the fast with all the neutrons with higher energy. Denoting with 1 the fast group and with 2 the thermal one, it follows:

$$k_\infty = \frac{\bar{\nu}\Sigma_{f_2}}{\Sigma_{a_2}} \frac{\Sigma_{1\rightarrow 2}}{\Sigma_{a_1}} \varepsilon \tag{2.9}$$

this approximation is the so called Four-factor formula [27]. In here, ε account for the fast fissions, while $\Sigma_{1\rightarrow 2}/\Sigma_{a_1}$ is the probability that neutrons slow down from fission to thermal energies. If leakage is now considered, k_∞ has to be multiplied by the probabilities that fast and thermal neutrons to do not leak from the system, deriving k_{eff} as results of the Six-factor formula:

$$k_{eff} = k_\infty \, P_{NL}^{th} \, P_{NL}^{fast} \tag{2.10}$$

from this derivation of k_{eff} it is possible to understand all its dependences. Such physical dependences of the effective multiplication factor have been further discussed where accidental scenarios are considered. The relevance of the effective multiplication factor as a global parameter describing the reactor, linked to its dependence from nuclear data (not exact data), brings the need to estimate which nuclide and reaction affects more the k_{eff} value (i.e. sensitivity analysis).

Another useful definition (especially in a Monte Carlo frame) comes by the word "generation". Given a certain number of neutrons, they will react in many ways (scattering, capture, etc.). The number of neutrons inducing fission and consequently leading to new fission neutrons correspond to the new generation of fission neutrons, the ones sustaining the chain reaction. Thus is possible to define the effective multiplication factor as:

$$k_{eff} = \frac{\text{Number of neutrons in one generation}}{\text{Number of neutrons in preceding generation}}$$

this definition is used especially in Monte Carlo applications thanks to the possibility to properly count the number of neutrons between successive generations.

A new parameter that can be derived from the definition of the effective multiplication factor is the reactivity. Sometimes it is convenient to define the change in k_{eff} from its critical reference. For this purpose, it is customary in reactor physics to use the reactivity term to describe the change in the state of a reactor core talking from a critical point of view. The reactivity ρ or $\Delta k/k$ is defined by the following equation:

$$\rho = \frac{k_{eff} - 1}{k_{eff}} \tag{2.11}$$

mathematically, reactivity is a dimensionless number, but it can be expressed by various units. The most common one is the *pcm* (per cent mile), which is equal to 10^{-5} of $\Delta k/k$.

The multiplication factor and therefore the reactivity determine the criticality state [28]:

- $k < 1 \longleftrightarrow \rho < 0$, the system is *subcritical*, the chain reaction dies out and the number of neutrons exponentially decrease.

- $k = 1 \longleftrightarrow \rho = 0$, the system is *critical*, the number of fissions in each succeeding generation is constant and the chain reaction will continue at a constant rate.

- $k > 1 \longleftrightarrow \rho > 0$, the system is *supercritical*, the number of fissions increases with each succeeding generation making the chain reaction exponentially divergent.

The reactivity is a useful parameter that describes how far the reactor is from its critical condition and it is used to define the so called reactivity coefficient, described in Sections 2.1.4 2.1.5. The effective multiplication factor for the MYRRHA model (at excess reactivity conditions of operation) considered in the present study is equal to 1.01311 and this value comes from precise conditions considered during the modeling and further discussed in Section 3.

2.1.2 Effective delayed neutron fraction β_{eff}

During a fission event, the compound nuclide splits into generally two lighter nuclei, called fission fragments. The splitting is accompanied by the release of γ-radiation and new neutrons. Such neutrons are born within 10^{-14} seconds after the fission. Because of their quick release after the fission event they are called "prompt neutrons". Since the fission fragments are neutron-rich atoms and in an excited state, they generally decay into less excited species. The fission fragments and their radioactive decay products are called fission products. Some of the them can lead by decay to species that can themselves emit neutrons. Such neutrons are called delayed neutrons, and the corresponding fission fragments are called precursors of delayed neutrons.

For example, as Fig. 2.1 shows, a fission in ^{235}U could yield ^{89}Br as fission product. This isotope is radioactive and decays into an excited state of ^{88}Kr, which stabilizes by emitting a neutron. The production of this neutron is delayed respect to the fission event; delay that is associated to the radioactive decay of ^{89}Br, the precursor.

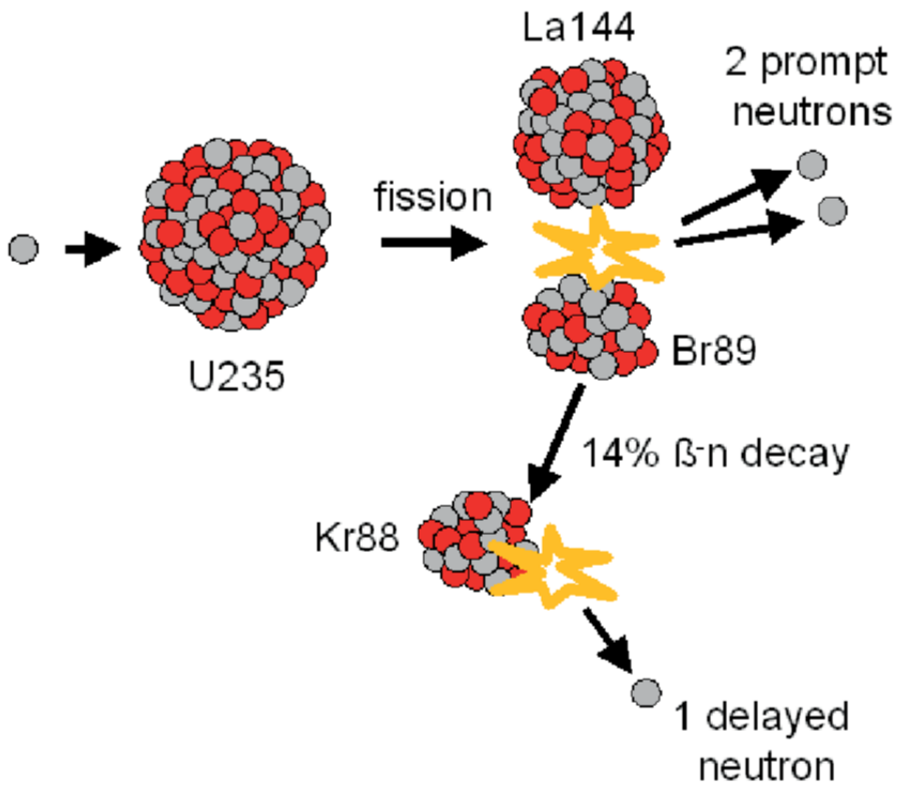

Figure 2.1: Prompt and Delayed neutrons example [29].

The parameter that accounts for this phenomena is the delayed neutron fraction:

$$\beta = \frac{\bar{\nu_d}}{\bar{\nu_p} + \bar{\nu_d}} = \frac{\text{delayed neutrons resulting from a fission event}}{\text{total number of neutrons emitted (prompt + delayed)}} \tag{2.12}$$

The β values depend on the incident neutron energy, but most importantly on the nuclides as shown in Table 2.1.

In Section 2.1, Eq. 2.13 does not account for this division of prompt and delayed neutrons. Considering the fraction of prompt neutron equal to $(1 - \beta)$, and the concentration of delayed neutron precursors $C(\bar{r}, t)$,

Table 2.1: Delayed neutron fraction for various nuclides.

Nuclide	β [%]
^{238}U	1.720
^{235}U	0.650
^{238}Pu	0.140
^{239}Pu	0.210
^{240}Pu	0.300
^{241}Pu	0.540
^{242}Pu	0.660

the integral differential form of the neutron transport equation becomes:

$$\begin{aligned} \frac{1}{v(E)}\frac{\partial\phi(\bar{r},E,\bar{\Omega},t)}{\partial t} + \nabla(\Omega\,\phi(\bar{r},E,\bar{\Omega},t)) + \Sigma_{tr}(\bar{r},E)\,\phi(\bar{r},E,\bar{\Omega},t) = \\ = S(\bar{r},E,\bar{\Omega},t) + (1-\beta)\oint d\Omega' \int dE'\,\bar{\nu}\,\Sigma_f(\bar{r},E')\,\phi(\bar{r},E',\bar{\Omega}',t)\,\frac{\chi_P(\bar{r},E)}{4\pi} + \\ + \sum_{i=1}^{R}\lambda_i C_i(\bar{r},t)\,\frac{\chi_d(E)}{4\pi} + \oint d\Omega' \int dE'\,\Sigma_s(\bar{r},E')\,\phi(\bar{r},E',\bar{\Omega}',t)\,f_s(\bar{r},E'\mapsto E,\bar{\Omega}'\mapsto\bar{\Omega}) \end{aligned} \tag{2.13}$$

where the third term on the right hand side accounts for the decay of delayed neutron precursors leading to the emission of delayed neutrons with a certain energy expressed by the delayed fission spectrum probability function. Since the precursors are more than 100, the decision of the early reactor physicists was to group them into 6 families, recently increased to 8 [30]. λ_i represents the decay constant defined as the probability of decay per unit time [1/s].

The aforementioned definition of β does not account for the different importance that neutrons have inside a reactor. The neutron importance at a certain position $\bar{r}$ with direction $\bar{\Omega}$ and energy E is the total number of fissions that these neutrons are able to produce [31]. On the other hand, defining the adjoint flux or importance ($\phi^\dagger$) as the fundamental eigenfunction of the adjoint problem going as follows:

$$(\mathbf{L}^\dagger - \mathbf{S}^\dagger)\phi^\dagger = \frac{1}{k_{eff}}\mathbf{F}^\dagger\phi^\dagger. \tag{2.14}$$

From reactor kinetics theory is possible to define the *effective* delayed neutron fraction β_{eff} weighted (over space, energy and angle) on the importance. This weighting is fundamental because delayed neutrons are emitted with an average energy spectrum of about 150 keV, significantly lower respect to the 2 MeV of the prompt neutrons.

$$\beta_{eff} = \frac{\langle\phi^\dagger, \frac{1}{k_{eff}}\mathbf{F_d}\phi\rangle}{\langle\phi^\dagger, \frac{1}{k_{eff}}\mathbf{F}\phi\rangle} \tag{2.15}$$

In here, the brackets $\langle\rangle$ represent the inner product integrated over all independent variables (space, energy and angle).

One of the implication of having a fast spectrum in MYRRHA is $\beta_{eff} < \beta$, since the importance of delayed neutrons is lower compared to the prompt one. Table 2.2 shows β_{eff} reference value for different reactor types.

Table 2.2: β_{eff} kinetic parameters in different reactor types. [32]

Kinetic parameters	LWR	CANDU	Fast Reactor
β_{eff}	0.006	0.005	0.0035

The effective delayed neutron fraction for the MYRRHA model considered in this study is equal to 0.33% which corresponds to 330 pcm. MYRRHA adopts reprocessed MOX fuel with an enrichment of 30% on the heavy metal and thus, it is expected to have a relatively low β values as shown in Table 2.1. A low β_{eff}

value of the system increases even more the impact of delayed neutrons on reactor kinetics, leading to a more challenging reactor control. In fact, supposing an increasing positive reactivity insertion (e.g. due to accidental scenario):

- $\rho < \beta_{eff}$, the velocity of the transient and the rate of energy release do not change much if the reactivity continues to increase;
- $\rho = \beta_{eff}$, this is the so called prompt criticality condition, a situation with safety concerns because the chain reaction is already sustained with prompt neutrons alone, without the delayed neutron contribution;
- $\rho > \beta_{eff}$, in super-prompt criticality condition the fission rate and therefore the power growth exponentially with time.

These considerations (e.g. transient velocity) can be integrated defining the second kinetic parameter Λ_{eff}. Further considerations on the relevance of delayed neutrons inside the reactor can be find in the next Section.

2.1.3 Effective prompt generation time Λ_{eff}

The effective prompt neutron generation time Λ_{eff}, is the timescale of the phenomena that happen in a nuclear reactor. It is defined as the time between the birth of a neutron and a subsequent absorption inducing fission. A definition that is useful for the sensitivity discussion of Section 2.3.2.3 is:

$$\Lambda_{eff} = \frac{l_{eff}}{k_{eff}} \tag{2.16}$$

where l_{eff} is the effective prompt lifetime, expressed from reactor kinetics theory as:

$$l_{eff} = \frac{\langle \phi^\dagger, \frac{1}{v}\phi \rangle}{\langle \phi^\dagger, \frac{1}{k_{eff}}\mathbf{F}\phi \rangle}. \tag{2.17}$$

From the integral nature of Eq. 2.17 it can be deducted that also Λ_{eff} is a parameter that concerns the whole reactor.

From one energy group diffusion theory is possible to derive a further approximation of Λ_{eff} that is useful to understand the physics of the sensitivity results of Section 5.2.3, assuming a non-leaking system:

$$\Lambda_{eff} = \frac{l}{k_\infty} = \frac{\frac{1/\Sigma_a}{v}}{\bar{\nu}\Sigma_f/\Sigma_a} = \frac{1}{v\bar{\nu}\Sigma_f} \quad [s] \tag{2.18}$$

where v is the neutron velocity and l is the average neutron lifetime that can be expressed as the mean free path over the neutron velocity. Typical values for Λ_{eff} in thermal and fast reactors can be seen in Table 2.3. The MYRRHA model considered in this study has $\Lambda_{eff} = 0.65\,\mu s$. A small value of Λ_{eff} has safety concerns (as well as the small value of β_{eff} discussed before). A complete interpretation of all these parameters can be deducted from the point kinetic equation [27]:

$$\frac{\partial N(t)}{\partial t} = \frac{\rho(t) - \beta_{eff}}{\Lambda_{eff}} N(t) + \sum_{i=1}^{R} \lambda_i C_i(\bar{r}, t) \tag{2.19}$$

from a first analysis, it is possible to do not consider the delayed neutrons and their precursors in order to understand their relevance. Therefore equation 2.19 becomes:

$$\frac{\partial N(t)}{\partial t} = \frac{\rho(t)}{\Lambda_{eff}} N(t) \tag{2.20}$$

from which is analytically possible to find a solution assuming at the initial time a neutron concentration equal to N(0):

$$N(t) = N_0\, e^{(t\,\rho/\Lambda_{eff})} \tag{2.21}$$

It arises that assuming a 1 pcm increase in reactivity would lead to the **doubling** of the neutron flux and hence the power level, in about 0.65 μs. That is definitely a dangerous condition. Fortunately, the presence of delayed neutrons increase the neutron lifetime and slows down the reactivity change effect making the reactor more controllable.

Table 2.3: Λ_{eff} kinetic parameter in different reactor types. [32]

Kinetic parameters	LWR	CANDU	Fast Reactor
Λ_{eff} $[s]$	2×10^{-5}	1×10^{-3}	4×10^{-7}

2.1.4 Void coefficient α_{coolant}

The void reactivity coefficient α_{coolant}, also called coolant density coefficient or coolant void worth, is a number that estimate how much the reactivity changes as voids form in the reactor coolant.

$$\alpha_{\text{coolant}} = \frac{d\rho}{dV} \quad \left[\frac{pcm}{\%\,void\,volume}\right] \tag{2.22}$$

It follows that having a positive void coefficient implies a positive reactivity insertion. It can be expressed in different ways, such as [pcm/K], since an increase of the coolant temperature is equal to a decrease of its density, thus an increase of the void volume.

From classical perturbation theory, it can be defined as:

$$\alpha_{\text{coolant}} = \frac{\langle \phi^\dagger, \Sigma_{\text{t,coolant}}\phi \rangle}{\langle \phi^\dagger, \frac{1}{k_{eff}}\mathbf{F}\phi \rangle} \tag{2.23}$$

where $\Sigma_{\text{t,coolant}}$ is the total neutron interaction operator in the coolant (i.e. scattering and capture operators).

It is one of the most important parameter related to safety and it is extremely sensitive to the location where the void is injected. After the Chernobyl accident, this parameter became even more important, since Reactor Bolshoy Moshchnosti Manalnyy (RBMK) reactors have a dangerously high positive void coefficient [33]. This was one of the main causes of the explosion of the reactor number 4 [34].

In a LBE-cooled reactor, such as MYRRHA, where the Lead-Bismuth Eutectic serves both as coolant and neutron reflector, voiding partially the core will arise to different physical phenomena, as discussed in detail in Section 4. In there, several accidental scenarios related to different void injections are considered.

2.1.5 Doppler coefficient α_{Doppler}

The multiplication factor and therefore the reactivity are dependent on several parameters, which at the same time vary depending on the temperature of the fuel. The Doppler effect is defined as the change in fuel temperature that leads to a reactivity change.

There are two main phenomena related to the Doppler effect. The first is the increase in neutron capture by fuel nuclei in the resonance region. This effect arises from the dependence of neutron cross sections on relative velocity between neutron and nucleus. Therefore, raising the temperature causes that the nuclei vibrate more rapidly within their lattice structures, effectively broadening the energy range of neutrons that may be resonantly absorbed in the fuel, as shown in Fig. 2.2. Thus the resonance becomes shorter and wider than when the nuclei are at rest [36].

The second effect that counterbalances the increase in capture, is the increase in neutron production from fissile nuclei. The Doppler coefficient (α_{Doppler}) is defined as the change in reactivity per degree change in the fuel temperature:

$$\frac{\alpha_{\text{Doppler}}}{T_{\text{fuel}}} = \frac{d\rho}{dT_{\text{fuel}}} \tag{2.24}$$

therefore, the reactivity behaves logarithimically as a function of the fuel temperature:

$$d\rho = \alpha_{\text{Doppler}} \ln\left(\frac{T_1}{T_0}\right) \tag{2.25}$$

This parameter is very important in reactor stability.

For some applications, especially during accidental condition the Doppler coefficient is the first and the most important feedback. The velocity of the response is extremely higher with respect to the Void coefficient, because the time of heat transfer phenomena to the coolant is measured in seconds, while the one respect to the fuel is almost instantaneous. Even if in small fast reactors with high enrichment of ^{239}Pu the Doppler coefficient could be positive [37], MYRRHA has a considerably negative Doppler coefficient of about -300 pcm [18].

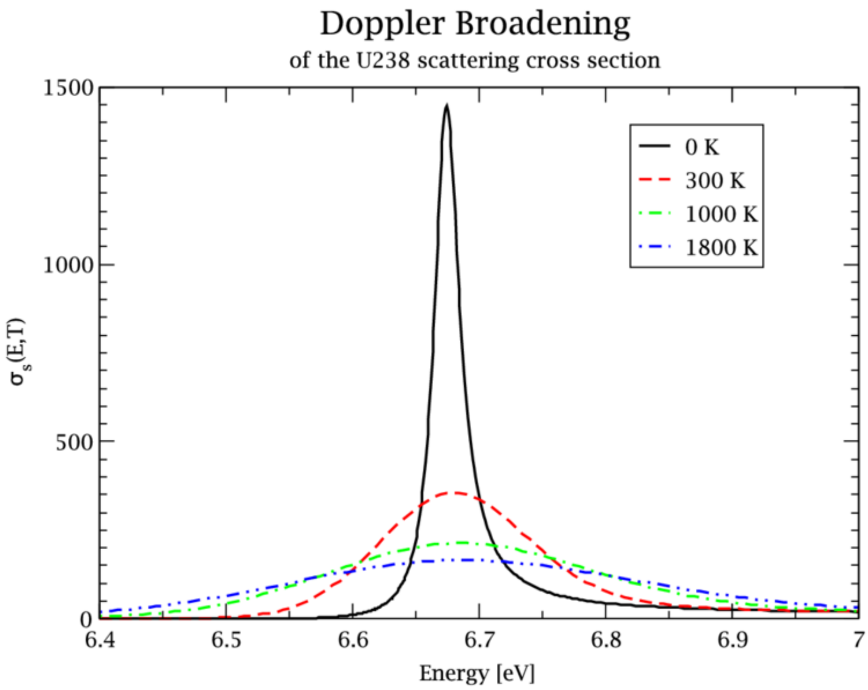

Figure 2.2: Doppler broadening of ^{238}U scattering cross section [35].

2.2 SERPENT2

SERPENT2 is a continuous energy multi purpose three-dimensional Monte Carlo neutron and photon transport code. Its development started in 2004 and, up to this day, the code has been continuously under development by VTT Technical Research Center of Finland. The version of the code used for the present study is SERPENT2 2.1.31.

One of the main advantages of SERPENT2, which is carried out while analyzing the routine dedicated to the geometrical domain, has to do with Woodcock delta-tracking [38]. Usually, other Monte Carlo transport code are based on a ray-tracing algorithm when dealing with complicated geometries. The latter presents some limitations, such as the characterization of small volume or low collision rate regions, as well as being computationally slower than the Woodcock delta-tracking methodology.

Another characteristic of SERPENT2 is the use of a uniform energy grid for all cross sections. In other methods, each nuclide is associated with its own energy grid point, thus, every time that the energy index is needed, the code has to repeat an iterative grid search, which slow down the calculation. The drawback of the method exploited in SERPENT2, is that a large number of redundant data points need to be stored, which increases considerably the amount of computer memory required. On the other hand, having stored all data needed, considerably speeds up the code cutting to a minimum that time consuming iteration. The uniform energy grid and the use of the delta-tracking method are the main reasons why SERPENT2 runs significantly faster compared to MCNP [9].

With SERPENT2 it is possible to compute different type of analyses, like criticality, depletion, transient, sensitivity calculations and moreover [9]. Starting from *criticality* calculations, the k-eigenvalue criticality source method is used as the default mode. At the initial state, the source points are chosen randomly in the fissile cells by the code. Then, the simulations run in cycles with a fixed number of neutrons per cycle (both the number of particles per cycle and the number of discarded and active cycles need to be defined by the user). In the end, the total number of active neutron histories is the one determining the statistical accuracy of the results. In the criticality source method, the fission reaction distributed from the previous cycle forms the next source distribution. SERPENT2 can also simulate an external source, but in this study this function was not used, since the critical version of the MYRRHA core was analyzed.

For the evaluation of user defined reaction rates over energy and averaged in space, SERPENT2 uses the collision estimate of neutron flux:

$$R = \frac{1}{V}\int_V \int_{E_{i+1}}^{E_i} f(r,E)\,\phi(r,E)\,d^3r\,dE \tag{2.26}$$

In which, V is the volume of the material where the collision is scored and $f(r,E)$ is the detector response function that determines the type of calculation.

Two different methods can be used to account for these collisions. In the analog one each neutron counts as all the others, while the implicit method leads to neutrons with different statistical weights. This different statistical weight comes from the assumption that when a neutron is captured it is not killed by the code, but its weight is reduced and any other collision accounts for this reduction. Thanks to this process, implicit treatment has lower statistical errors with respect to the analog one.

2.3 Sensitivity calculations

The uncertainty in nuclear data is one of the most important sources of uncertainty in reactor physics simulations. Sensitivity calculations and then uncertainty analyses are needed to improve the predictive power of simulations, with the purpose to meet the target accuracy and reliability needed for nuclear reactor applications and thus to guide future works [39].

Sensitivity analysis studies how data (nuclear data, geometrical data, etc.) perturb particular response functions. Therefore, the accuracy of the response function depends on the accuracy of the data. For example, nuclear data are not exact because they come from experimental evaluations which, in return, are affected by approximations. Moreover, if they are instead evaluated based on simulations, modeling uncertainties then are the ones affecting the data nominal value. The sensitivity analysis based on perturbation theory allows to verify data in the reactor without doing separate calculations[10]. Generally speaking, sensitivity analysis relies on first-order perturbation theory approximation (first-order Taylor's expansion) [40].

The aforementioned response functions can be formed by several safety parameters, therefore the sensitivity calculations play a key role in the safety analysis. The parameter that governs the sensitivity analysis is the sensitivity coefficient S_x^R of the response function R with respect to a perturbation on x:

$$S_x^R = \frac{dR/R}{dx/x} \tag{2.27}$$

as it will be observed later, the parameter x might be any reaction cross sections or nuclear data of any nuclides present in the system in a specific volume at any incident neutron energy. In perturbation analysis, the effect of a perturbation of a parameter x on the response R is expressed in relative terms, because useful parameters such as the neutron flux and the fundamental adjoint have an arbitrary normalization, hence their concept should be understood in relative terms[41].

The parameter x (e.g. the fission cross section) can be strongly energy dependent, thus the sensitivity coefficient itself is remarkably energy dependent. As seen before, the energy dependence can be treated by a discretization of the energy domain, for this reason the sensitivity coefficient is always linked to an energy grid made by several energy bins. The width and the numbers of the energy bins in the energy grid are not fixed, but they should be selected based on their convenience. For example, in the case of a reactor with an hard spectrum, an energy grid with a significant number of bins in the fast region is more suitable.

In the attempt to avoid the energy dependence of the sensitivity coefficient to get results comparable with any energy grid, sensitivity analysis relies on another important coefficient: the Integrated Sensitivity Coefficient (ISC). It can be seen as the integral or sum of all the sensitivity coefficients over the energy domain or bins:

$$\mathrm{ISC} = \sum_{i=1}^{n} S_{x_i}^R \tag{2.28}$$

where i is the the energy bin index.

A useful interpretation of these two coefficients should be deducted form their definition in relative terms. Assuming for example, the fission cross section of a certain nuclide as the perturbed parameter x and the effective multiplication factor k_{eff} as a response function, if a 1 % perturbation is applied to the nuclide's fission cross section at all energies, the relative increase/decrease on the overall k_{eff} is equal to ISC. Similar interpretations should be derived for the sensitivity coefficient, with the only exception that the domain is just one energy bin instead of all the energies.

2.3.1 Monte Carlo vs Deterministic method

Different methods based on deterministic or probabilistic approach have been used to execute sensitivity calculations. Deterministic methods solve the differential or the integral forms of the transport (or diffusion) equation using one of the standard methods. In general, they aim at solving the energy weighted-averaged form of the equation which is known as the "multi-group form".

In *deterministic* methods, the equations governing the sensitivity analysis are solved explicitly after reducing/simplifying the complexity of the task in a series of sequentially performed calculations. Deterministic codes are mostly based on local analysis, thus studying the behavior of system responses locally around a chosen point. Local sensitivity relies on first order contribution to the total response variation and it well-approximates the response function if small data perturbations are introduced.

Deterministic methods were developed with the primary objective to be fast running methods, because of the excessive computing burden of the probabilistic method. They are efficient in computing time but limited to the linearity of the system response. The main limitation of such methods resides in the possible lack of accuracy due to the introduced approximations.

Stochastic methods are usually used for global analyses, which aim at determining all of the system's critical points over the entire space of parameter variations. In the probabilistic methods (often referred to as Monte Carlo methods) the probability of occurrence of a nuclear reaction/process is used to sample neutron life histories throughout the system. Using a very large number of such histories, the true behavior of neutrons in the system can be reproduced. Due to the size and complexity of the systems usually modeled, Monte Carlo techniques are an extremely expensive computing techniques typically used for reference calculations.

Global sensitivity analyses can be conducted with these codes, taking into account high-order terms (non-linearity). For this reason, sensitivity analyses conducted with Monte Carlo codes should reach much accurate results than deterministic methods.

2.3.1.1 SERPENT2

SERPENT2 performs sensitivity calculations with a *"collision history and weight perturbation"* based approach extended to Generalized Perturbation Theory, presented in detail in [41].

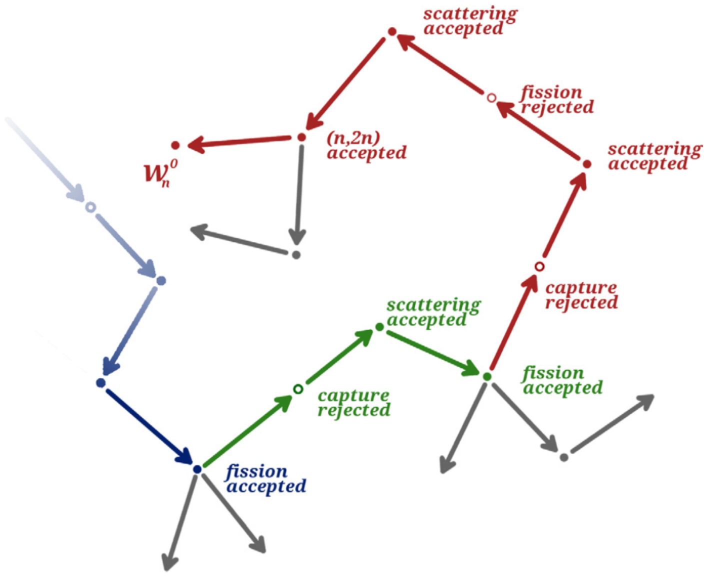

$$w_n{}^* \simeq w_n{}^0 \cdot \left(1 + \frac{d\Sigma_{n,2n}}{\Sigma_{n,2n}}\right) \cdot \left(1 + \frac{d\Sigma_s}{\Sigma_s}\right) \cdot \left(1 - \frac{d\Sigma_f}{\Sigma_f}\right) \cdot \left(1 + \frac{d\Sigma_s}{\Sigma_s}\right) \cdot \left(1 - \frac{d\Sigma_c}{\Sigma_c}\right) \cdot$$
$$\cdot \left(1 + \frac{d\Sigma_f}{\Sigma_f}\right) \cdot \left(1 + \frac{d\Sigma_s}{\Sigma_s}\right) \cdot \left(1 - \frac{d\Sigma_c}{\Sigma_c}\right) \cdot \left(1 + \frac{d\Sigma_f}{\Sigma_f}\right) \ldots$$

Figure 2.3: Collision history and weight perturbation [41].

A simplified description of the processes performed by the code is presented. The first step consists in the increase of the cross section by a factor f. When the reaction occurs, it is rejected with a probability equal to $(1 - 1/f)$. This *virtual* event is scored thanks to the cross section perturbation. On the contrary, when the reaction occurs and it is not rejected, it is accepted and the event is scored as *real*. Secondly, the next process is the compression and the propagation of the information for the successive generations. This operation is done by Iterated Fission Probability (IFP) methods [42], the one used also for the calculation of adjoint-weighted kinetic parameters. At the end, the initial weight w_n^0 of the particle is adjusted to compensate the bias introduced, as can be observed in Fig. 2.3. After each scored reaction, by adopting first order expansion, the adjusted weight w_n^* increases if it accounts for *real* event and decreases for *virtual* one.

The Iterated Fission Probability scheme is illustrated in Fig. 2.4. During sensitivity calculations, the Iterated Fission Probability method stores data for every so called progenitor neutron at each generation g [43]. It compresses and propagates the information for M latent generations until scoring the asymptotic population (or number of descendants) associated to the original event. Since in the Monte Carlo frame more events correspond to lower statistical errors, the IFP cycle is repeated a certain number of time to reach better estimation of the asymptotic population.

SERPENT2 uses a more complicated algorithm with an overlapping approach, where even in the latent generations each neutron is treated as a progenitor. This overlapping method permits to improve more the statistics with a small waste of extra memory [44].

Since each response function has a different physical meaning and it is governed by a distinct phenomenon, their sensitivity coefficients S_x^R are calculated with various equations, as stated in the following Chapters. In particular, SERPENT2 calculates each term of the sensitivity coefficient equations using relations among accepted and rejected events that are properly importance-weighted by the IFP method.

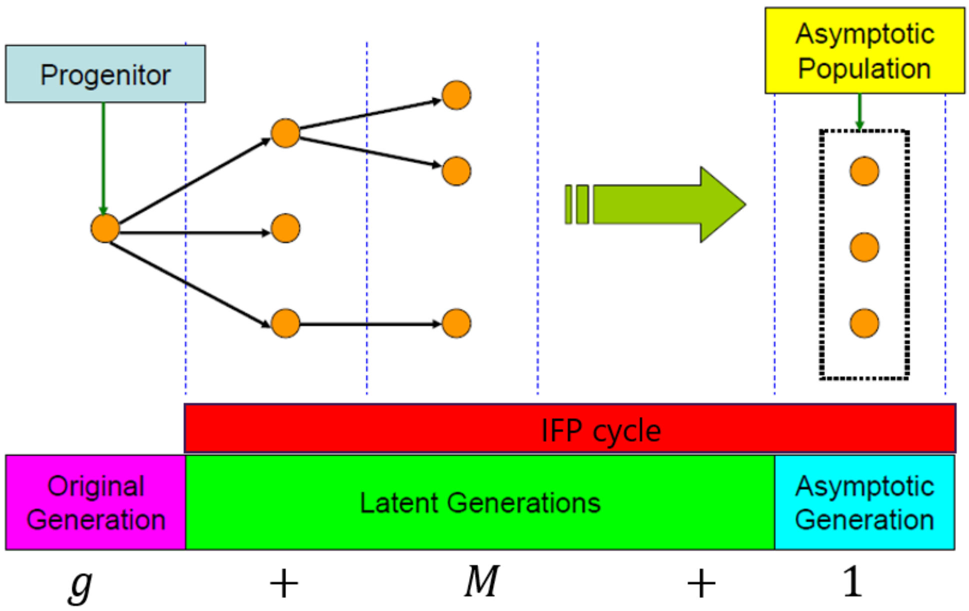

Figure 2.4: Iterated Fission Probability mechanism [45].

2.3.1.2 Other codes

A list of the different tools to compute sensitivity analysis is presented below. These codes are the ones used for comparisons either on benchmark systems and successively for MYRRHA sensitivity calculations.

- MCNP (Monte Carlo N-Particles), developed at LANL (USA) [6]. It represents a well-validated Monte Carlo code for reactor physics applications. MCNP is able to perform sensitivity analyses using methods such as differential operator and IFP with a non-overlapping approach presented in the previous Chapter.
- SUSD3D deterministic code, developed at JSI (Slovenia) [46]. Several comparisons has been done since different sensitivity studies on MYRRHA has been performed using this code, including parameters such as k_{eff} and β_{eff}. It uses first order Generalized Perturbation Theory to compute sensitivity analysis.
- SCALE, developed at ORNL (USA) [47], it is based on probabilistic Monte Carlo methods. With the tool TSUNAMI-3D, sensitivity analysis can be performed using Equivalent Generalized Perturbation Theory (EGPT) method [48].
- ERANOS deterministic code [49] and Tripoli-4 Monte Carlo code [50] developed at CEA (France). Both have been used for comparisons. The latter uses the same IFP overlapping approach developed for SERPENT2.
- MARBLE-SAGEP deterministic code, developed at JAEA (Japan) [51]. This has been also taken into account since several previous sensitivity analyses on MYRRHA were performed with this code.

2.3.2 Response functions

In the following Sections, the parameters set as response functions are presented. Response functions of interest for this study are: the effective neutron multiplication factor k_{eff}, the effective delayed neutron fraction β_{eff}, the effective prompt neutron generation time Λ_{eff} and the void reactivity coefficient α_{coolant}. Moreover, with sensitivity calculations is possible to evaluate also the value of α_{coolant} and α_{Doppler} coefficient.

2.3.2.1 Effective multiplication factor k_{eff}

The k_{eff} eigenvalue sensitivity coefficient can be calculated from the Standard Perturbation Theory [52] as follows:

$$S_x^{k_{eff}} = \frac{\langle \phi^\dagger, \frac{1}{k_{eff}} \frac{\frac{\partial \mathbf{F}}{\partial x}}{x} \phi \rangle - \langle \phi^\dagger, \frac{\frac{\partial \mathbf{L}}{\partial x}}{x} \phi \rangle + \langle \phi^\dagger, \frac{\frac{\partial \mathbf{S}}{\partial x}}{x} \phi \rangle}{\langle \phi^\dagger, \frac{1}{k_{eff}} \mathbf{F} \phi \rangle} \tag{2.29}$$

where x is the perturbed parameter. The numerator terms are respectively the total fission F, loss L and scattering S neutron production rate, which have been weighted on the importance of the emitted neutrons, while the denominator is the total importance-weighted fission production operator [41].

2.3.2.2 Effective delayed neutron fraction β_{eff}

For the kinetic parameter β_{eff}, the response function is expressed as ratios of bi-linear functions of forward and adjoint flux as shown in Eq. 2.15. For the three kinetic parameters of interest the response function can be generalized as:

$$R = \frac{\langle \phi^\dagger, \Sigma_1 \phi \rangle}{\langle \phi^\dagger, \Sigma_2 \phi \rangle} \tag{2.30}$$

where Σ_1 and Σ_2 represent two general reaction operators. In particular, the definition of Eq. 2.15 for the response function β_{eff} can be expressed as follows:

$$\beta_{\text{eff}} = \frac{\langle \phi^\dagger, \frac{1}{k_{eff}} \chi_d \bar{\nu}_d \Sigma_f \phi \rangle}{\langle \phi^\dagger, \frac{1}{k_{eff}} \chi_t \bar{\nu}_t \Sigma_f \phi \rangle} \tag{2.31}$$

For this type of response functions, the sensitivity coefficient can be expressed as a first order expansion from extended Generalized Perturbation Theory [48] and it is characterized by direct and indirect terms:

$$S_x^R = \frac{\langle \phi^\dagger, \frac{\partial \Sigma_1}{\partial x/x}\phi\rangle}{\langle \phi^\dagger, \Sigma_1 \phi\rangle} - \frac{\langle \phi^\dagger, \frac{\partial \Sigma_2}{\partial x/x}\phi\rangle}{\langle \phi^\dagger, \Sigma_2 \phi\rangle} + \frac{\langle \phi^\dagger, \Sigma_1 \frac{\partial \phi}{\partial x/x}\rangle}{\langle \phi^\dagger, \Sigma_1 \phi\rangle} - \frac{\langle \phi^\dagger, \Sigma_2 \frac{\partial \phi}{\partial x/x}\rangle}{\langle \phi^\dagger, \Sigma_2 \phi\rangle} + \frac{\langle \frac{\partial \phi^\dagger}{\partial x/x}, \Sigma_1 \phi\rangle}{\langle \phi^\dagger, \Sigma_1 \phi\rangle} - \frac{\langle \frac{\partial \phi^\dagger}{\partial x/x}, \Sigma_2 \phi\rangle}{\langle \phi^\dagger, \Sigma_2 \phi\rangle} \tag{2.32}$$

where the first couple of terms represents the direct effect of R to x. While the second and the third couples represent respectively the effect of ϕ and $\phi^\dagger$ to the perturbed parameter x.

Since this sensitivity calculations are time consuming and computationally intensive respect to k_{eff}, two solutions were adopted. Firstly, an increment of the number of particles ($1.5e6$ in total) to increase the number of events and consequently reduce the statistical errors. Secondly, to run an independent analysis based on a different method with a subsequent comparison of the results. In this second analysis the sensitivity coefficient is derived from an approximation of the response β_{eff}, known as the Bretscher prompt k-ratio definition [53]:

$$\beta_{eff} \simeq 1 - \frac{k_p}{k} = \frac{k - k_p}{k} \tag{2.33}$$

$$S_x^\beta = \frac{x}{\beta_{eff}} \frac{\partial \beta_{eff}}{\partial x} = -\frac{xk}{k - k_p} \frac{\partial (k_p/k)}{\partial x} = \frac{k_p}{k - k_p} \frac{x}{\partial x} \frac{\partial k}{k} - \frac{k_p}{k - k_p} \frac{x}{\partial x} \frac{\partial k_p}{k_p} = \frac{k_p}{k - k_p} \left(S_k - S_{k_p}\right)$$

$$S_x^\beta = \frac{1 - \beta_{eff}}{\beta_{eff}} \left(S_k - S_{k_p}\right) \tag{2.34}$$

where k_p and S_{k_p} are respectively the effective multiplication factor and the sensitivity coefficient, both computed when the delayed neutrons are switched off during the calculations.

2.3.2.3 Effective prompt generation time Λ_{eff}

A different discussion has to be done for the second kinetic parameter Λ_{eff}, because the response function that can be set from sensitivity calculations is l_{eff}. In Eq. 2.17 the fission operator can be expand as:

$$l_{eff} = \frac{\langle \phi^\dagger, \frac{1}{v}\phi\rangle}{\langle \phi^\dagger, \frac{1}{k_{eff}} \chi_t \bar{\nu}_t \Sigma_f \phi\rangle} \tag{2.35}$$

the inability to perform directly the sensitivity to Λ_{eff} leads to additional calculations:

$$S_{\Lambda_{eff}} = \frac{\sigma}{\Lambda_{eff}} \frac{\partial \Lambda_{eff}}{\partial \sigma}$$

Λ_{eff} can be substituted as shown in Eq 2.16:

$$S_{\Lambda_{eff}} = \frac{\sigma k_{eff}}{l_{eff}} \frac{\partial \left(\frac{l_{eff}}{k_{eff}}\right)}{\partial \sigma} = \frac{\sigma}{\partial \sigma} \frac{k_{eff}}{l_{eff}} \frac{\partial l_{eff} k_{eff} - \partial k_{eff} l_{eff}}{k_{eff}^2} = S_{l_{eff}} - S_{k_{eff}} \tag{2.36}$$

where $S_{l_{eff}}$ can be calculated using Eq. 2.32.

The number of particles in the simulation is the same as in β_{eff} (1.5E6). Also in this case, the sensitivity coefficient can be obtained from an approximation of the response l_{eff}. This method does not require the solution of the adjoint neutron transport problem and it is the so called "$1/v$ absorber method" [53]. A good agreement between the results obtained from the SERPENT2 GPT capabilities and the "$1/v$ absorber method" approach using TSUNAMI-1D EGPT has been already proved in [41]. The decision for this thesis was firstly to obtain the same result in several benchmark experiments presented in Section 5.2.1 and then to apply directly the SERPENT2 capabilities to MYRRHA.

2.3.2.4 Void coefficient α_{coolant}

Such as the previous kinetic parameters, the reactivity coefficient α_{coolant} can be expressed as ratios of bi-linear functions of the forward and the adjoint flux. The fission operator of Eq. 2.23 can be explicit leading to:

$$\alpha_{\text{coolant}} = \frac{\langle \phi^\dagger, \Sigma_{\text{t,coolant}} \phi\rangle}{\langle \phi^\dagger, \frac{1}{k_{eff}} \chi_t \bar{\nu}_t \Sigma_f \phi\rangle} \tag{2.37}$$

then, the sensitivity to α_{coolant} can be calculated with Eq. 2.32.

Another method to calculate the sensitivity to α_{coolant} can be done introducing directly a perturbation in the coolant density and computing the sensitivity to k_{eff}. With a comparison between the k_{eff} sensitivity of the nominal case and the one perturbed it is possible to derive the sensitivity to α_{coolant} [24].

An additional application of the sensitivity analysis is to directly calculate the value of some coefficients, and not the sensitivity related to them. As stated in Eq. 2.22, α_{coolant} is a ratio of derivatives and therefore it is a sensitivity coefficient that can be calculated by the code. The calculation of the void reactivity coefficient can be performed running a sensitivity analysis on k_{eff} and set a perturbation to the total macroscopic cross section of the coolant $\Sigma_{\text{t,coolant}}$. The mathematically explanation can be deducted from the following formula:

$$\Sigma = N\sigma \tag{2.38}$$

because perturbing Σ has the same meaning of perturbing N (atomic density of the material).

The sensitivity coefficient calculated with this procedure indicates the change in k_{eff} due to the 1% increase in the coolant density. Since α_{coolant} is expressed in [pcm/% void volume], the results must be multiplied for -0.01, because the 1% increase in void volume corresponds to the 1% decrease in density [54]. The results of this calculation are shown in Section 5.3.

2.3.2.5 Doppler coefficient α_{Doppler}

Similar discussion can be done for the Doppler coefficient α_{Doppler}. As can be seen in Eq. 2.24, it is also expressed as a ratio of derivatives. The first step to calculate the Doppler coefficient is to broaden the cross sections. For this purpose different software can be used (e.g. Janis [55]). Secondly, the code needs a file with those relative change in microscopic cross section, using as reference the core operative temperature. Finally, the response to k_{eff} has to be set.

In order to obtain the Doppler coefficient from the integrated sensitivity coefficient, some post processing operations have to be done. Firstly, it is necessary to multiply by k_{eff} to get the perturbation, since sensitivities are by definition relative quantities. Secondly, dividing by the temperature difference used for broadening the cross sections it is possible to get the unit of [pcm/K]. Finally, multiplying by the fuel temperature it is possible to obtain the Doppler coefficient linked to the cross section broadening.

$$\alpha_{\text{Doppler}} = \text{ISC} * k_{eff} * 10^5 * T_{\text{fuel}} \tag{2.39}$$

Chapter 3

Full core model of MYRRHA

Since 1998 the MYRRHA core design has been changed and improved, for the present study the 1.6 version of 2014 is considered [18]. In the past, the model of the MYRRHA 1.6 critical core has been deeply examined in different neutronic code: MCNP [6], OpenMC [12], etc. The present study, in which the SERPENT2 Monte Carlo code was employed, represents a further implementation with new analyses and results. The MYRRHA core is analyzed at Beginning of Cycle (BOC), i.e. when the reactor is started and the burnup distribution depends on the fuel management strategy. In the model configuration considered all the control and safety roads are withdrawn (excess of reactivity condition). Fig. 3.1 shows a radial view of the core in correspondence of the fuel axial mid-plane.

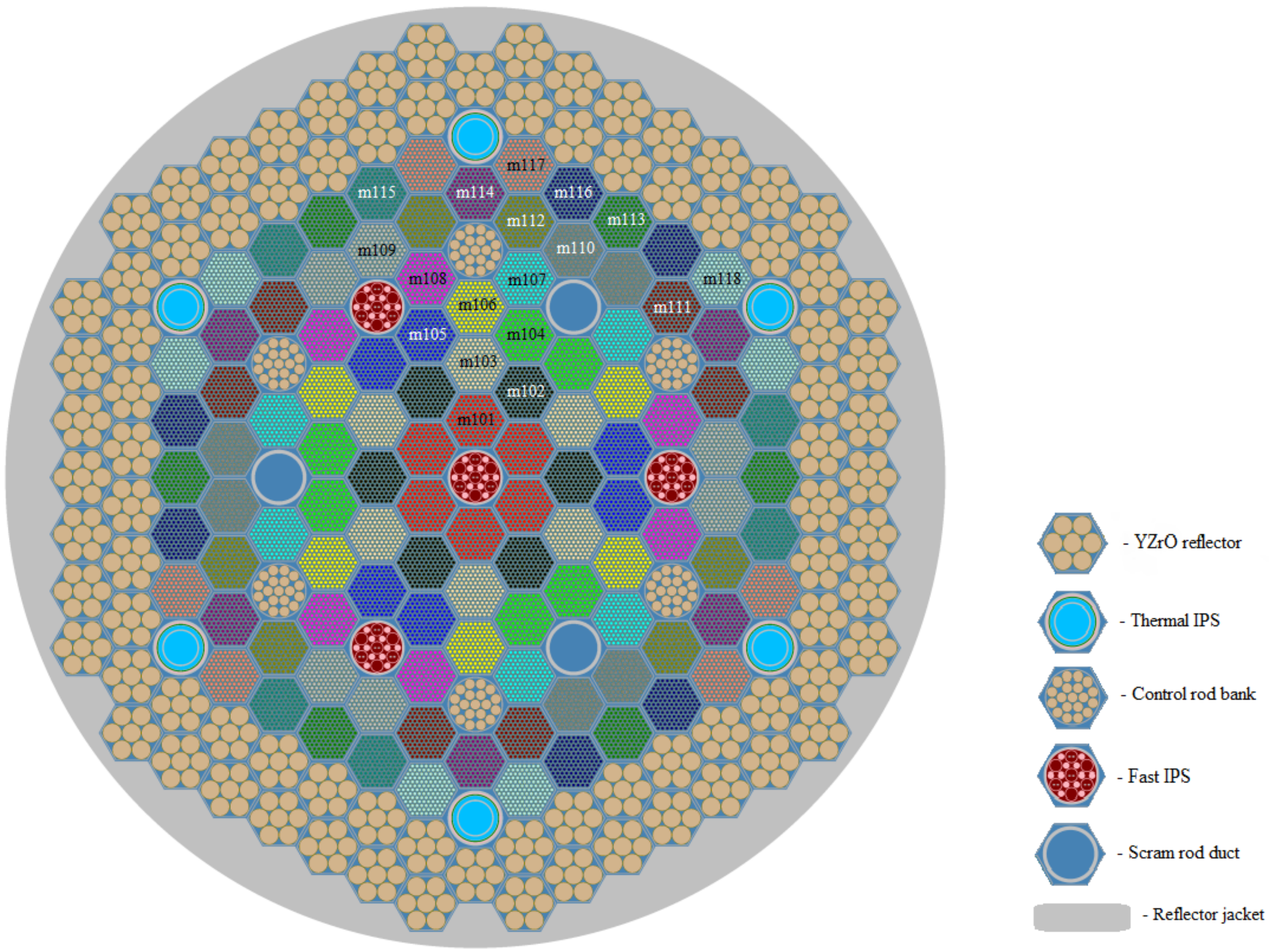

Figure 3.1: MYRRHA 1.6 critical core (xy-plane) [56].

The core contains 108 FAs distributed in 18 burnup batches. Each batch is formed by 6 FAs with identical average-burnup indicated with the same color in Fig. 3.1. The fresh fuel (m101) is located in the center of the core because there is higher neutron flux. The burnup increases up to its maximum value in 9^{th} batch (m109) and it consequently decreases moving towards the periphery up to the 18^{th} batch (m118). The MYRRHA fresh fuel is highly-enriched MOX (more than 30%-HM enriched).

In Fig. 3.1 two different types of safety high-absorbing rods are present. Three scram-rod gravity-driven located in the 4^{th} ring for the shut down of the reactor and six buoyancy-driven control-rods located in the same ring that are used for reactivity control in normal operation. Two other types of IPSs (In-Pile-Sections) constitute the core and they are distinguished by the operating spectrum. Four fast spectrum IPSs, one located in the center of the core and the other three in the 4^{th} ring are used for irradiation and displacements-per-atom (dpa) analyses. Six thermal spectrum IPSs are located in the 6^{th} ring for radio-nuclide production, especially ^{99}Mo.

The last two rings of the core contain beryllium rods and act as neutron reflector. At the end, the most outward element containing all these 127 assemblies/channels is the stainless steel jacket, indicated by the gray color in Fig. 3.1.

The two associated axial plots of the core are presented in Fig. 3.2. For the calculation point of view, the outside of these two figures is considered as vacuum, thus neutrons crossing these limits are removed from the system (vacuum boundary conditions).

For what concerns the temperatures of the elements aforementioned, it has to be noted that a radial temperature gradient among fuel – gap – cladding was imposed ranging between 1300 K to 750 K. While in the LBE an axial gradient between 550 K for the lower assembly up to a maximum of 750 K was considered.

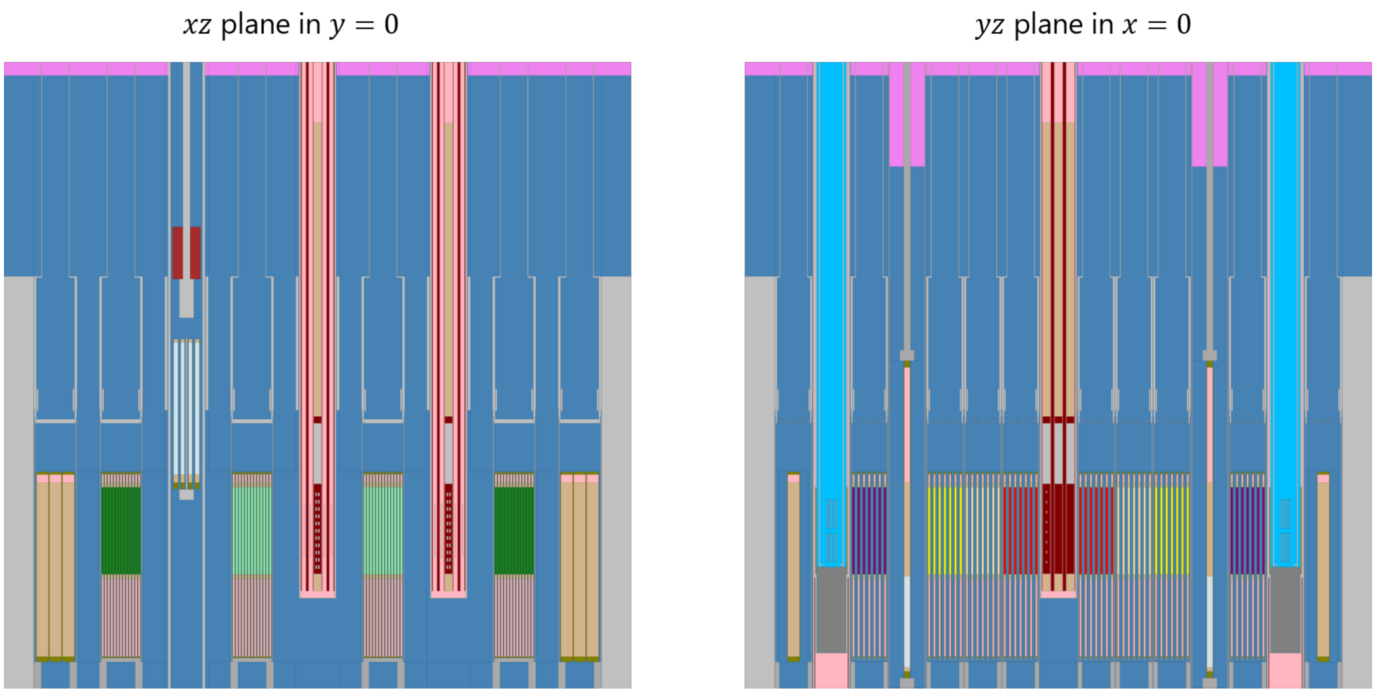

Figure 3.2: MYRRHA 1.6 axial views.

3.1 MYRRHA results

Several criticality calculations were run for the MYRRHA 1.6 core model in nominal condition to better understand how the SERPENT2 user choices affect the result, the computational time, the statistical error and the memory usage. The nominal condition corresponds to the core version presented in Fig. 3.1, at BOC and when the control rods are out of the active zone (i.e. excess of reactivity condition).

The neutron flux calculated using Monte Carlo methods is arbitrarily normalized and its value depend on the number of simulated neutron histories. The present study is rarely focused on absolute values of flux or reaction rates, but in such cases it is normalized on the nominal core power, i.e. 100 MW [18].

To find the maximum value of the neutron flux two calculations were performed. The first one has been conducted along the z height on the radial center of the reactor. Fig. 3.3 shows that the maximum is reached in $z = 0$. Successively, the second calculation was performed in the plane $z = 0$ to find the radial maximum. Fig. 3.4 shows the 3D behavior of the flux, the absolute maximum is located in the fresh fuel assemblies. This behavior has been confirmed by Fig. 3.5, that shows two symmetrical peak located near the center of the reactor. The peak is not located in correspondence of the central assembly (the fast IPS) because it do not contained fuel nuclides. From Fig. 3.5 two relative peaks can be also seen. They are the direct consequence of the reflector action located around the core. They are geometrically in correspondence to the thermal IPS. From this analysis the maximum value of the neutron flux has been found, i.e. 1.3^{17} $[cm^{-2}s^{-1}]$.

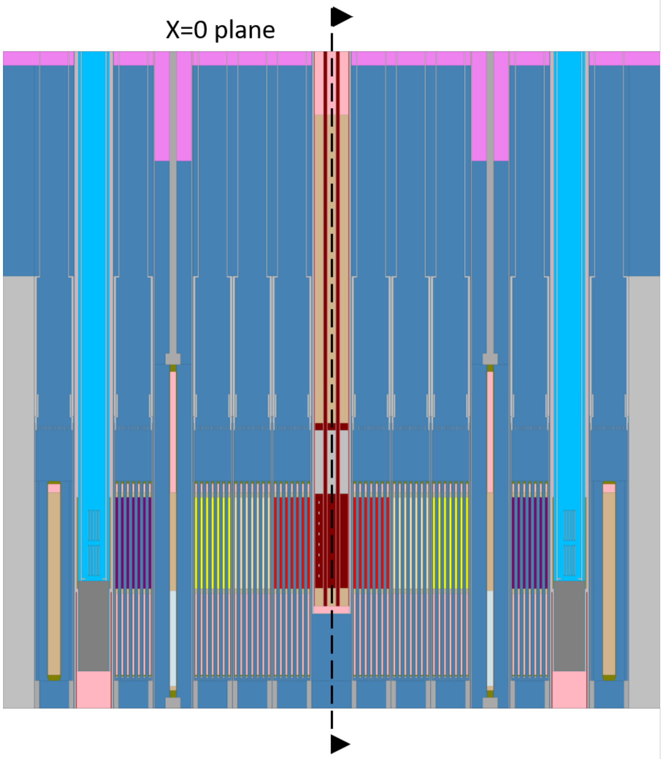

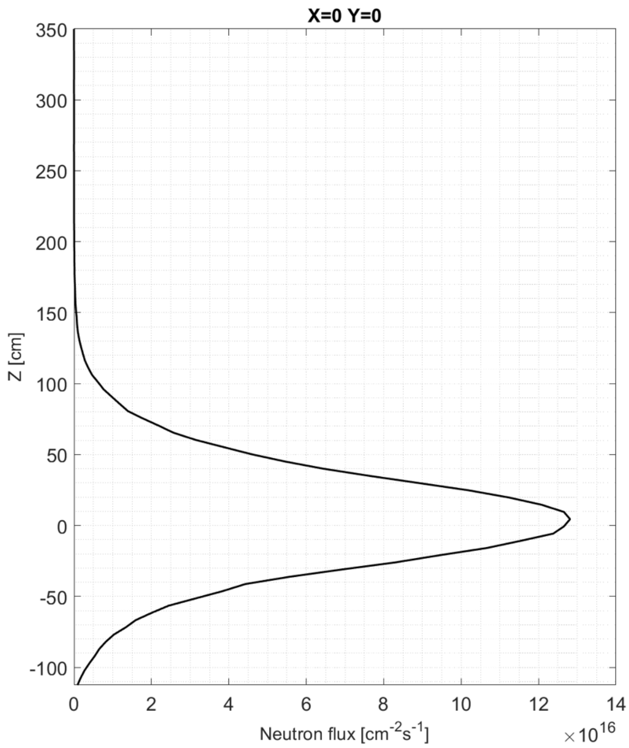

Figure 3.3: MYRRHA 1.6 neutronic flux along the core height in the center line.

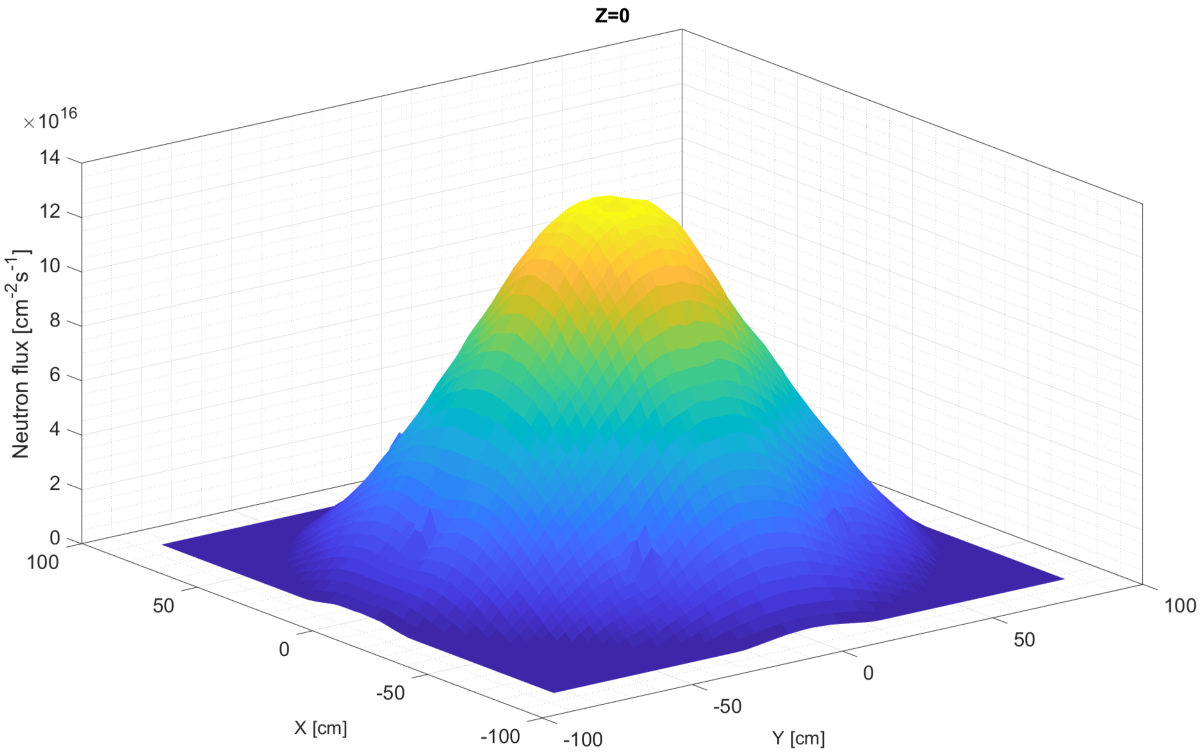

Figure 3.4: MYRRHA 1.6 neutronic flux (xy-plane).

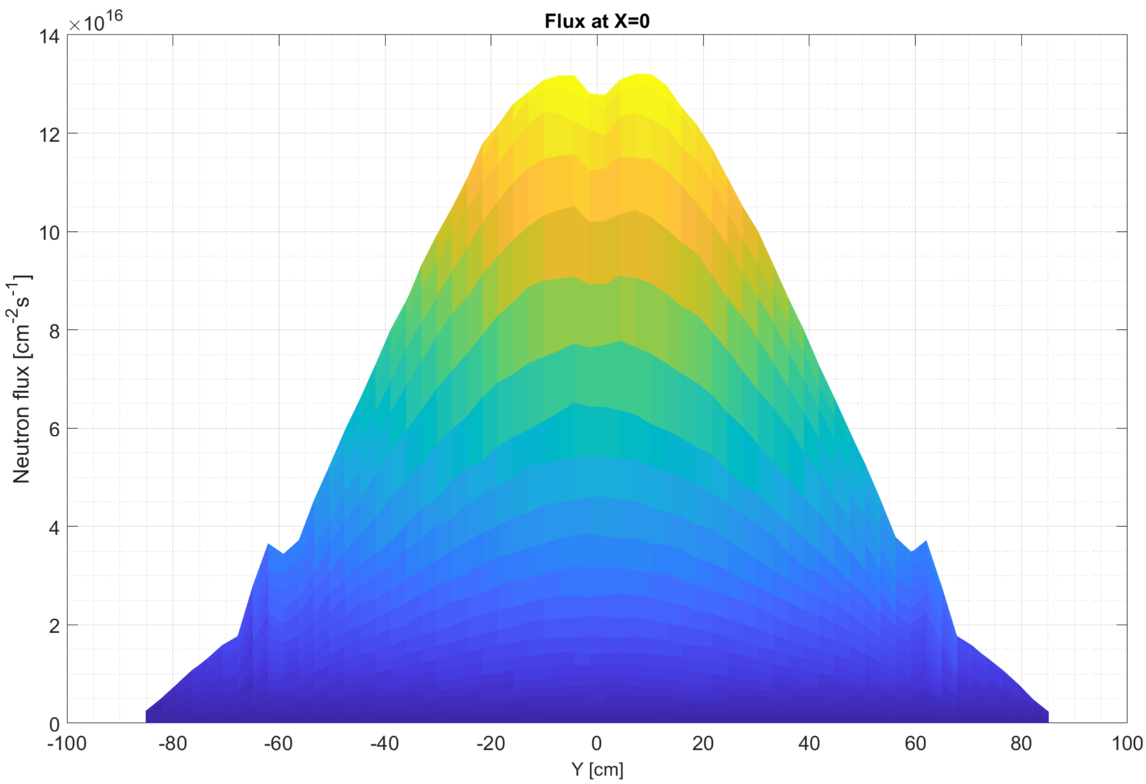

Figure 3.5: MYRRHA 1.6 neutronic flux (yz-plane).

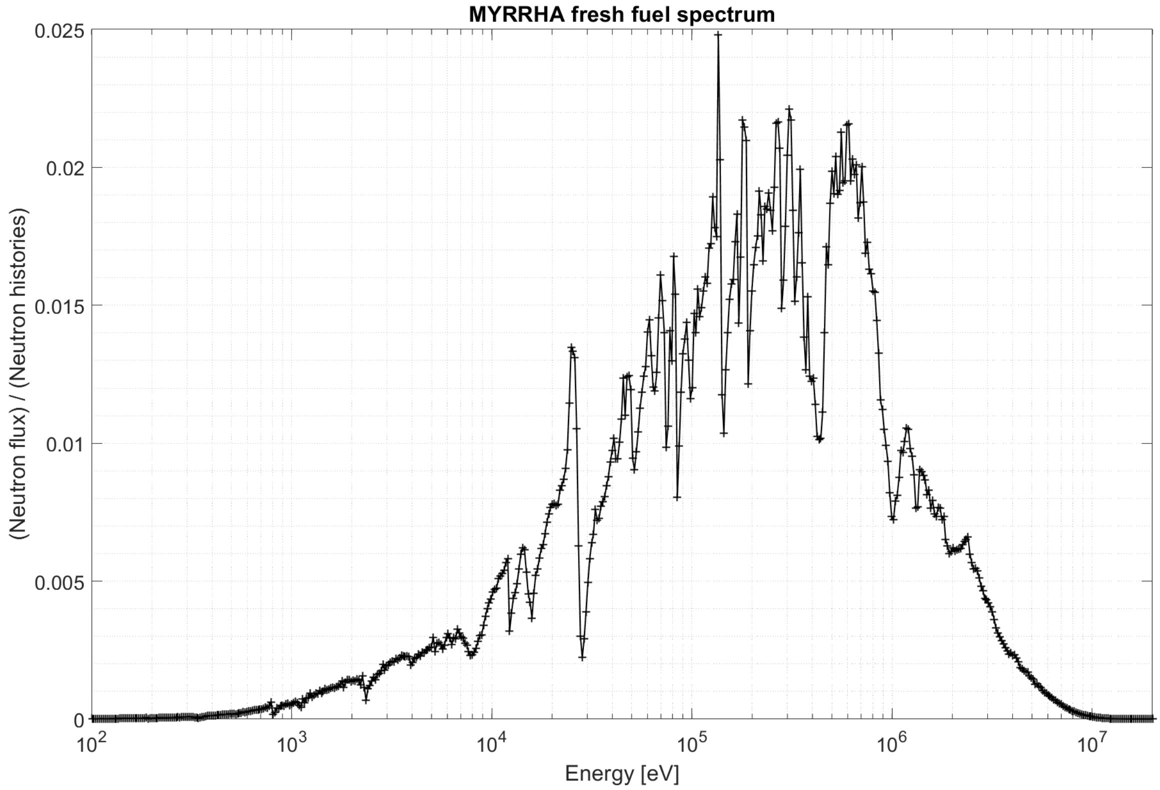

Figure 3.6: MYRRHA 1.6 spectrum in fresh fuel.

Fig. 3.6 shows that MYRRHA has a fast spectrum. Going from the center of the core to the outwards, not only the absolute value of the neutron flux decreases, but even its spectrum become slightly softer.

All the presented MYRRHA results were obtained with 2e6 particles per cycle and 1e4 active cycles, leading to $2{\times}10^{10}$ histories. Such high number was employed to obtain reference results very accurate, as shown in Table 3.1.

In Monte Carlo simulations, the k_{eff} parameter can be calculated via *analog* approach (scoring the physical interactions) or via *implicit* estimator (based on the expected occurrence of the event) that is derived from the analog estimator with the purpose of obtaining better statistics [9]. The analog approach results are the one listed in Table 3.1. It can be said that the mean value of the implicit one is the same, with the only difference that it presents a lower statistical error by a factor 2 respect to the analog one. k_{eff} is considerably higher compared to 1 (the critical value), because of the excess of reactivity condition analyzed.

Table 3.1: MYRRHA 1.6: main parameters comparison between SERPENT2 and MCNP

MC code	k_{eff}	β_{eff}	Λ_{eff}
SERPENT2	1.01311± 1e-5	$0.00330 \pm 2e-6$	0.6403± 2e-4 μs
MCNP	1.01312± 9e-5	$0.00329 \pm 1e-5$	0.6401± 4e-3 μs

The kinetic parameters Table 3.1 are calculated during the criticality calculation using the IFP method. They are calculated with different methods and all the results are given in the output file, it can be said that a good agreement has been found among all the methods with extremely low statistical errors (several order of magnitudes lower respect to their mean values).

Table 3.1 shows also a good agreement between the SERPENT2 results and the ones coming from the well-validated MCNP code. The mean values are very similar while the statistical errors are different because the two simulations rely on different number of cycles and particles. In this specific case SERPENT2 can run faster than MCNP of a factor from 5 to 15 [9].

Chapter 4

Void propagation

In this Chapter, a study regarding the impact that different LBE volumetric void configurations have from a reactivity change point of view is described. The analysis was carried out taking as reference/nominal state the MYRRHA 1.6 critical core model at BOC and at excess of reactivity configuration, presented in the previous Chapter.

In a nuclear reactor, the coolant voiding of the core is one of the most important issue to consider during the reactor design in order to fulfill the safety requirements. Especially for reactors that run on fast neutrons, because of the absence of high efficiency moderators (e.g. light water) in the reactor leading to a positive void coefficient [57].

Even if a vast literature regarding void studies for fast reactors can be found on Sodium Fast Reactors (SFR), a not negligible effect is expected to happen in lead-cooled type of systems, since the boiling temperature of lead coolant is exceptionally high of about 1745°C. For Lead-Bismuth Eutectic coolant the boiling temperature is 1670°C [21], much higher than the coolant temperature in nominal condition and this might be the reason of not even considering this a safety cause of concern [58].

Anyhow, loss of coolant and steam injection scenarios were considered in the present study, since unlikely but still possible accidental events could lead to these dangerous situations. The dangerousness comes from the fact that in this type of fast systems, fissions are maximized to occur above the epithermal energy region, thus hardening the spectrum will not necessarily produce a decreased in the number of fissions. Since the probability that a fission event occurs inside a reactor is not constant, the impact on the system reactivity level brought by the abrupt change of density of a certain material of the domain (e.g. reactor coolant) will depend not only on the degree of such change but also on its location along the system (e.g. reactor core).

In order to investigate such aspects, the choice was to monitor the change of the effective multiplication factor at different volumetric void configurations is described. For each study an analysis of the physics behind such change is also carried out by observing the behavior of the most important phenomena that contribute to the overall void effect.

The reduction of interaction between neutrons and coolant nuclides leads to three main effects:

- Spectral hardening: less neutrons-coolant scattering interactions bring to a decreasing neutrons moderation. More high energy neutrons are present in the system $\rightarrow$ reactivity increases.
- Increased leakage: neutrons with higher energy have less probability to be absorbed (since absorption cross sections usually decrease with the neutron velocity) $\rightarrow$ reactivity decreases.
- Reduction of neutron capture: coolant density reduction leads to a decreasing number of neutrons captured in the coolant $\rightarrow$ reactivity increases.

As can be imagined, the reactivity effect and its magnitude depends on the sum of these three aspects. After a certain void volume, leakage becomes predominant and the reactivity drastically decreases. The aim of this study is to find the geometrical configuration leading to this limit corresponding to the maximum reactivity enhancement, called *worst condition*.

4.1 LBE voiding scenario

In this Section, two voiding strategies with their respective results and the safety concerns are analyzed. The first voiding strategy is related to radially and axially void expansions due to different loss of coolant scenarios. The second voiding strategy simulates the localized gas release inside a single fuel assembly. In the following, a detailed explanation on how the physical problem was implemented in SERPENT2 and the relative results are presented.

4.1.1 Ring voiding

In order to simulate a loss of coolant with the aim to find the so called *worst condition*, the idea was to start from the most critical point of the core, located in the nearby of the radial center and at $z = 0$ (corresponding to the exact half of the fuel active length) and expand volumetrically the void along the LBE to the outward of the core. Successively, once found the highest reactivity insertion condition, the aim was to verify if a continued void volume increase will cause the reduction of reactivity due to predominant neutron leakage phenomena.

Practically, in the SERPENT2 Monte Carlo code, simulating a void injection is a geometrical problem. The method used consists in replacing in the universe of interest the void instead of LBE. In the so called *nominal* core configuration, it has to be noted that the central assembly contains a fast IPS and therefore, in the nearby of the point where the flux has its highest point (where the neutron importance via the adjoint component is the highest) no LBE is present. Thus, the first void formation begins in the volume occupied by the small LBE layer surrounding the central IPS, condition called *ring central* in the results Section.

As can be seen in Fig. 4.1 (where black regions correspond to voided regions) the next step was to radially expand the void towards the periphery, finding other three configurations: the void up to the first, the second and up to the third ring of fuel assemblies. For this first step, the void condition was considered only when the full rings were voided. As can be seen from the yz views of Fig. 4.2, also the z axial height was taken into account in order to create a void mesh. For each of the fourth radial configurations, different void height were considered ranging from 18 to 34 cm. The mesh limits of the axial and radial analyses have been reasonably chosen for some expected physics aspects discussed in detail in the results Section. The voided (black) region shown in Fig. 4.2 (right), where the radial void is up to the third ring and the axial height is the maximum (34 cm) is called the *black zone* for the rest of the study.

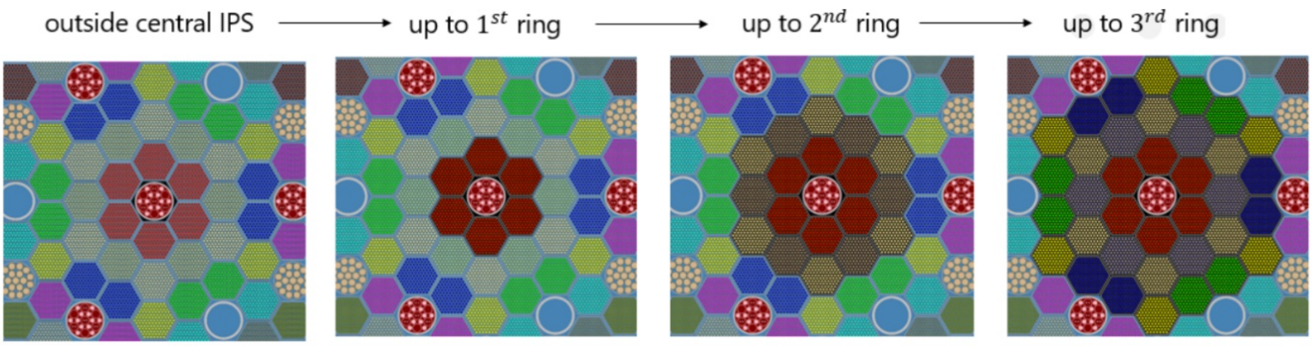

Figure 4.1: Radial expansion of LBE void.

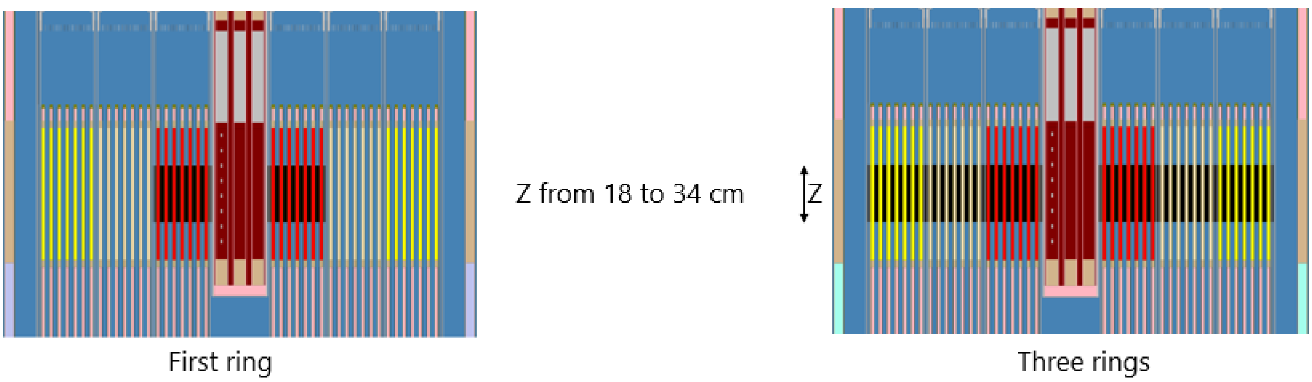

Figure 4.2: Axial expansion of LBE void.

Successively, since the reactivity insertion peak has been found inside the imposed radial limits, the choice was to investigate also conditions related to half-ring. As can be seen in Fig 4.3, other three conditions were taken into account. Starting from the void up to the half of the first ring (where just the half part of the fuel assemblies that face the center of the core was voided), the so called *ring 0.5*. The other two condition took the same nomenclature, even if they do not represent exactly the half of the assembly voided, because in the corners of the hexagon region voided, just 1/3 of the LBE volume inside the assembly was substituted with void for geometrical reasons.

Regarding these new half ring conditions, only the axial height corresponding to the maximum reactivity insertion that was previously found was analyzed.

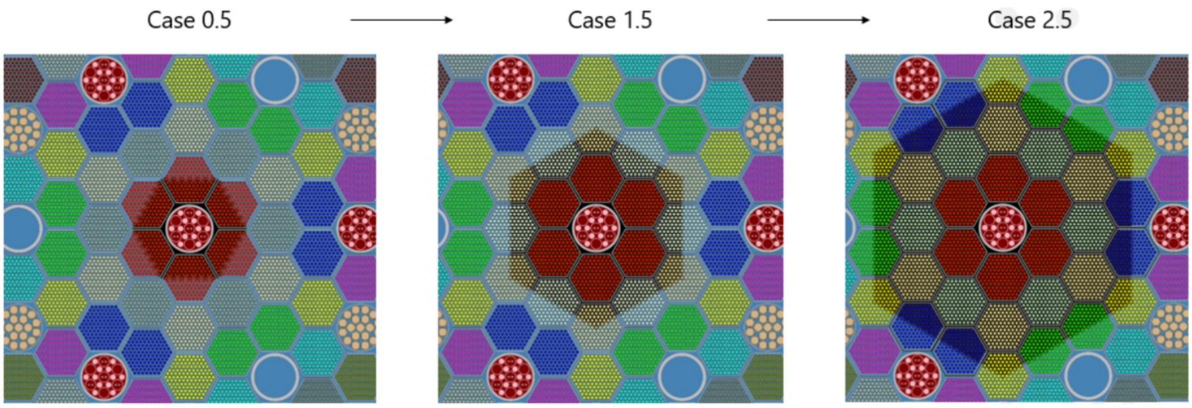

Figure 4.3: Half ring radial expansion of LBE void.

4.1.1.1 Full ring voided results

The primary results coming from the full ring voiding analysis are shown in Fig. 4.4. The graph shows how the aforementioned volumetric void mesh affects the value of k_{eff}. The first conclusion that can be drawn is that every void injection causes a positive k_{eff} increase. It can be also observed that the maximum reactivity increase (the temporary *worst case*) happens when the second ring is fully voided at an axial distance from the center of 34 cm (e.g. from -17 to $+17$ cm). Since the maximum increase of reactivity was found at the axial limit (34 cm), even $36 - 38 - 40$ cm have been investigated for the second ring void case, but their multiplication factors were smaller than the *worst case*.

In first approximation, to reach the desired balance between precision and fast results, the simulations were run with $1e6$ particles and 250 active cycles, that required 40 minutes to provide an analog k_{eff} results with a standard deviation of 10 pcm with a computational power of 72 cores in parallel. After identifying that the voided-second ring corresponded to the one leading to the maximum insertion of reactivity, a deeper analysis was conducted on the axial height. These analyses relied on the same number of particle as before, $1e6$, but with an increased number of active cycles, $2e3$, leading to an analog k_{eff} results with a standard deviation of 2 pcm. This condition is presented in Fig. 4.4 and Fig. 4.5. Successively, once identified the worst case, an additional simulation was run with the same statistics of the nominal condition to compare results with the same precision. It can be finally concluded that for the *worst case*, the effective multiplication factor is $k_{eff} = 1.01720 \pm 1$ pcm. The associated positive reactivity insertion is 398 pcm with respect to the nominal case.

In order to fully understand the phenomena leading to different reactivity insertions, other studies were carried out with the aid of the tallying capabilities of SERPENT2. A study on the relative variation (which is derived from the reference value) of the total core fission – capture – leakage rates for the radial-axial volumetric void mesh was performed. Since the effective multiplication factor is formed by the ratio of fission to losses (i.e. capture plus leakage) rates, then such figures can be used to deduct which of these effects is dominating along the spatial distribution of the LBE volumetric void.

As can be deducted from Fig. 4.6, from the fission point of view, the major enhancement is detected radially at the second ring voided condition and axially at 34 cm of void height (i.e. situation that exactly corresponds to the *worst condition*).

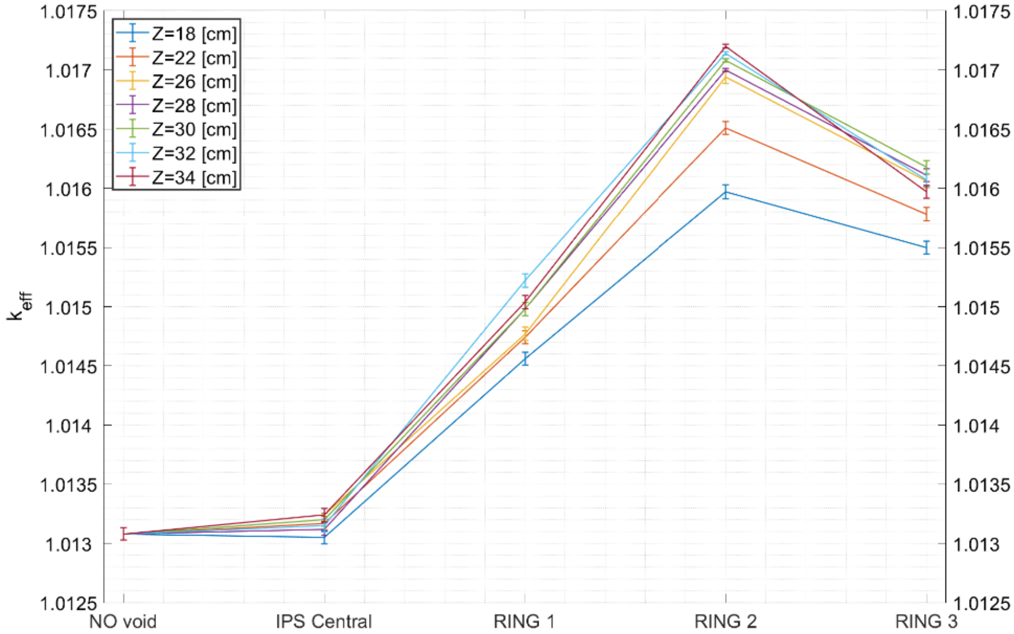

Figure 4.4: Effective multiplication as function of voided rings.

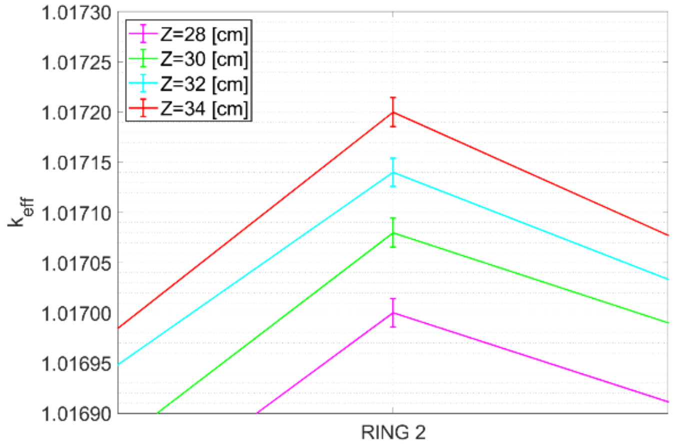

Figure 4.5: Zoom of the effective multiplication factor in the second ring voiding condition.

A more local-oriented analysis based on the relative change (from the nominal calculation) of fission rates of important fuel nuclides for different void configurations can be found in figures Fig. 4.7 and Fig. 4.8. The main idea was to see how some important fissionable and fissile nuclides from all fuel batches along the core behave under the presence of void.

From this local analysis of the relative variation of the nuclides fission reaction rates, it can be observed at the maximum point of reactivity insertion (up to 2nd ring at 34 cm) the maximum increase of fissions in ^{240}Pu. Also at this point, there is a large increase in the number of fissions in ^{238}U, while the relative change in fissile ^{239}Pu and ^{241}Pu under any degree of void is a negative relative decrease in comparison to the nominal calculation. This means that the neutron spectral shift in the fuel (due to the presence of coolant void) enhances fission reactions in fissionable nuclides (e.g even-nuclides) while, on the other hand, it creates the opposite effect in fissile ones (e.g odd-nuclides). An interesting observed feature in the ^{238}U behavior is that the fission rate actually increases until the voiding of the third ring. Nevertheless, between the second and the third ring the fission rate in ^{240}Pu strongly decreases.

Another fruitful discussion regarding ^{238}U and ^{239}Pu fission reactions at different energy (that confirms these conclusions) can be found in Section 5.1, where the k_{eff} sensitivity results are explained making use of the fission macroscopic cross section of these two nuclides.

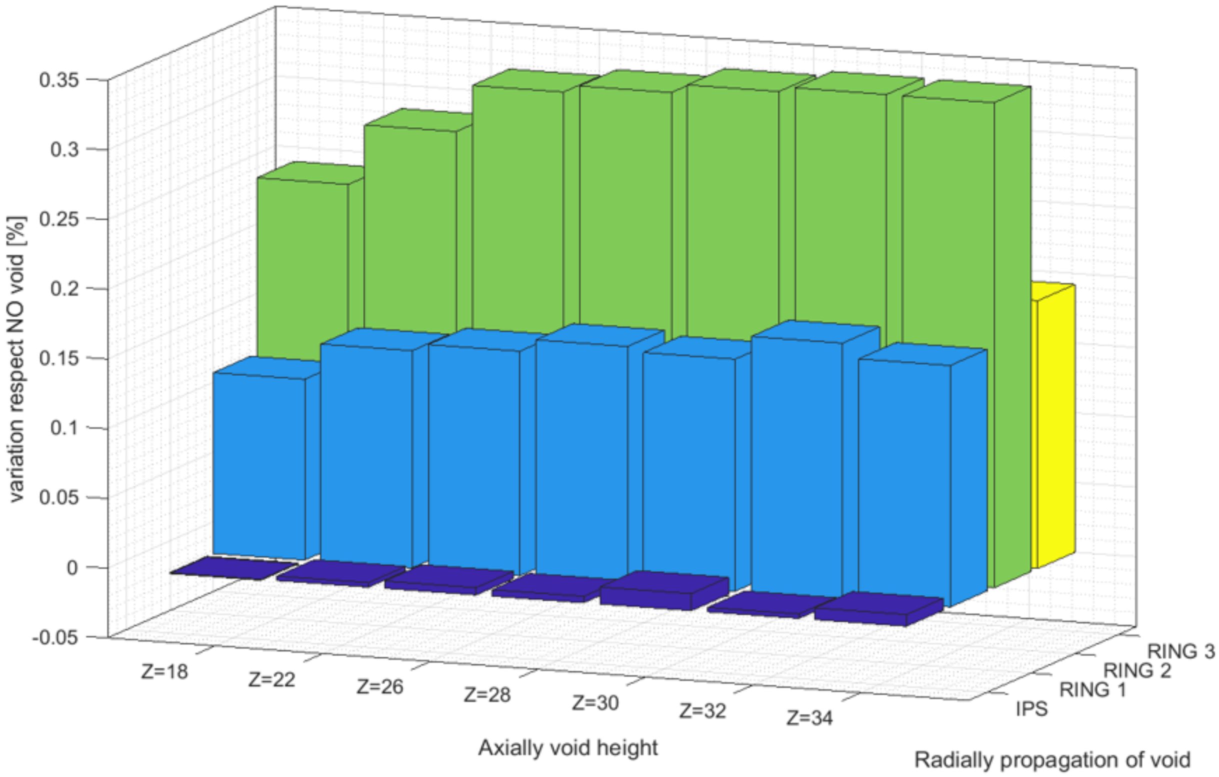

Figure 4.6: Total core fission rate variation respect to the nominal condition.

The results from Fig. 4.9 show that losses due to radiative capture are always negative when void is present with respect to the reference calculation. This is an expected conclusion, since the reduction of coolant nucleus can only bring to a decreasing number of neutrons captured into it. In fact, continuing to enhance the volume voided across the rings (even after the second ring) the number of capture reactions continue decreasing.

The conclusions deducted up to now can just explain why the reactivity increases with the enhancement of void volume. However, no explanation can be derived on the fact that after the second ring void condition the reactivity starts its negative trend.

Fig. 4.10 fills this shortcoming, because leakage in the third ring condition is about five times higher respect to the second ring value. Nevertheless, the large increase of fission reactions during the voiding up to the second ring, combined with the weak leakage interaction at this degree of radial voiding, creates the maximum reactivity injection at an axial height of void of 34 cm. After that, if an additional full voided ring is added to the domain of study, leakage becomes very strong dominating the scenario and finally, becoming the strongest physical phenomena that in the end would lead to a sudden decrease of reactivity.

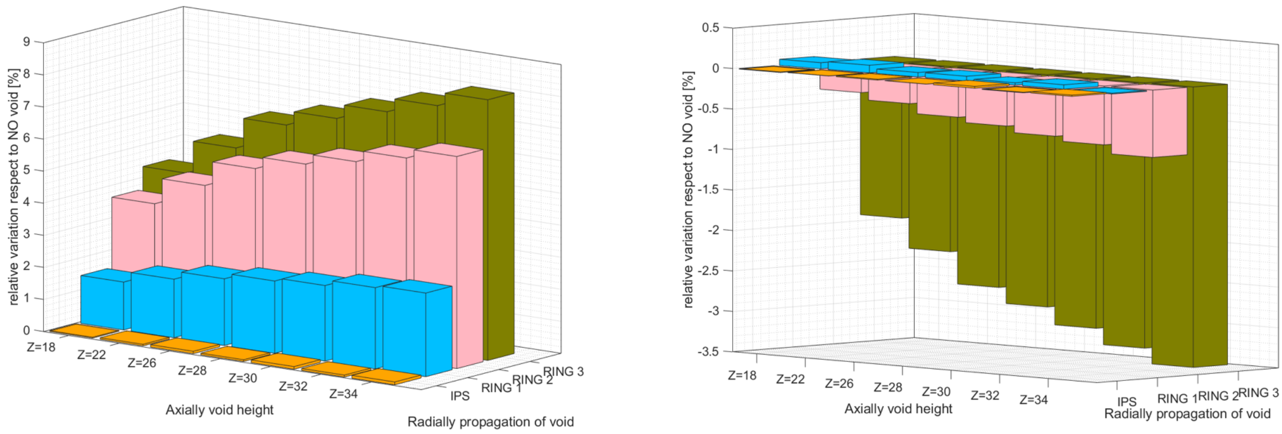

Figure 4.7: ^{238}U (left) and ^{239}Pu (right) fission reaction rates variation respect to the nominal condition.

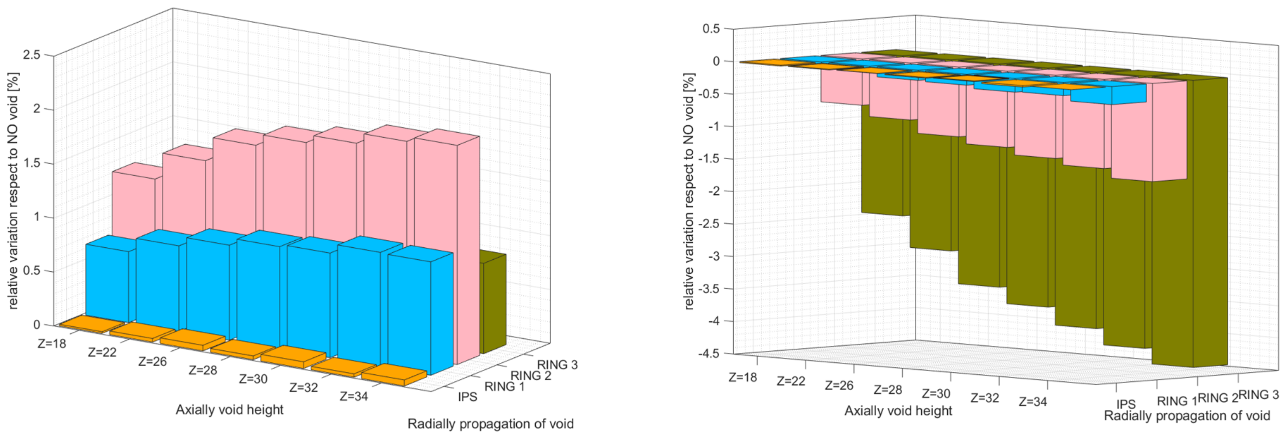

Figure 4.8: ^{240}Pu (left) and ^{241}Pu (right) fission reaction rates variation respect to the nominal condition.

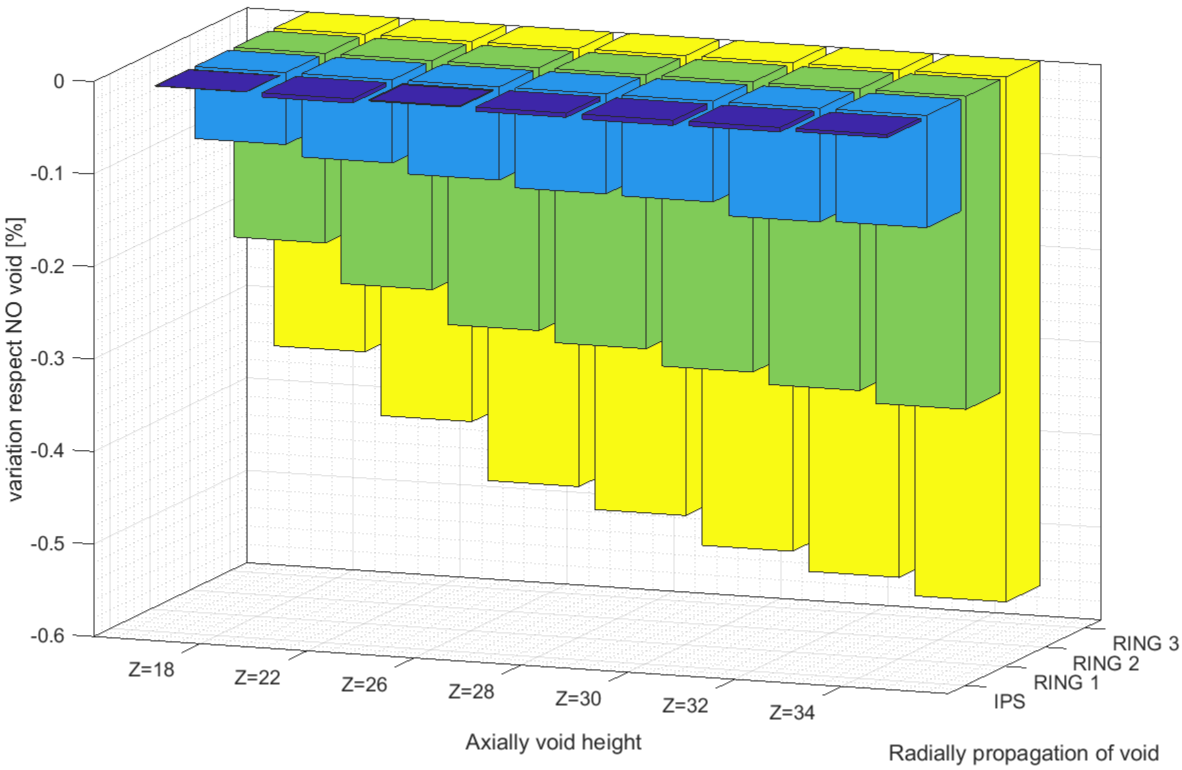

Figure 4.9: Total core capture rate variation respect to the nominal condition.

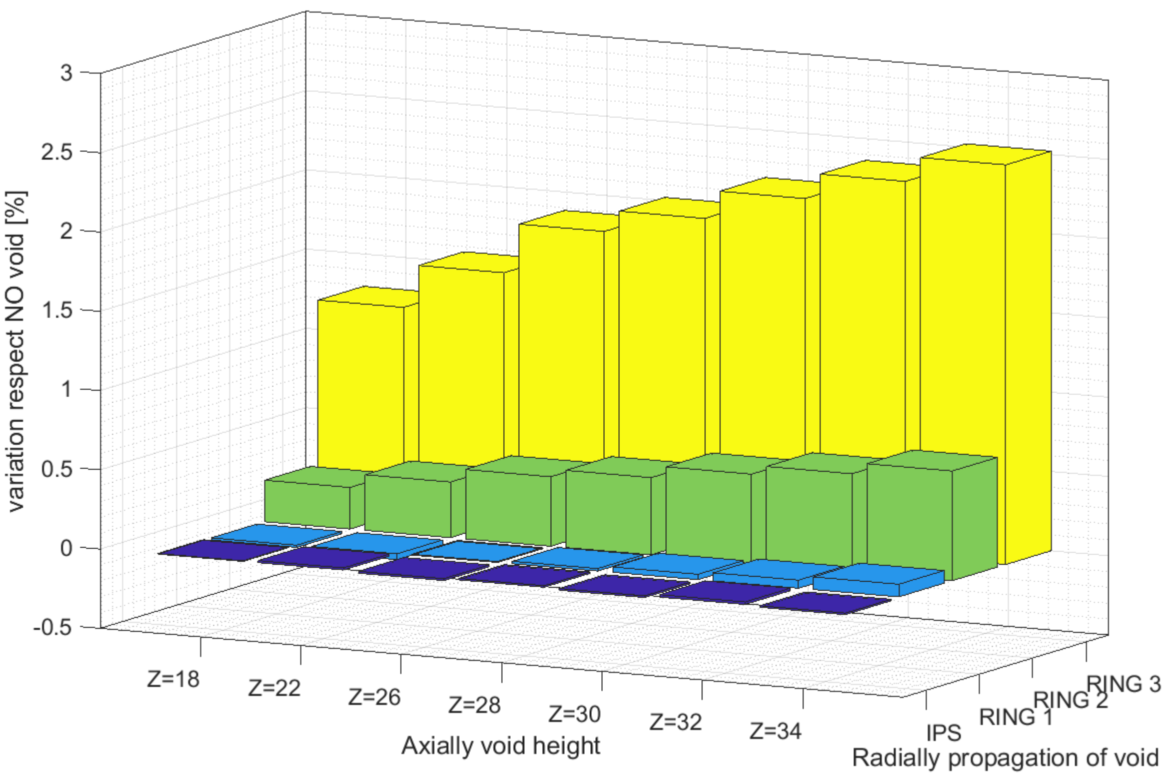

Figure 4.10: Total core leakage rate variation respect to the nominal condition.

4.1.1.2 Half ring voided results

Successively, since the results found up to this point were physically explainable and understandable, the decision was to investigate also the half ring radial void condition taking as reference the 34 cm of axial height. The expectation was to find in the half ring void condition a value between the previous full ring voided and the successive one. In correspondence of the *worst condition*, two possibilities were taken in consideration, to find a k_{eff} value between the previous full ring voided and the successive one, or even to find a new maximum value. As can be seen in Fig. 4.11, the latter possibility was the right on.

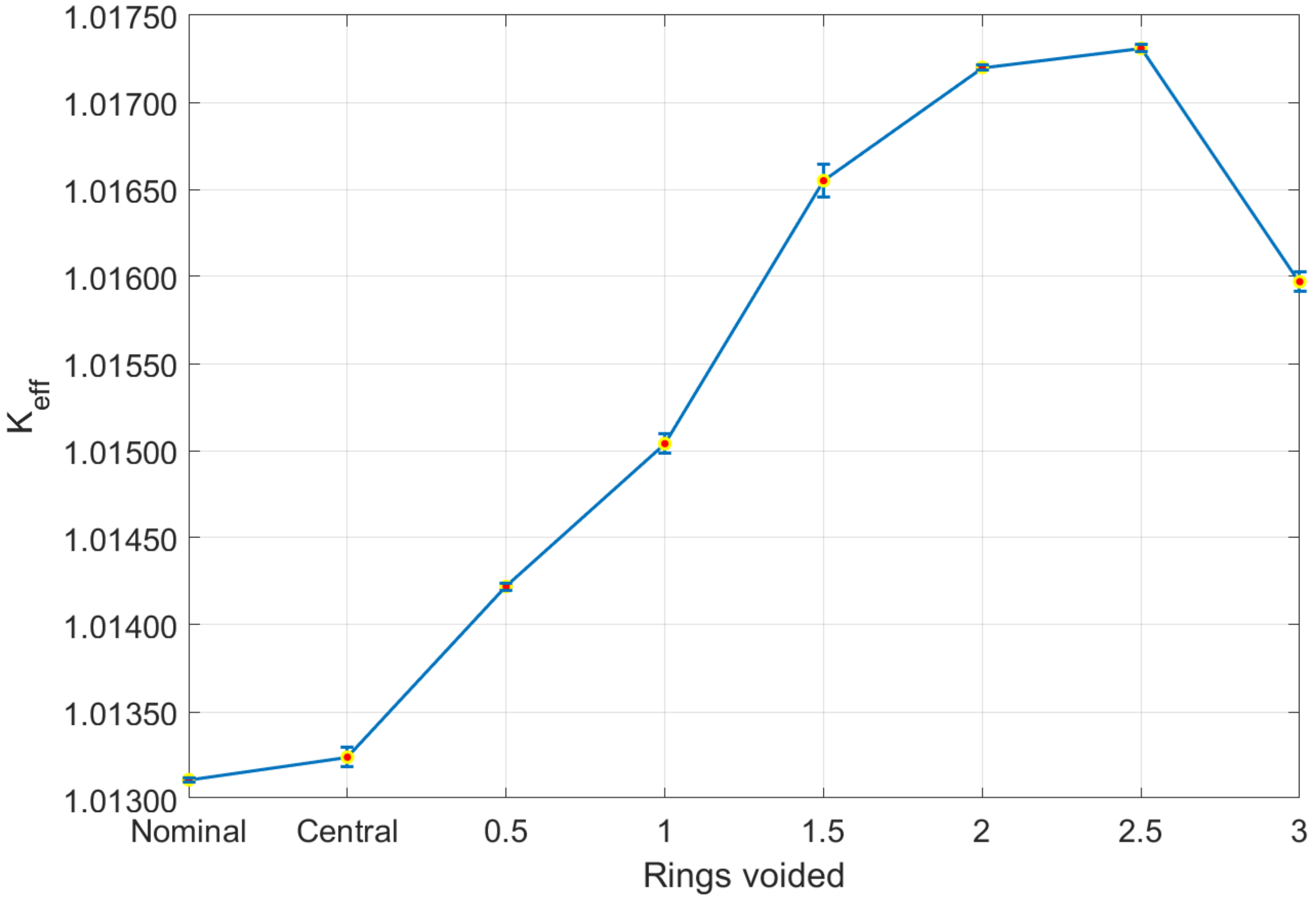

Figure 4.11: Effective multiplication as function of voided rings.

The graph shows that a new maximum, thus a new *worst condition*, was achieved in the second ring and a half voided condition. The new maximum is now: $k_{eff} = 10732 \pm 1$ that leads to a positive reactivity insertion of 408 pcm respect to the nominal case. Nevertheless, since it is not a significant change in comparison to the worst case that was previously found out while voiding up to the second ring, the previous reaction rate calculations were not repeated.

The most important conclusion that can be deducted from the half ring analysis is not the fact that the highest reactivity insertion occurs at an axial height of 34 cm while voiding up to the volume corresponding to 2.5 rings. Instead, the most important results is that this analysis permits to refine the k_{eff} data available for different volumes of void injection. This is shown in Fig. 4.12.

It can be seen a radical change on the x-axis respect to the previous graphs of k_{eff} behavior, since they have been based as a function of number of voided rings, giving the illusion that the reactivity insertion is wherever non-linear. Alternatively, in Fig. 4.12 the x-axis represents the percentage of void in the system with respect to the volume of the so called *black zone*. This zone represents the volume of LBE voided in the system when it is expanded radially up to the third ring and axially up to 34 cm. This behavior corresponds exactly to the behavior that could be found if the considered abscissa was the ratio between the void volume over the total LBE volume present in MYRRHA. This can be mathematically derived as follows:

$$V_{LBE_{MYRRHA}} = V_{LBE_{black}} + V_{LBE_{no\,black}} \tag{4.1}$$

where $V_{LBE_{MYRRHA}}$ is the total volume of LBE in the MYRRHA reactor. $V_{LBE_{black}}$ is the volume of LBE radially inside the third ring and axially at a height of 34 cm, which is equal to $5.16e4\ cm^3$. $V_{LBE_{no\,black}}$ corresponds to the volume of LBE in the MYRRHA reactor outside of the black zone. Since they are fixed volumes for the rest of the calculation, it can be deducted that $V_{LBE_{black}}$ represents a small fraction of $V_{LBE_{MYRRHA}}$. Thus, when the void is injected:

$$\frac{Vvoid}{V_{LBE_{black}}} \propto \frac{Vvoid}{V_{LBE_{MYRRHA}}} \tag{4.2}$$

where $Vvoid$ is the volume of the void injection. It can be concluded that the relative distances on the x-axis of Fig. 4.12 remain the same as the void volume was compared to the total volume of LBE in MYRRHA. It is also observed that the shape of the curve should remains the same.

With this new way of showing the k_{eff} results, depicted in Fig. 4.12, it can be observed firstly a more linear behavior of the effective multiplication factor from the beginning of voiding and up to 30% of it (corresponding to ring 1.5) and successively a smooth increase up to the maximum insertion of reactivity (corresponding to ring 2.5). Finally, a drastically decrease of k_{eff} and in consequence, of the reactivity insertion from its maximum value takes place due to the predominant leakage effect.

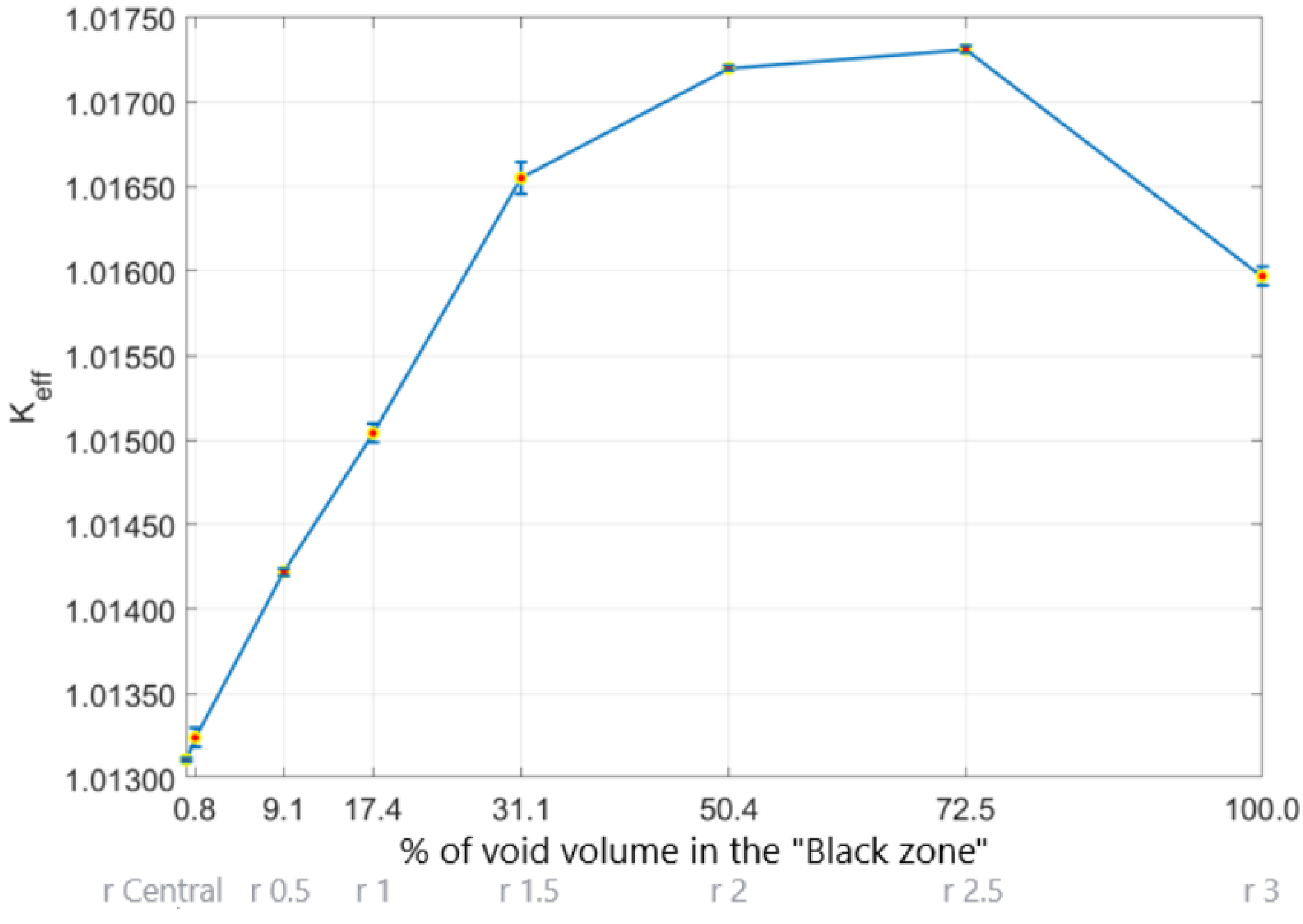

Figure 4.12: Effective multiplication factor as a function of LBE volume voided rings.

4.1.2 Single assembly voiding

The second voiding strategy has the aim to simulate an accidental situation inside a single assembly, occurring the void formation in a very localized region of the core. It can be the case of an unprotected assembly blockage, where a pin failures leads to a fast generation of fuel debris blockage. This means that once a pin fails the release of fuel chunks, accompanied by the release of gas around the sub-channels, would lead to the reduction of coolant flow which, in return, may bring other pins to fail due to the combination of low cooling flow and the addition of heating (i.e. avalanche effect). In the end, the maximum amount of released gas could form different void configurations along the assembly. More information related to the scenario of this phenomena can be found in [59].

The maximum volumetric void due to the aforementioned conditions corresponds to 91.2 cm^3, which is relatively small compared to the volumes seen in the previous Section. On the contrary this accidental situations are much more realistic than the previous ones. Modeling such scenarios in SERPENT2 leads to the choice of a single assembly belonging to the first ring (i.e. fresh batch fuel), to which different degrees of void configurations were applied by changing both radial and axial dimensions, equaling each of these to the maximum volume of the void. Some examples are illustrated in Fig. 4.13, where the axial length of the void is indicated in the upper part of the plots. The total length H is divided in half starting from the center of the axis for the first four scenario. For the last one (H = 32.5 scenario) the axial length corresponds the whole axial height comprised between the origin of the axis and the end of the active part of the fuel.

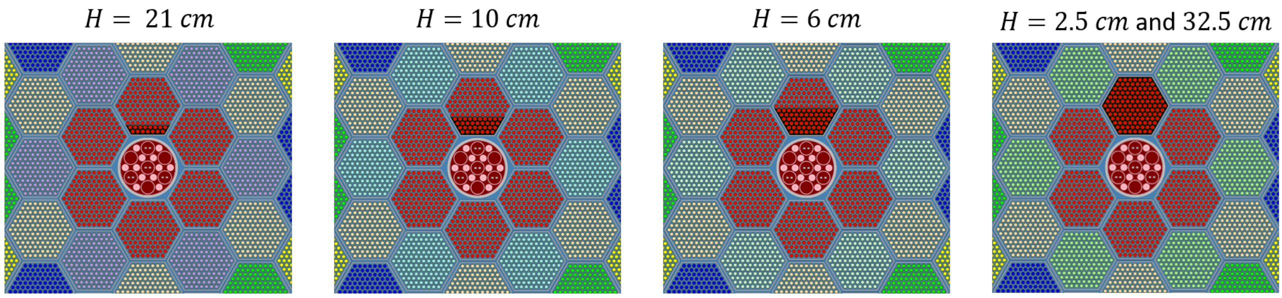

Figure 4.13: Single assembly expansion of LBE void.

4.1.2.1 Single assembly results

The effective multiplication factor of all these results can be graphically found in Fig 4.14. It can be appreciated with a black horizontal line the reference k_{eff} (1.01311 ± 1 pcm). Since an extremely little variation of k_{eff} was expected for all the cases, the simulations were run with the same statistics of the nominal condition. This little variation is comparable to the results of the previous analyses, showing that for small void injection in the black zone (up to the 30%), the increase of k_{eff} can be approximated as linear. The outcome of this linear approximation shows that all the results should have an average increase of k_{eff} of around 2 pcm. It can be calculated using the following proportion:

$$(0.311 \times V_{black}) : (\rho_{1.5} - \rho_{nom}) = V_{void} : x \tag{4.3}$$

where the first term $(0.311 \times V_{black})$ represents the void volume of the the ring 1.5 condition coming from the previous study. The second term $(\rho_{1.5} - \rho_{nom})$ is the respective increase in reactivity due to that void condition. The third term is the new void volume of 91.2 cm^3 corresponding to the first four cases. The fourth term is the unknown, which is nothing else than the expected increase of reactivity due to the new void condition.

As Fig 4.14 shows, this rough estimation is extremely near to the real results, since the maximum deviation from the nominal condition occurs either at the configuration with an axial height of 6 cm, or the one corresponding to the height of 2.5 cm (both with a $k_{eff} = 1.01316 \pm 1$).

The final safety conclusion coming from this single assembly voiding is that there is almost no increase in reactivity due to this type of scenario.

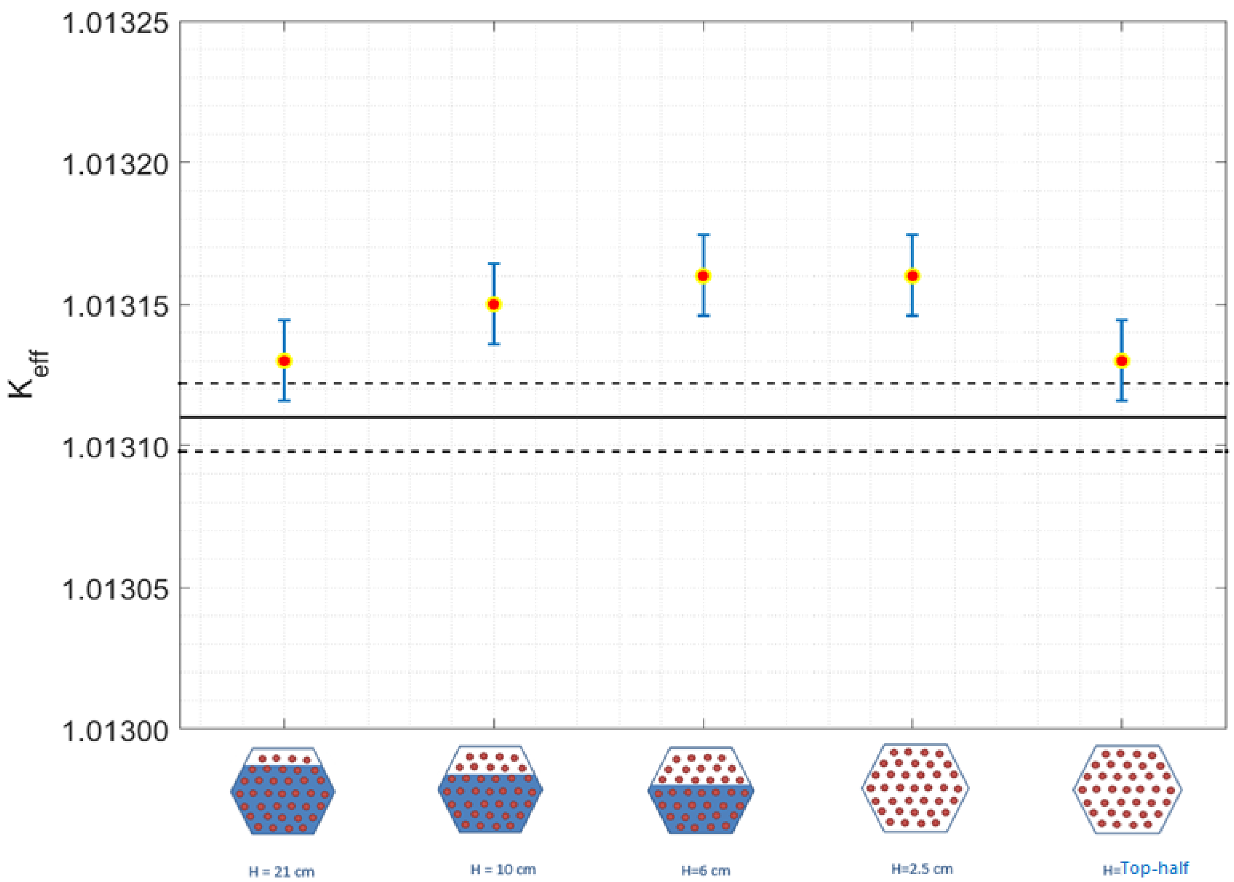

Figure 4.14: Effective multiplication as function of voided assembly.

Chapter 5

Sensitivity analysis

In this Chapter the results of the sensitivity analyses conducted on the MYRRHA 1.6 core are presented and explained. Some calculations have been conducted directly on the MYRRHA core, while others have been previously conducted on benchmark experiments. Most of the times the simulations were run with the following main input parameters:

- $1.5e6$ number of neutrons per generation and $1.0e4$ active cycles leading to $1.5e10$ neutron histories. They have been selected in order to achieve low statistical errors and to run simulations in a reasonable time with the available cluster memory;
- 15 latent generations and 10 iterated fission probability cycles. Previous studies [41] [44] have shown that these numbers are sufficient to make the descendant neutrons convergent to the adjoint flux;
- ECCO 33 multi-group energy grid has been chosen since it aimed at benchmarking fast reactor calculations [60] and because the small numbers of energy bins makes the graphs more suitable for comparisons of different nuclides;
- batch size equal to 25. It represents the number of consecutive cycles in a batch. The aim is to combine several consecutive cycles and tallying the interested quantities by averaging the tallies of cycles in a batch.

For the present calculations, the nuclear data library used is the JEFF-3.1.2. It is a general purpose library in ENDF-6 format that contains incident neutron data for 381 isotopes or elements [61].

5.1 Effective multiplication factor k_{eff}

In this Section the k_{eff} sensitivity results with respect to some reaction cross sections of different nuclides are presented. Previous analyses [24, 39, 62, 63], carried out on different versions of the homogenized MYRRHA core have shown a high sensitivity of k_{eff} to some nuclear reactions and nuclides such as ^{239}Pu($\bar{\nu}$), ^{239}Pu(n, f) and ^{238}U(n, γ), which is confirmed by the present study.

In Table 5.1 the energy integrated k_{eff} sensitivities of the main nuclides are ranked in a descending order on the absolute Integrated Sensitivity Coefficient value. The two nuclear data types to which the MYRRHA k_{eff} is most sensitive are the prompt nubar and the fission cross sections of ^{239}Pu. In a first approximation, it can be thought that ^{238}U should be the predominant nuclide since it is the most abundant in the fuel mixture.

The following discussion on the macroscopic cross sections can be useful to justify the predominance of ^{239}Pu and to interpret and compare the sensitivity profiles of different reactions and nuclides. Fig. 5.1 shows the fission macroscopic cross section of ^{239}Pu and ^{238}U in the MYRRHA reactor. It can be seen that the Σ_f of ^{239}Pu is several orders of magnitude higher than the more abundant ^{238}U, especially for energies lower than 3 MeV. Above that energy, the highest Σ_f is the one corresponding to ^{238}U. The exact same behavior can be find in Fig. 5.2. In fact, from incoming neutron energies below 3 MeV the ^{239}Pu sensitivity profile is considerably higher, then ^{238}U has the highest step-sensitivity coefficients. It can be thus concluded that macroscopic cross sections (the one appearing in the neutron transport equation 2.13) and sensitivity profiles for a certain nuclide and reactions have a similar behavior.

Table 5.1: MYRRHA 1.6: k_{eff} sensitivity ranking table.

Isotope	Reaction	Sensitivity Coeff. (%/%)	Std. dev. (2σ)
^{239}Pu	$\bar{\nu_p}$	+0.68081	±0.00005
^{239}Pu	(n,f)	+0.48347	±0.00006
^{238}U	(n,γ)	−0.11652	±0.00004
^{241}Pu	$\bar{\nu_p}$	+0.08988	±0.00003
^{240}Pu	$\bar{\nu_p}$	+0.08798	±0.00003
^{238}U	$\bar{\nu_p}$	+0.07254	±0.00003
^{241}Pu	(n,f)	+0.06482	±0.00003
^{240}Pu	(n,f)	+0.06077	±0.00003
^{239}Pu	(n,γ)	−0.04557	±0.00002
^{238}U	(n,f)	+0.04530	±0.00003
^{209}Bi	(n,n)	+0.04418	±0.00023
^{238}U	(n,n')	−0.02479	±0.00010
^{240}Pu	(n,γ)	−0.02262	±0.00002
^{235}U	$\bar{\nu_p}$	+0.01993	±0.00001
^{56}Fe	(n,n)	+0.01920	±0.00020
^{238}U	(n,n)	+0.01658	±0.00029
^{235}U	(n,f)	+0.01292	±0.00001
^{56}Fe	(n,n')	−0.01101	±0.00003
^{56}Fe	(n,γ)	−0.01000	±0.00001
^{206}Pb	(n,n)	+0.00768	±0.00010
^{209}Bi	(n,n')	−0.00681	±0.00002
^{241}Pu	(n,γ)	−0.00456	±0.00001
^{209}Bi	(n,γ)	−0.00301	±0.00001
^{206}Pb	(n,n')	−0.00281	±0.00002
^{239}Pu	(n,n)	+0.00240	±0.00013
^{239}Pu	(n,n')	−0.00214	±0.00004
^{235}U	(n,γ)	−0.00175	±0.00001
^{206}Pb	(n,γ)	−0.00161	±0.00001
^{240}Pu	(n,n')	−0.00149	±0.00001
^{240}Pu	(n,n)	+0.00148	±0.00010
^{239}Pu	$\bar{\nu_d}$	+0.00132	±0.00001
^{238}U	$\bar{\nu_d}$	+0.00109	±0.00001

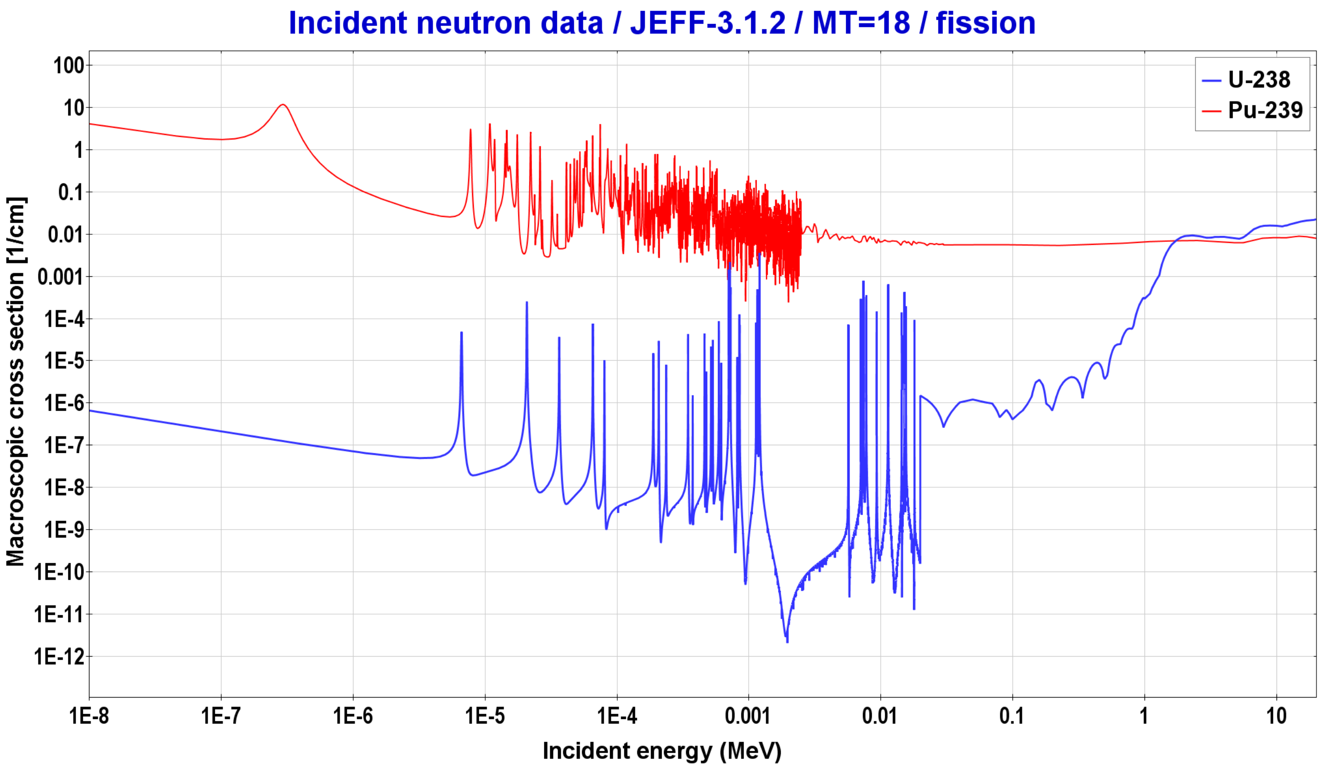

Figure 5.1: MYRRHA 1.6: ^{238}U and ^{239}Pu macroscopic fission cross-sections comparison.

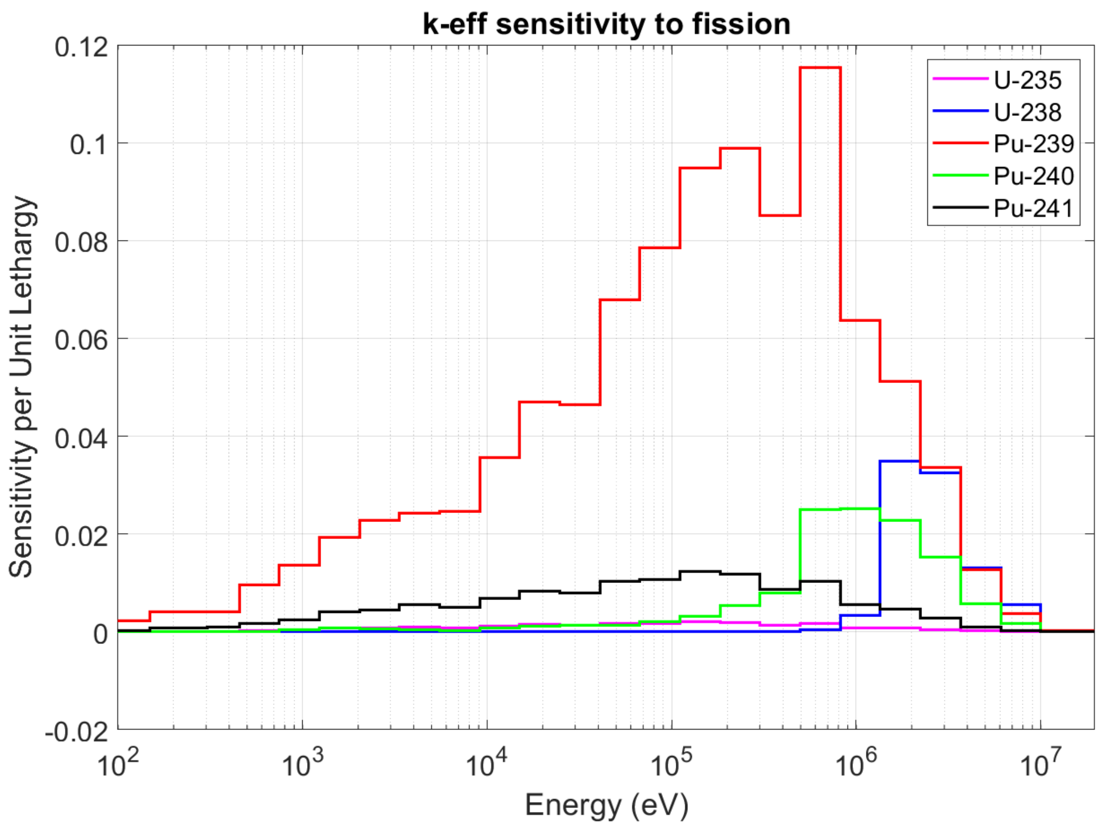

Figure 5.2: MYRRHA 1.6: k_{eff} sensitivity with respect to fission cross-sections.

Fig. 5.2 and 5.3 show that the sensitivity profiles for fission and prompt nubar have similar shape. It can be explained by the fact that a perturbation (e.g. positive) of one parameter or the other, leads to the same physical result: an increase in the number of neutrons in the system. However, since nubar prompt and the fission cross section are different parameters with different dependences (e.g energy dependence), the magnitude of their sensitivity coefficient is different. The positive effects that such perturbations induce can be also mathematically explained since Σ_f and $\bar{\nu}_p$ can be find at numerator in Eq. 2.8, thus a positive perturbation lead to an increase in k_{eff}.

In Fig. 5.4 the sensitivity profiles for delayed nubar perturbations are shown. The pick of ^{238}U is due to its higher value of delayed neutron fraction respect to the other nuclides, but this is analyzed more in detail in Section 5.2.2.

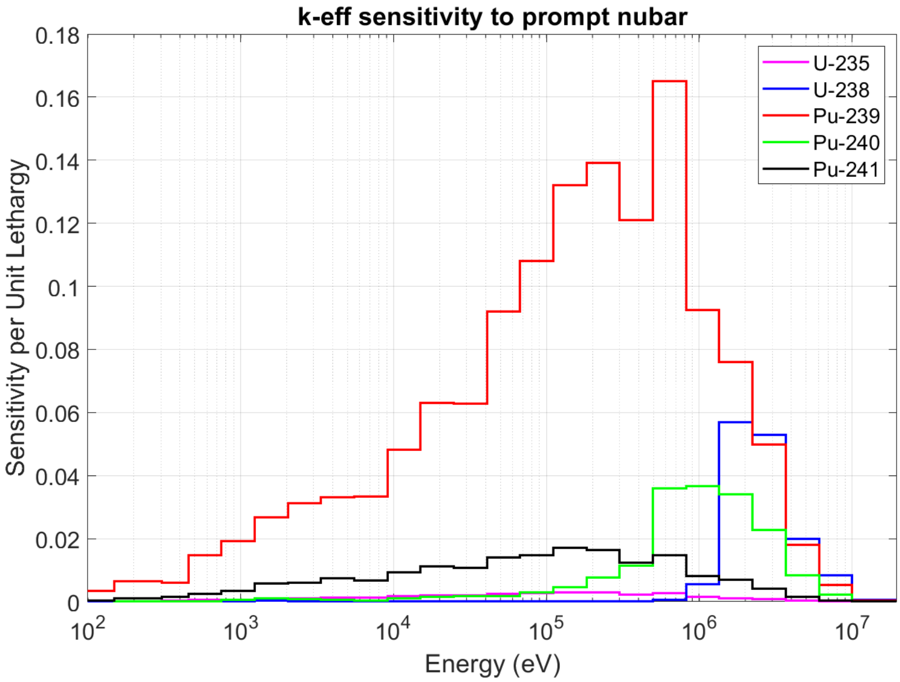

Figure 5.3: MYRRHA 1.6: k_{eff} sensitivity with respect to prompt nubar.

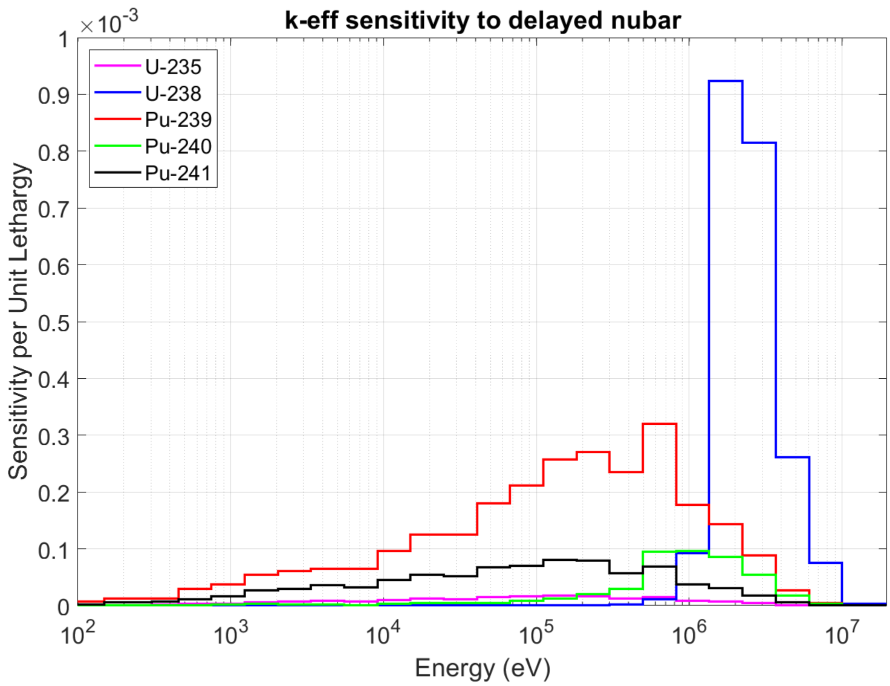

Figure 5.4: MYRRHA 1.6: k_{eff} sensitivity with respect to delayed nubar.

A negative sensitivity profile leads to a negative ISC, therefore an increment of that perturbed quantity leads to a decrease of k_{eff}. For this reason, the k_{eff} ISC to capture of ^{238}U appears with the minus sign in Table 5.1. It can be justified physically, since an increase in the radiative capture cross section (at any energy) leads to a rise probability that a neutron is removed from the system and consequently to a less number of fission events. It can be also mathematically explained, since the capture contribution can be find at denominator in the multiplication factor definition of Eq. 2.8.

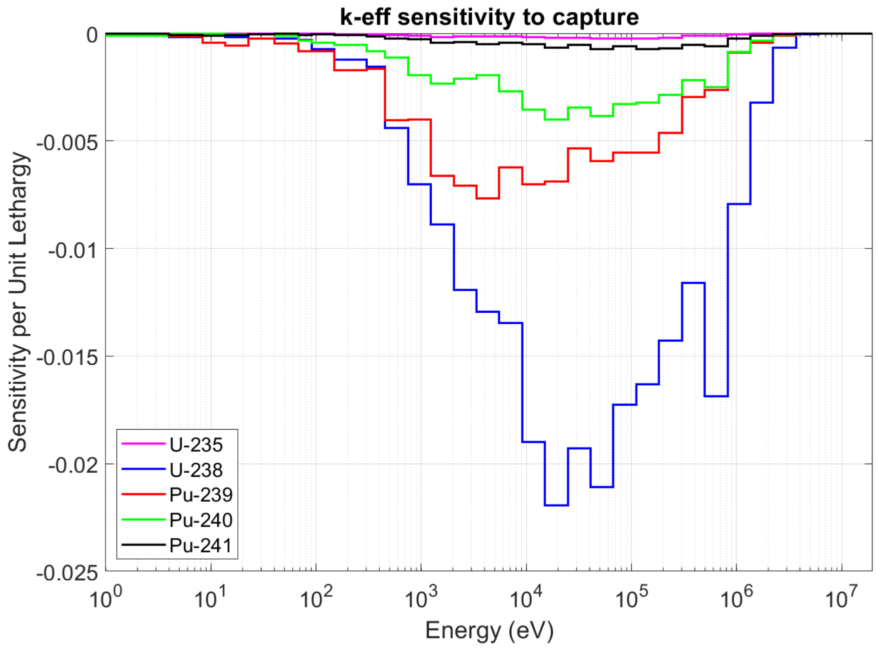

Figure 5.5: MYRRHA 1.6: k_{eff} sensitivity with respect to capture.

The absence of prompt and delayed fission spectra from Table 5.1 can be justified by its positive and negative shape profile of Fig. 5.6 which makes its integral value null. It can be demonstrate by the nature of such nuclear data, that the fission spectra is a probability density function and that its integrated value as a function of energy is equal to unity. For this reason, a positive perturbation of χ in a certain energy range must be counterbalanced by a negative perturbation in the other energy range. This is the so called constrained approach [64].

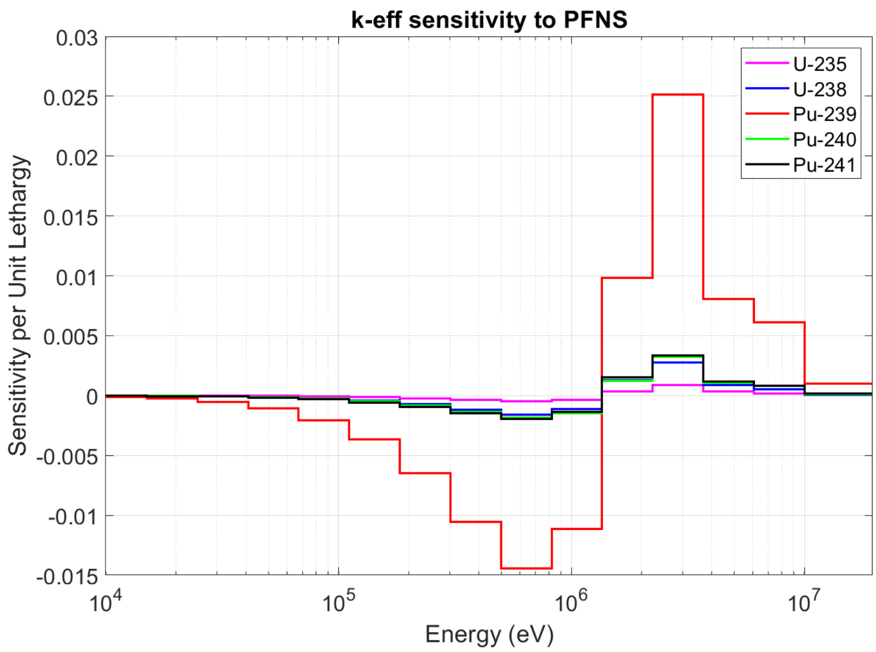

Figure 5.6: MYRRHA 1.6: k_{eff} sensitivity with respect to PFNS.

Precise sensitivity results to the elastic and inelastic scattering reactions are the most difficult ones to obtain due to the slow convergence of the sensitivity coefficient. This convergence problem occurs in particular in resonance region, where the reactions relevance changes drastically with very small changes in energy. For this reason, the ISC related to a perturbation of ^{238}U elastic scattering reaction is accompanied by one of the highest statistical error (the 2σ column). However, the high number of particles and cycles that characterize this simulation makes the statistical error very low, as can be seen from Fig. 5.7.

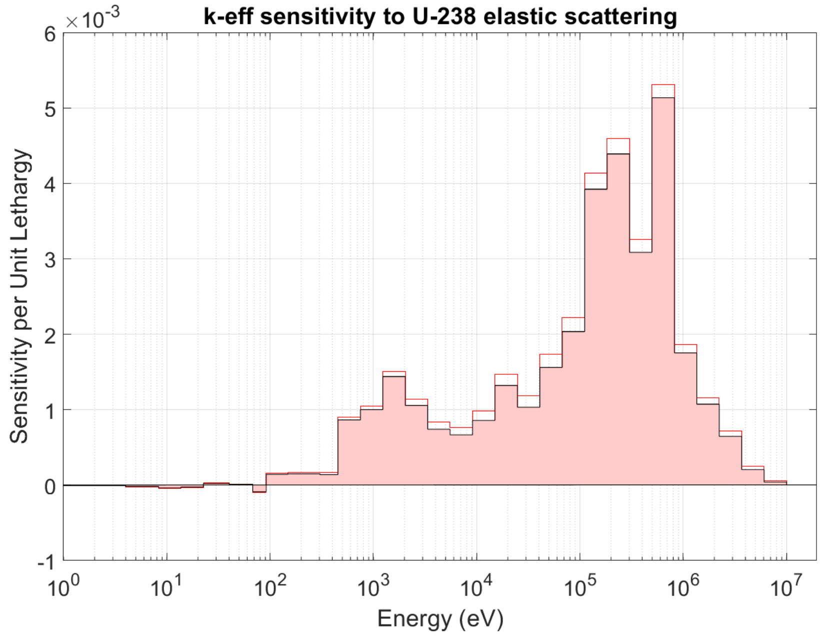

Figure 5.7: MYRRHA 1.6: k_{eff} sensitivity with respect to elastic scattering of U-238.

As expected from the nature of the reaction, the inelastic scattering shows a threshold energy also in its sensitivity profile of Fig. 5.8. Therefore the sensitivity profile becomes non-null after this energy (e.g. ^{238}U have an inelastic scattering threshold energy of 45 KeV, and it exactly falls in the first (blue) non-zero sensitivity profile step in Fig. 5.8). When neutrons undergo inelastic scatterings they lose a great amount of energy. Therefore this process removes neutrons with energies above the threshold of ^{238}U fission reaction leading to neutrons more likely to get captured than causing fast fission in the most abundant fuel nuclide. For this reason in Table 5.1 all the inelastic scattering reactions have a negative ISC.

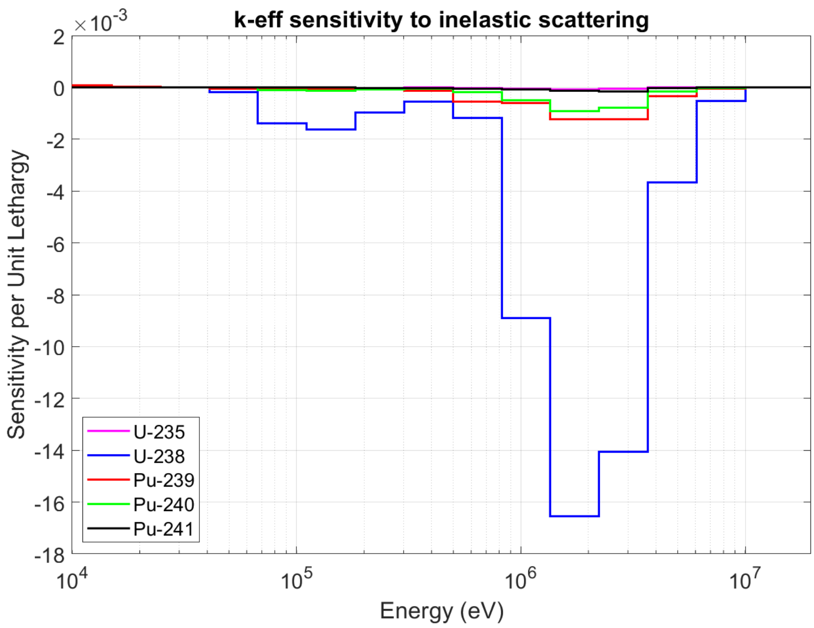

Figure 5.8: MYRRHA 1.6: k_{eff} sensitivity with respect to inelastic scattering.

The contribution of other abundant nuclides non characterizing the fuel, such as ^{209}Bi, ^{206}Pb, ^{56}Fe, is mostly relevant only for capture and scattering reactions. Same discussion as before can be done for the capture reaction that leads to a negative k_{eff} contribution. For what concerns the elastic scattering reaction, it has a positive effect especially in lead and bismuth as shown in Fig. 5.9. On the other hand, Fig. 5.10 shows that inelastic scattering is strongly negative for iron.

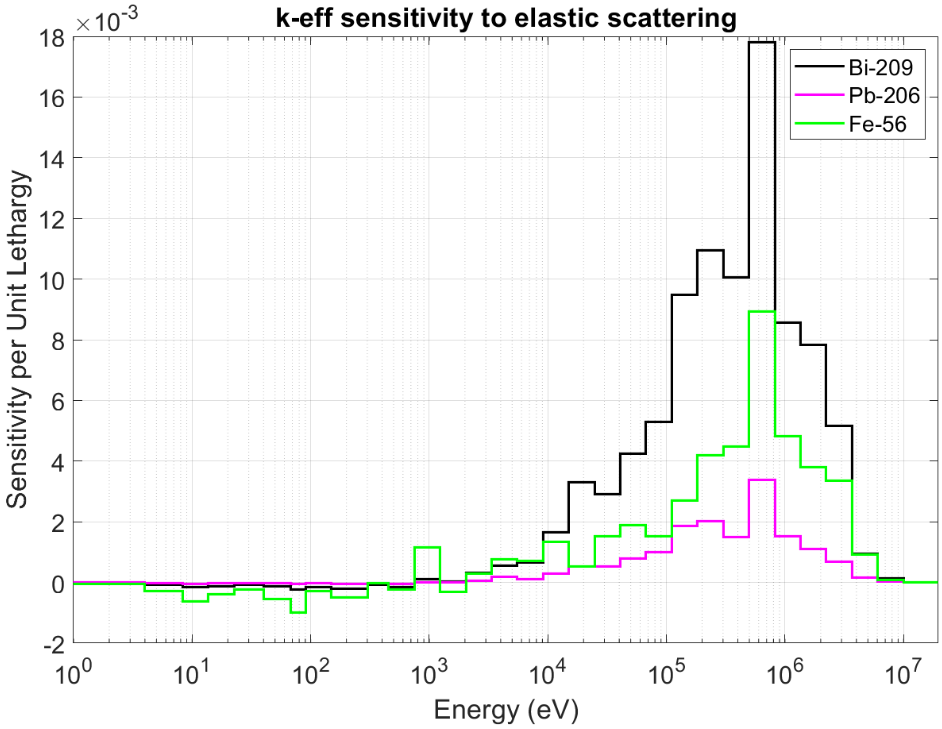

Figure 5.9: MYRRHA 1.6: k_{eff} sensitivity with respect to inelastic scattering.

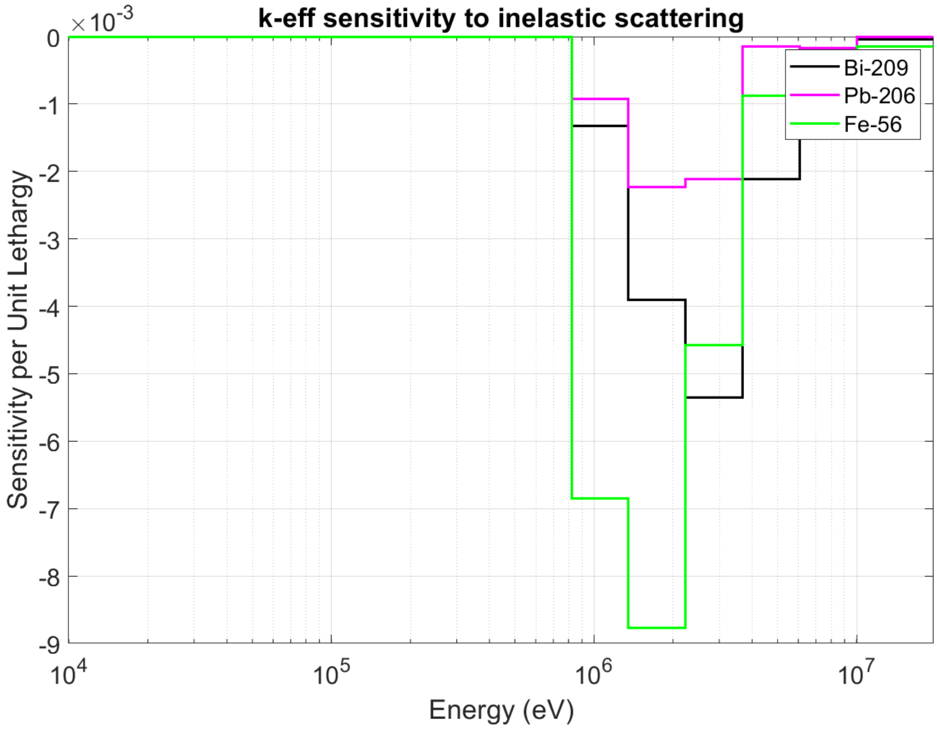

Figure 5.10: MYRRHA 1.6: k_{eff} sensitivity with respect to inelastic scattering.

5.2 Kinetic parameters

As discussed in Section 2.1.2 and 2.1.3, the kinetic parameters are the ones characterizing the discipline that studies the behavior of neutron population as function of time in a non-critical configuration, the so called reactor kinetics. Before presenting the results of the sensitivity analyses of such parameters on MYRRHA, these have been investigated before in benchmark experiments.

This intermediate step has been done to compare the results with other codes and better understand the SERPENT2 capabilities and how the user choices affect the results. This verification has been done only for kinetic parameters, because their sensitivities are more computationally intensive to calculate respect to the multiplication factor and because of the wide MYRRHA results literature that exists for k_{eff} sensitivity. The kinetic parameters analyzed as response functions are β_{eff} and Λ_{eff}. No analysis was possible for $\alpha_{\mathrm{coolant}}$ reactivity coefficient, because of the absence of coolant in the benchmark systems considered. The choice of the benchmark experiments (among all the possible options) was not random, but it can be justified analyzing them one by one.

5.2.1 Benchmarks

In general these experiments have simple geometry and a well defined material composition. These features make them easier to analyze during measurement operations of reference parameters. They are useful also for the simulation point of view, because a small number of neutron histories and short computing time are required to reach good results with low statistical errors.

Among all the possibilities, three of them were analyzed because of different similarities with MYRRHA. For each one, a brief description of the systems is presented, followed by a comparison of the SERPENT2 results with the ones found in the wide literature that characterize these experiments.

5.2.1.1 JEZEBEL

Jezebel, more properly identified as PU-MET-FAST-001, is a plutonium bare sphere used for benchmark experiments [65]. This experiment was conducted for the first time in 1954 at Los Alamos National Laboratory. The aim was to determine the critical mass of this spherical, bare (unreflected), homogeneous Pu-Ga alloy, see Fig. 5.11.

The plutonium phase with lowest density is the delta-phase. Although existing only in the range temperature of 310 − 452°C, it can be stabilized at room temperature adding gallium. This is mainly because in this phase plutonium has better metal properties than in the alpha-phase that makes it hard, brittle and more difficult for shaping operations. Apparently disadvantageous from the viewpoint of criticality, because of its lower density, the plutonium stabilized in the delta-phase actually undergoes a sudden transformation to the alpha-phase (of higher density) when submitted to strong shock compression [66].

The referred experiment for the present study is the one corresponding to 2016 reevaluation with a more detailed geometry and material composition [67]. This experiment has been chosen for two main reasons: the first one is related to the isotopes, since Jezebel is mainly characterized by ^{239}Pu, as can be seen in Table 5.2. The same plutonium isotope that with ^{238}U represent the most abundant nuclides in the MYRRHA MOX fuel. The second one can be deducted from the fast spectrum similarity that characterizes JEZEBEL and MYRRHA, showed respectively in Fig. 5.12 and 3.6.

Table 5.2: Jezebel: material composition.

Nuclide	Mass fraction
Ga	0.034
^{239}Pu	0.920
^{240}Pu	0.043
^{241}Pu	0.003

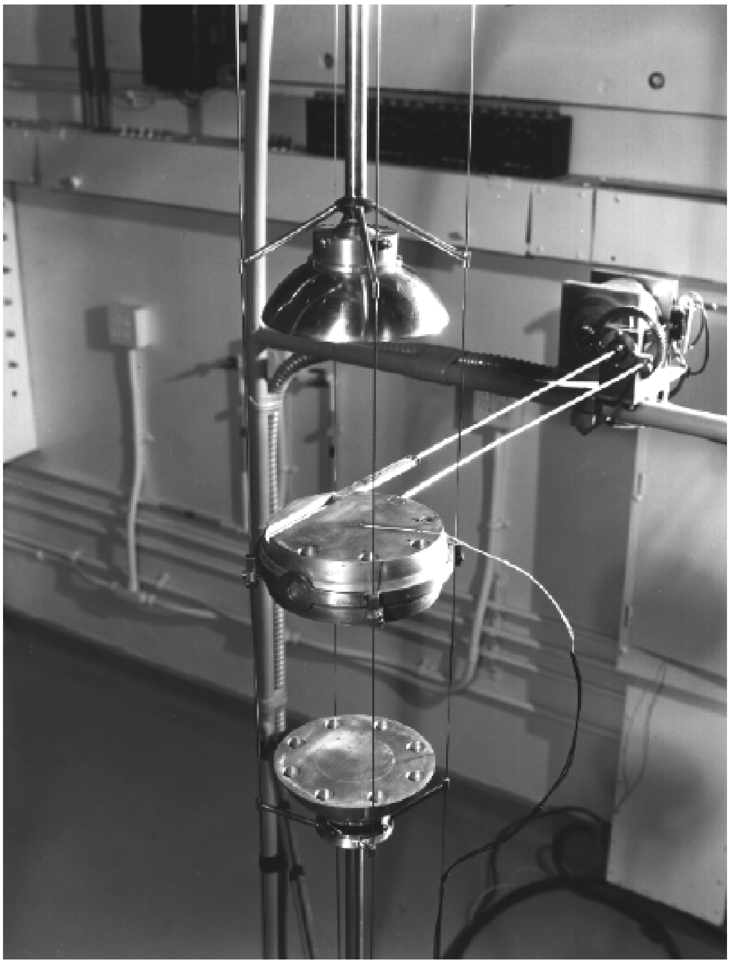

Figure 5.11: Jezebel experiment, Jan 24 1955 [67].

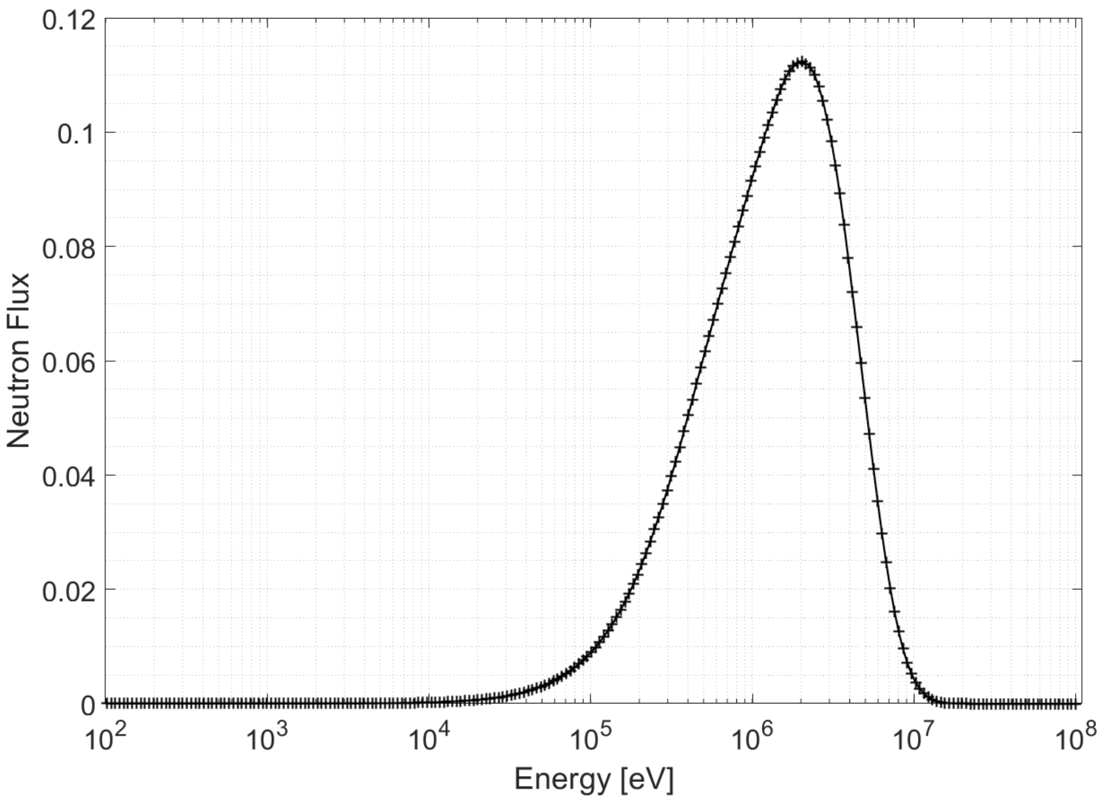

Figure 5.12: Jezebel neutron spectrum.

The sensitivity analysis has been conducted setting as main input parameters: $1e6$ particles, $2e4$ active cycles, 15 latent generations and 10 IFP cycles. With these inputs and a parallelization in the cluster with 72 CPUs, the SERPENT2 code was able to provide all the results in 25 hours, with relatively low statistical errors.

The results for β_{eff} sensitivity are presented in Table 5.3 and they are compared with the ISC obtained using the SUSD3D deterministic code in a previous study presented here [68]. The relative difference column, where the SUSD3D results has been considered as the reference value, shows a good agreement between the 2 studies. For low ISC value the relative difference are not considered, since small absolute differences led to huge relative differences, but not relevant for the present consideration.

Table 5.3: Jezebel: β_{eff} sensitivity to nuclear data.

		S_x^R (%/%)		
		JEFF-3.1.2	ENDF/B-VII.0	
Isotope	Reaction	SERPENT2	SUSD3D	Rel. Diff. (%)
^{239}Pu	$\bar{\nu}_d$	$+0.948 \pm 0.0\%$	$+0.948$	$+0.0$
^{239}Pu	$\bar{\nu}_p$	$-0.945 \pm 0.1\%$	-0.947	-0.2
^{239}Pu	(n,n)	$+0.083 \pm 4.0\%$	$+0.079$	$+5.6$
^{240}Pu	$\bar{\nu}_p$	$-0.051 \pm 0.9\%$	-0.049	$+4.6$
^{240}Pu	$\bar{\nu}_d$	$+0.043 \pm 0.4\%$	$+0.043$	$+0.0$
^{239}Pu	(n,γ)	$-0.020 \pm 1.0\%$	-0.022	$-$
^{239}Pu	(n,f)	$-0.012 \pm 13.0\%$	-0.014	$-$
^{240}Pu	(n,n)	$+0.004 \pm 16.0\%$	$+0.005$	$-$
^{240}Pu	(n,f)	$-0.003 \pm 16.0\%$	-0.002	$-$
^{240}Pu	(n,γ)	$-0.001 \pm 5.9\%$	-0.001	$-$

For what concern the second kinetic parameter, the effective prompt lifetime (l_{eff}), the results are presented in Table 5.4. It can be seen a very small statistical error and a good agreement with previous results calculated with the deterministic tool TSUNAMI-1D, that makes use of EGPT to estimate this sensitivity adopting the $1/v$ absorber method. The relative differences between the code are in the order of few percentage for most of the considered parameters, overcoming the 15% just for one reaction.

Table 5.4: Jezebel: l_{eff} sensitivity to nuclear data.

		S_x^R (%/%)		
		JEFF-3.1.2	ENDF/B-VII.0	
Isotope	Reaction	SERPENT2	TSUNAMI	Rel. Diff. (%)
^{239}Pu	(n,f)	$-0.242 \pm 0.1\%$	-0.246	-1.6
^{239}Pu	(n,n)	$+0.240 \pm 0.1\%$	$+0.230$	$+4.3$
^{239}Pu	(n,n')	$+0.162 \pm 0.1\%$	$+0.201$	-19.4
^{239}Pu	(n,γ)	$-0.035 \pm 0.1\%$	-0.037	-5.4
^{240}Pu	(n,f)	$-0.014 \pm 0.3\%$	-0.013	$+5.3$
^{240}Pu	(n,n)	$+0.013 \pm 0.5\%$	$+0.013$	$+0.0$
^{240}Pu	$\bar{\nu}_t$	$-0.011 \pm 0.3\%$	-0.010	$-$
^{239}Pu	$\bar{\nu}_t$	$-0.010 \pm 0.4\%$	-0.008	$-$
^{240}Pu	(n,n')	$+0.009 \pm 0.1\%$	$+0.008$	$-$

5.2.1.2 Popsy

Popsy (Flattop), more properly identified as PU-MET-FAST-006, is a plutonium sphere surrounded by a thick reflector of natural uranium used for benchmark experiments [69]. The experiment was originally located at the Los Alamos National Laboratory, then moved to the Nevada National Security Site where it is continuing to operate. In 2012, Popsy was used for key demonstration of the use of nuclear power for space applications in collaboration with NASA [70].

Popsy is characterized by a fast spectrum at the center of the core and a degraded spectrum in the reflector. This system is one of the benchmark critical assemblies whose characteristics have been established over a period of years. Popsy assemblies are used principally in a continued program of neutron activation and reactivity coefficient measurements [69].

This experiment has been chosen due to its material composition because of the presence of both ^{239}Pu and most importantly ^{238}U. The material mass fractions are listed in Table 5.5.

Table 5.5: Popsy: material composition.

Nuclide	Mass fraction
^{238}U	0.541
^{239}Pu	0.416
^{240}Pu	0.021
^{31}Ga	0.017
^{235}U	0.004
^{241}Pu	0.001
^{234}U	–

With respect to Jezebel, Popsy runs faster in SERPENT2 thanks to the thick reflector of natural uranium that surrounds the plutonium sphere. Therefore, good statistical errors have been reached with 5e5 particles and 2e3 active cycles in 2.5 hours. The β_{eff} sensitivity results are listed in Table 5.6. They are compared with previous results obtained using the SUSD3D deterministic code[71]. The highest relative difference found in the main sensitivity contributor reactions and nuclides is about the 10%. However, these slightly higher relative differences are affected by already high statistical errors coming from the SERPENT2 sensitivity profile.

Table 5.6: Popsy: β_{eff} sensitivity to nuclear data.

		S_x^R (%/%)		
		JEFF-3.1.2	ENDF/B-VII.0	
Isotope	Reaction	SERPENT2	SUSD3D	Rel. Diff. (%)
^{239}Pu	$\bar{\nu}_p$	$-0.869 \pm 0.4\%$	-0.879	-1.1
^{239}Pu	$\bar{\nu}_d$	$+0.576 \pm 0.3\%$	$+0.588$	-2.0
^{238}U	$\bar{\nu}_d$	$+0.372 \pm 0.4\%$	$+0.361$	$+3.0$
^{239}Pu	(n,f)	$-0.320 \pm 2.0\%$	-0.305	$+4.9$
^{238}U	(n,f)	$+0.269 \pm 1.2\%$	$+0.261$	$+3.0$
^{238}U	(n,n')	$-0.176 \pm 5.9\%$	-0.170	$+3.5$
^{238}U	$\bar{\nu}_p$	$-0.092 \pm 3.3\%$	-0.083	$+10.8$
^{238}U	(n,γ)	$-0.052 \pm 5.7\%$	-0.050	$+4.0$
^{239}Pu	(n,n')	$-0.043 \pm 14.0\%$	-0.042	$+2.4$
^{240}Pu	$\bar{\nu}_p$	$-0.043 \pm 3.4\%$	-0.043	$+0.0$
^{235}U	(n,f)	$+0.027 \pm 5.0\%$	$+0.027$	$+0.0$
^{240}Pu	$\bar{\nu}_d$	$+0.024 \pm 1.8\%$	$+0.024$	$+0.0$

The consistent behavior of SERPENT2 respect to ^{238}U sensitivity is a good point for the applications on MYRRHA. This present study has not been just conducted on the integrated sensitivity coefficient, but also to the sensitivity profiles obtained adopting an energy grid. Even in these cases pretty equal shapes have been found.

On the other hand, in Table 5.7 the results coming from the effective prompt lifetime sensitivity are listed. No comparisons can be done this time because no sensitivity coefficients have been found in literature. It resulted in a merely analysis on the statistical errors that are relatively low even with the drastic reduction in the simulated neutron histories respect to the Jezebel analysis. Once again the highest statistical errors can be found in scattering reactions.

Table 5.7: Popsy: l_{eff} sensitivity to nuclear data.

		S_x^R (%/%)
		JEFF-3.1.2
Isotope	Reaction	SERPENT2
^{238}U	(n,n)	$+0.61451 \pm 1.1\%$
^{238}U	(n,γ)	$-0.48877 \pm 0.2\%$
^{239}Pu	(n,f)	$-0.47139 \pm 0.3\%$
^{238}U	(n,n')	$-0.21826 \pm 1.0\%$
^{239}Pu	$\bar{\nu}_p$	$-0.14490 \pm 0.5\%$
^{238}U	$\bar{\nu}_p$	$+0.09963 \pm 0.5\%$
^{235}U	$\bar{\nu}_p$	$+0.07447 \pm 0.3\%$
^{239}Pu	(n,γ)	$-0.06438 \pm 0.5\%$
^{235}U	(n,f)	$+0.04507 \pm 0.7\%$
^{239}Pu	(n,n)	$-0.03976 \pm 6.3\%$
^{238}U	(n,f)	$+0.03561 \pm 1.6\%$
^{240}Pu	(n,f)	$-0.02772 \pm 1.2\%$
^{240}Pu	$\bar{\nu}_p$	$-0.02639 \pm 1.1\%$
^{235}U	(n,γ)	$-0.00707 \pm 1.3\%$
^{240}Pu	(n,γ)	$-0.00401 \pm 1.8\%$

5.2.1.3 Flattop23

Flattop23, more properly identified as U233-MET-FAST-006, is a U-233 sphere surrounded by a thick reflector of natural uranium used for benchmark experiments. It has been analyzed in order to investigate the behavior of the SERPENT2 sensitivity capabilities when natural uranium (^{235}U and ^{238}U) is either in the central sphere and in the reflector. This feature was actually not present in the previous two benchmark experiments. Table 5.8 shows the material composition.

Table 5.8: Flattop23: material composition.

Nuclide	Mass fraction
^{233}U	0.488
^{234}U	0.006
^{235}U	0.004
^{238}U	0.502

From the simulation point of view, the number of histories is the same used in Popsy for the same reason. The code execution was even faster (1.5 hours) thanks of the absence of plutonium isotopes. The contributions of ^{233}U and ^{234}U were not taken into account because of their very little presence in the MYRRHA fuel.

The β_{eff} sensitivity results are listed in Table 5.9. They are compared with the results obtained using the SUSD3D deterministic code[71].

The statistical errors and the relative differences are almost equal with the Popsy results, due to same number of histories and the presence of ^{238}U. The ^{235}U results are also very consistent, even if the percentage of this isotope in the system is little.

Table 5.9: Flattop23: β_{eff} sensitivity to nuclear data.

		S_x^R (%/%)		
		JEFF-3.1.2	ENDF/B-VII.0	
Isotope	Reaction	SERPENT2	SUSD3D	Rel. Diff. (%)
^{238}U	$\bar{\nu}_d$	$+0.283 \pm 0.4\%$	$+0.274$	$+3.3$
^{238}U	(n,f)	$+0.172 \pm 1.6\%$	$+0.167$	$+3.0$
^{238}U	(n,n')	$-0.140 \pm 5.2\%$	-0.129	$+8.5$
^{238}U	$\bar{\nu}_p$	$-0.109 \pm 2.1\%$	-0.104	$+4.8$
^{238}U	(n,n)	$+0.065 \pm 28.0\%$	$+0.075$	-13.3
^{238}U	(n,γ)	$-0.036 \pm 5.7\%$	-0.033	$+9.1$
^{235}U	(n,f)	$+0.026 \pm 6.2\%$	$+0.015$	$-$
^{235}U	$\bar{\nu}_d$	$+0.014 \pm 2.0\%$	$+0.014$	$-$

Table 5.10 shows the effective prompt lifetime sensitivity results. Since no comparison ISC results have been found, the following discussions that can be derived on the statistical errors are similar to the one addressed for POPSY.

Table 5.10: Flattop23: l_{eff} sensitivity to nuclear data.

		S_x^R (%/%)
		JEFF-3.1.2
Isotope	Reaction	SERPENT2
^{238}U	(n,n)	$+0.57993 \pm 1.1\%$
^{238}U	(n,γ)	$-0.51036 \pm 0.2\%$
^{238}U	(n,n')	$-0.23445 \pm 0.8\%$
^{238}U	$\bar{\nu}_p$	$+0.11007 \pm 0.5\%$
^{235}U	$\bar{\nu}_p$	$+0.07238 \pm 0.3\%$
^{238}U	(n,f)	$+0.04277 \pm 1.3\%$
^{235}U	(n,f)	$+0.04171 \pm 0.7\%$
^{235}U	(n,γ)	$-0.00750 \pm 1.2\%$
^{235}U	(n,n)	$+0.00397 \pm 13.0\%$
^{235}U	(n,n')	$-0.00273 \pm 5.5\%$
^{238}U	$\bar{\nu}_d$	$+0.00171 \pm 3.1\%$

5.2.2 Effective delayed neutron fraction β_{eff}

It can be said that the intermediate step to conduct kinetic parameter sensitivity calculations of benchmark experiments has led to good results. Thus the decision was to apply the SERPENT2 capabilities to perform such calculations to MYRRHA. In Table 5.11 the main energy integrated β_{eff} sensitivities are ranked in a descending order on the absolute ISC value. It can be seen that the two nuclides leading to the highest ISC are ^{239}Pu and ^{238}U, results confirmed by previous studies [24, 39].

Whereas k_{eff} and β_{eff} are different parameters governed by different physical quantities, also their Integrated Sensitivity Coefficients can be completely different. Indeed, observing the highest contributor in Table 5.11 it can be derived that the most important parameters are $\bar{\nu_p}$ and $\bar{\nu_d}$ (in k_{eff} they have little relevance).

A first interpretation of this result can be derived recalling the delayed neutron fraction β definition of Eq. 2.12. Therefore, a merely mathematical interpretation leads to positive sensitivity to $\bar{\nu_d}$ for every nuclides and a negative ones for $\bar{\nu_p}$, as shown in Fig. 5.13 and 5.14. A second interpretation comes from the definition of the number of statistical neutrons emitted per fission event $\bar{\nu}$. It can be deducted that a positive perturbation of the delayed neutrons emitted per fission event $\bar{\nu_d}$ must have a positive β_{eff} contribution at all energies, since the concentration of delayed neutrons in the system is increased thanks to the perturbation.

Table 5.11: MYRRHA 1.6: β_{eff} sensitivity ranking table.

Isotope	Reaction	Sensitivity Coeff. (%/%)	Std. dev. (2σ)
^{239}Pu	$\bar{\nu_p}$	−0.58384	±0.00199
^{239}Pu	$\bar{\nu_d}$	+0.39679	±0.00067
^{238}U	$\bar{\nu_d}$	+0.32948	±0.00064
^{238}U	(n, f)	+0.21117	±0.00148
^{239}Pu	(n, f)	−0.16736	±0.00301
^{238}U	$\bar{\nu_p}$	−0.14084	±0.00113
^{240}Pu	$\bar{\nu_p}$	−0.12852	±0.00118
^{241}Pu	$\bar{\nu_d}$	+0.12791	±0.00046
^{240}Pu	$\bar{\nu_d}$	+0.06796	±0.00034
^{241}Pu	$\bar{\nu_p}$	−0.06544	±0.00130
^{241}Pu	(n, f)	+0.06162	±0.00160
^{240}Pu	(n, f)	−0.04414	±0.00141
^{235}U	$\bar{\nu_d}$	+0.03425	±0.00024
^{242}Pu	$\bar{\nu_p}$	−0.02972	±0.00059
^{238}U	(n, n')	−0.02844	±0.00478
^{242}Pu	$\bar{\nu_d}$	+0.02806	±0.00023
^{238}U	(n, γ)	−0.02122	±0.00182
^{56}Fe	(n, n')	−0.02051	±0.00254
^{235}U	(n, f)	+0.01899	±0.00072
^{209}Bi	(n, n')	−0.01544	±0.00185
^{235}U	$\bar{\nu_p}$	−0.01397	±0.00064
^{239}Pu	(n, γ)	−0.01184	±0.00109

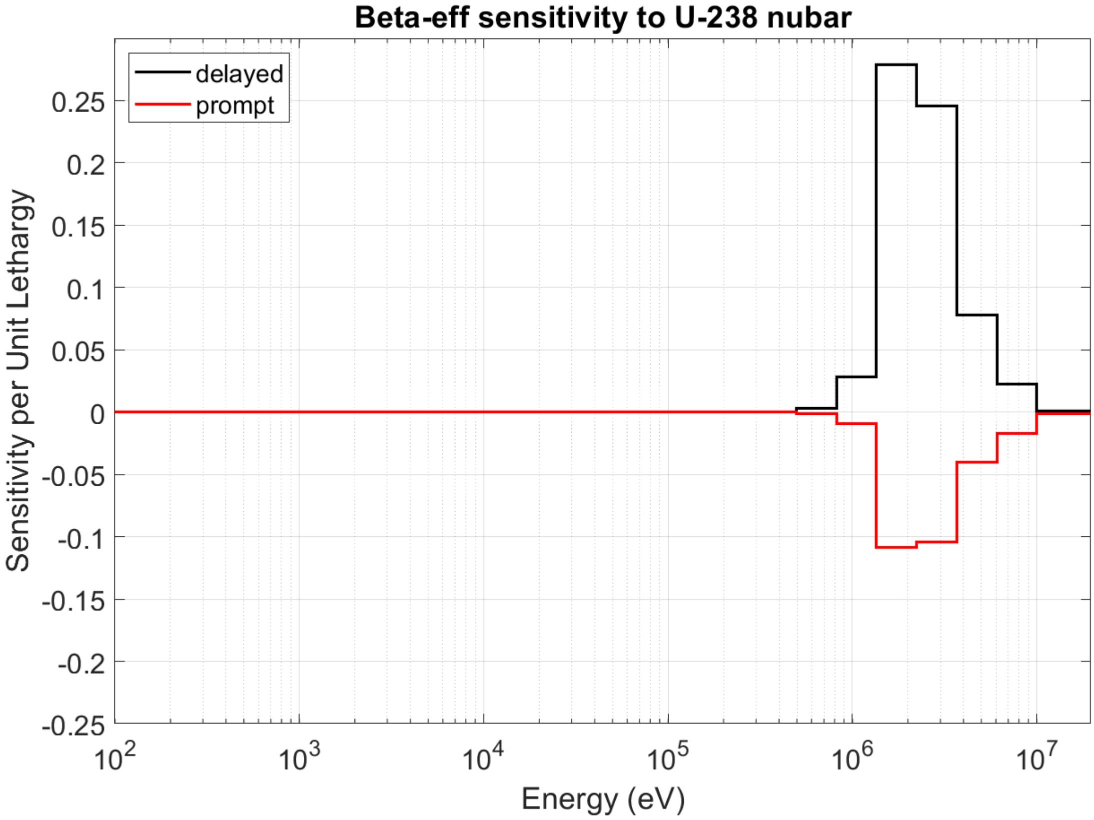

Figure 5.13: MYRRHA 1.6: β_{eff} sensitivity with respect to U-238 nubar.

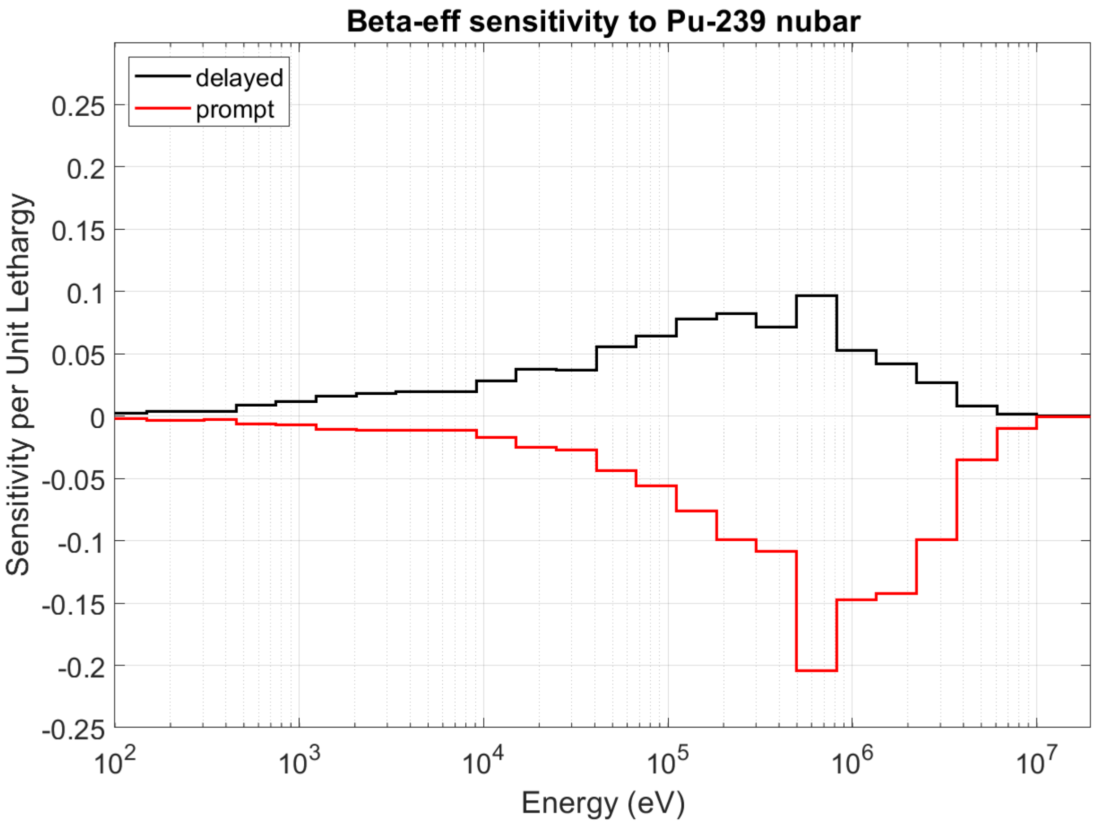

Figure 5.14: MYRRHA 1.6: β_{eff} sensitivity with respect to Pu-239 nubar.

To understand the contribution of fission cross sections perturbations to β_{eff} sensitivity, it is useful to recall that MYRRHA has $\beta_{eff} = 330$ pcm. Hence, the energy integrated sensitivities are negative for fission of isotopes with β values lower than 330 pcm (^{239}Pu and ^{240}Pu), and positive for isotopes with higher β (^{241}Pu, ^{238}U and ^{235}U). In Fig. 5.15 is possible to see profile that change their sign based on the incident neutron energy. Since ^{238}U strongly contribute only in fast region due to its threshold fission energy, every contribution for any other nuclides is small or negative in that region.

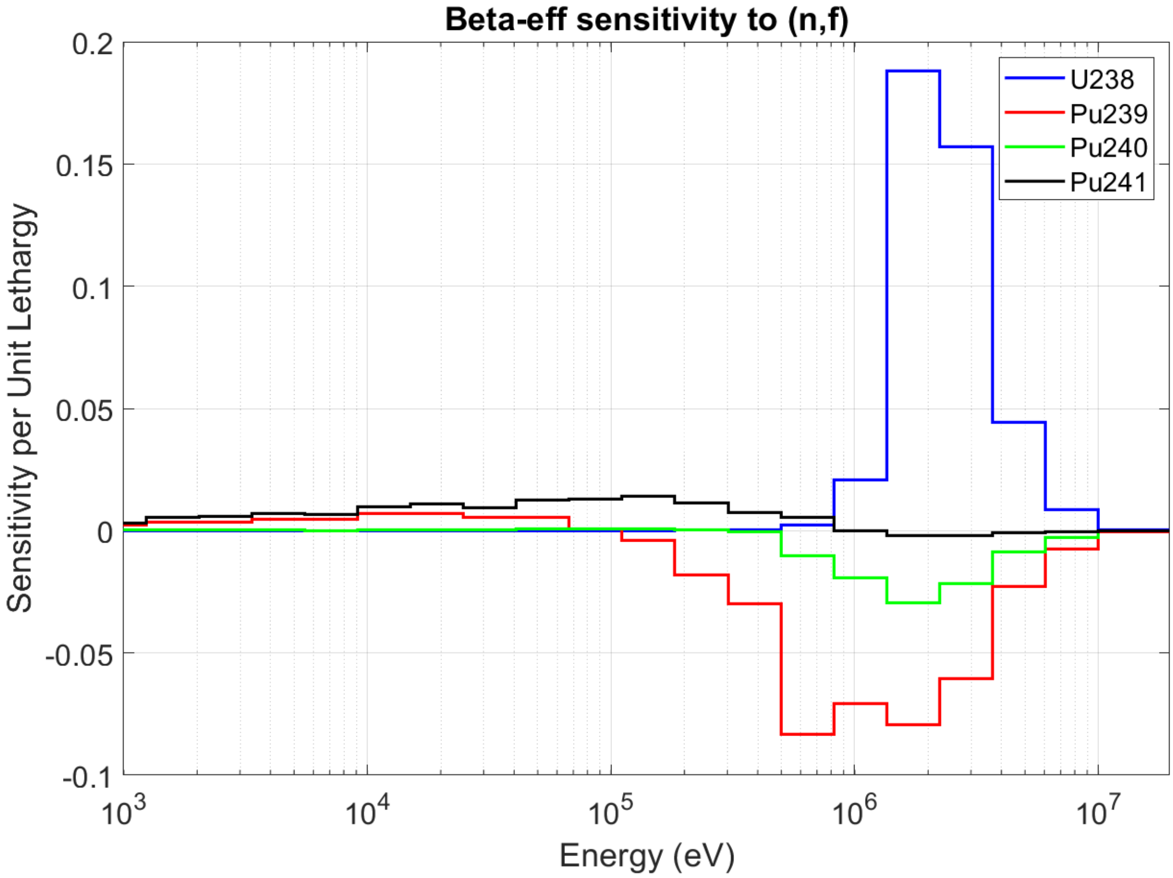

Figure 5.15: MYRRHA 1.6: β_{eff} sensitivity with respect to fission cross-sections.

The $2\,\sigma$ column of Table 5.11 is the proof that this kind of calculations are more computationally intensive compared to the k_{eff} sensitivity. They rely on the same number of simulated neutron histories but the statistical errors are in average more than 10 times higher. This fact can be seen even stronger in the scattering functions, because of the resonance region discussion of Section 5.1. From Table 5.11 it can be noticed that the inelastic scattering contribution is negative, because slow down neutrons makes the fission more likely to happen in nuclides with lower beta than ^{238}U.

For the first time in this study it is possible to observe a partial positive contribution of the capture reaction to a sensitivity profile in Fig 5.16. This can actually be understood by looking at the fission cross section spectra. In fact, this positive behavior corresponds to the peak of the ^{239}Pu fission cross section (1 MeV) [39]. Therefore, reducing the number of ^{239}Pu fissions at that energy has a positive effect on the overall β_{eff}.

In order to verify the results obtained from the discussed β_{eff} sensitivity analysis, the same outputs were obtained from another type of procedure. This comparison has been performed using the Bretscher prompt k-ratio approximation. Instead of setting as response function β_{eff}, another k_{eff} sensitivity analysis has been performed switching off the delayed neutrons. As for the mathematical derivation discussed in Section 2.1.2, β_{eff} sensitivities has been obtained. Fig 5.17 shows a good agreement between the two different methods.

With this method a further check of the results has been done. Since the Bretscher prompt k-ratio approximation has been used to analyze the MYRRHA β_{eff} sensitivities in several previous studies [39, 72], being the spatial homogenization the only difference between the present study and the other ones.

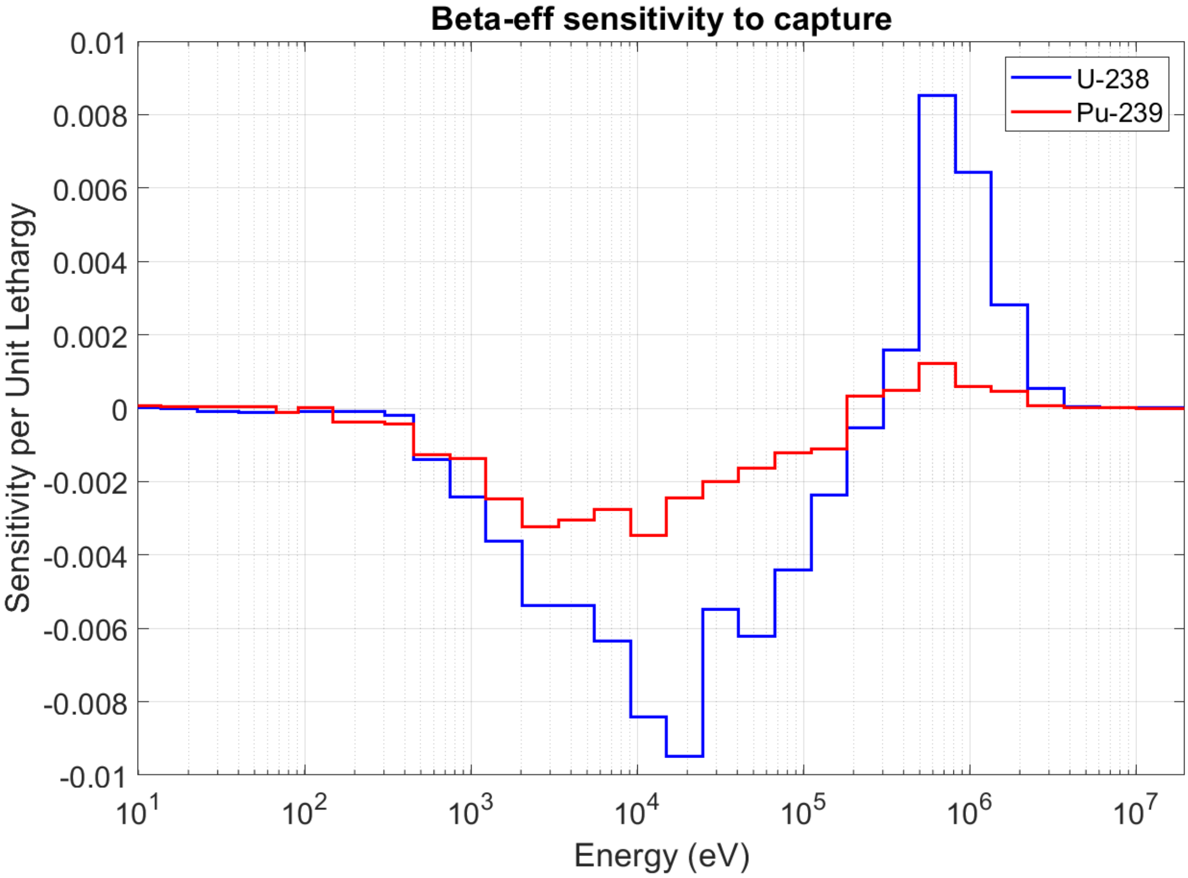

Figure 5.16: MYRRHA 1.6: β_{eff} sensitivity with respect to capture.

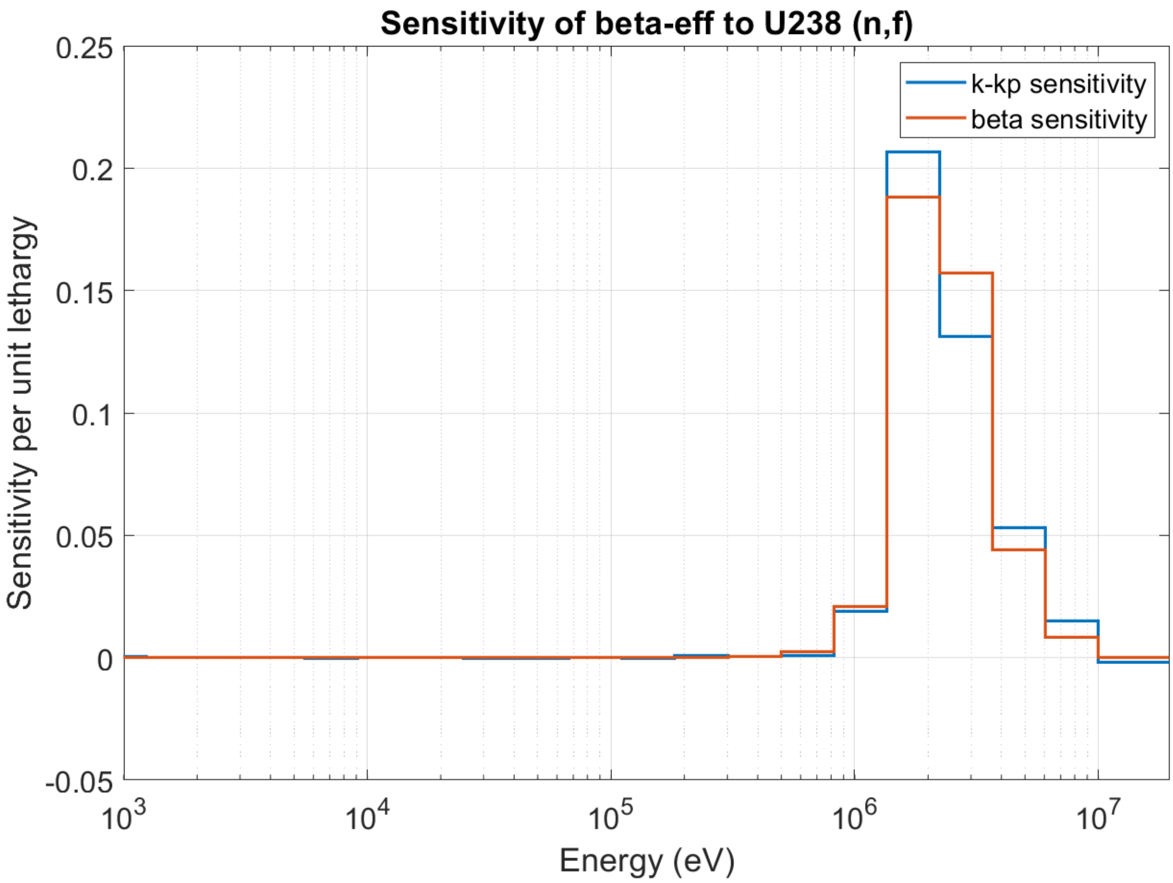

Figure 5.17: MYRRHA 1.6: β_{eff} sensitivity comparison with respect to ^{238}U fission cross-sections.

5.2.3 Effective prompt generation time Λ_{eff}

In this Section, the Λ_{eff} sensitivity results are presented. As previously discussed in Section 2.3.2.3, the Λ_{eff} sensitivity can be approximated as the l_{eff} sensitivity subtracted by the k_{eff} sensitivity. In Table 5.12 the different nuclides and their perturbed reactions are ranked in descendant order on the absolute Λ_{eff} ISC value. Since the code calculates the effective prompt lifetime sensitivity, these results have been added in Table 5.12.

Table 5.12: MYRRHA 1.6: l_{eff} and Λ_{eff} sensitivity ranking table.

		l_{eff}		Λ_{eff}	
Isotope	Reaction	Sensitivity Coeff. (%/%)	Std. dev. (2σ)	Sensitivity Coeff. (%/%)	Std. dev. (2σ)
^{239}Pu	(n,f)	-0.38736	±0.00248	-0.87083	±0.00557
^{239}Pu	$\bar{\nu}_p$	-0.08691	±0.00191	-0.76772	±0.01689
^{240}Pu	$\bar{\nu}_p$	-0.09764	±0.00104	-0.18562	±0.00197
^{238}U	$\bar{\nu}_p$	-0.09341	±0.00092	-0.16594	±0.00163
^{240}Pu	(n,f)	-0.09869	±0.00118	-0.15945	±0.00192
^{239}Pu	(n,γ)	-0.18100	±0.00101	-0.13543	±0.00076
^{238}U	(n,f)	-0.08544	±0.00106	-0.13074	±0.00162
^{238}U	(n,γ)	-0.24063	±0.00154	-0.12411	±0.00080
^{241}Pu	(n,f)	-0.01022	±0.00123	-0.07504	±0.00900
^{238}U	(n,n')	$+0.04908$	±0.00393	$+0.07387$	±0.00592
^{240}Pu	(n,γ)	-0.07754	±0.00070	-0.05493	±0.00070
^{241}Pu	$\bar{\nu}_p$	-0.04901	±0.00108	-0.04088	±0.00090
^{238}U	(n,n)	-0.02383	±0.01144	-0.04041	±0.01941
^{239}Pu	(n,n)	-0.01113	±0.00490	-0.01353	±0.00600
^{241}Pu	(n,γ)	-0.01711	±0.00031	-0.01255	±0.00023
^{239}Pu	(n,n')	$+0.00472$	±0.00142	$+0.07387$	±0.00592

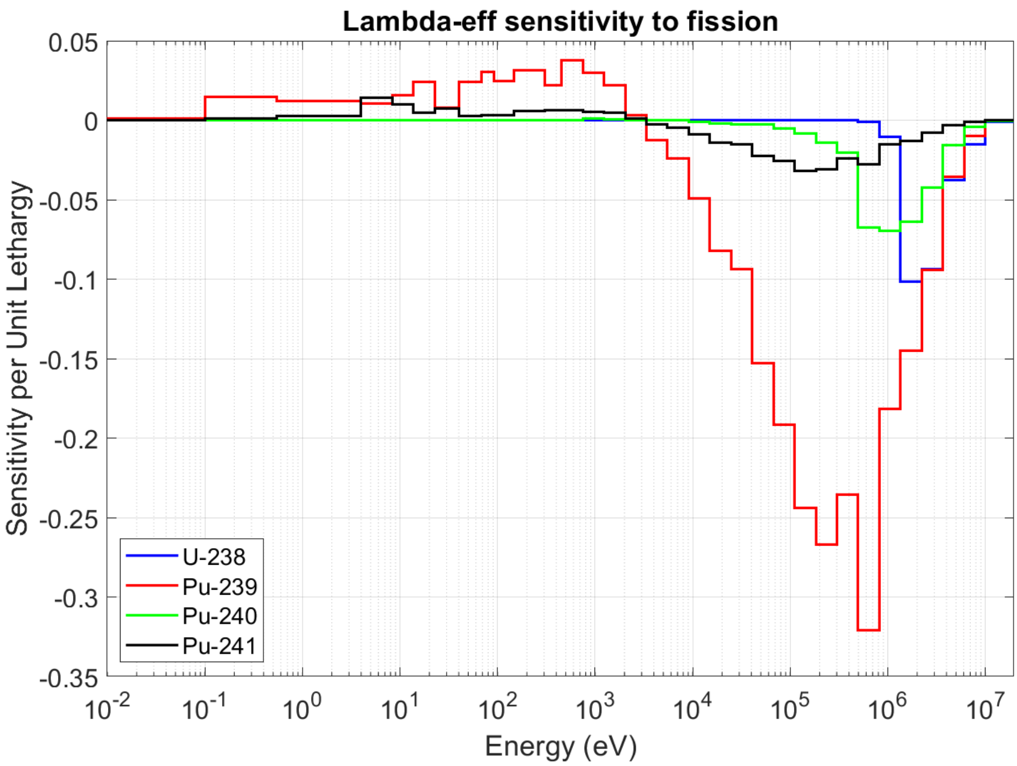

Figure 5.18: MYRRHA 1.6: Λ_{eff} sensitivity with respect to fission.

Fig. 5.18 shows that the fission contribution is negative at higher energies and null or slightly positive at lower energies. This effect can be understood from the definition of effective prompt generation time, since an enhancement in the probability to have fission at higher energies reduces the time between the birth of a neutron and the subsequent absorption inducing fission (Λ_{eff}), decreasing the number of neutrons available that induce fission at low energies.

For fissile nuclides the enhancement of the fission probability (especially in the resonance region) has a positive contribution, even if this is smaller than the negative one comprised in the fast region. The comparison between Fig 5.18 and Fig 5.19 shows a similar behavior between the two perturbed parameters contributions.

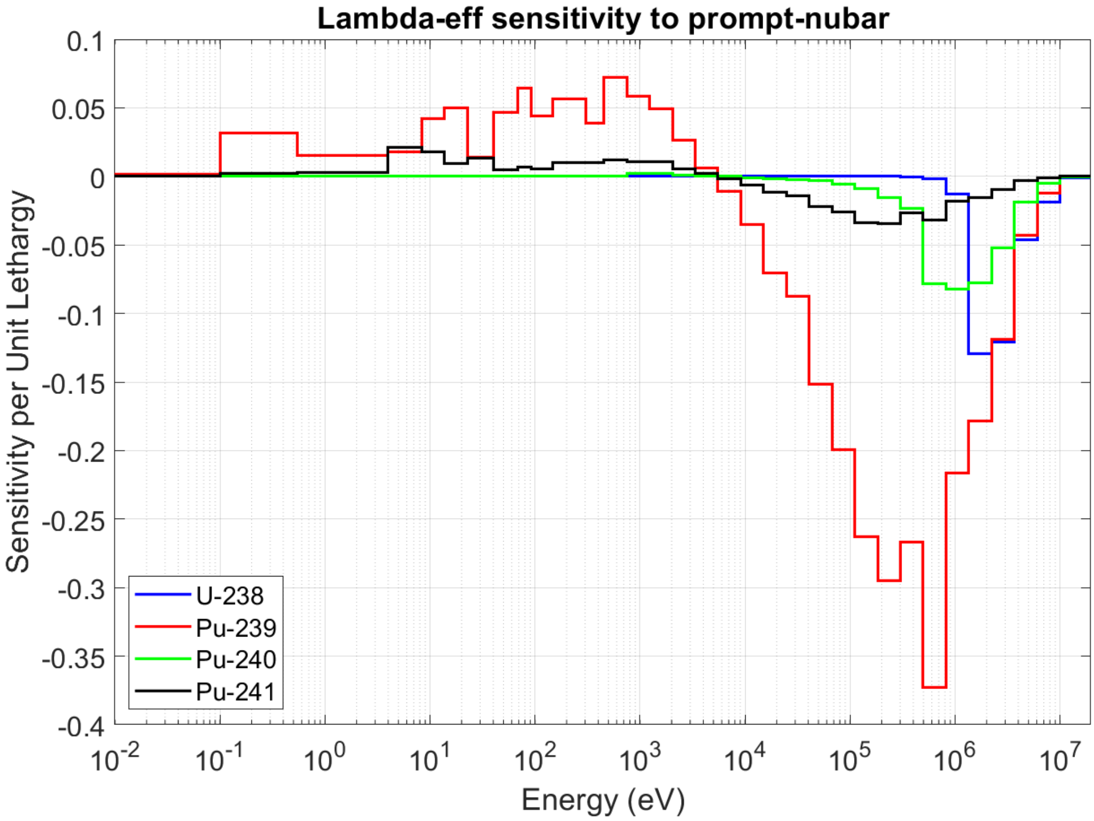

Figure 5.19: MYRRHA 1.6: Λ_{eff} sensitivity with respect to prompt-nubar.

From Table 5.12 it can be seen that capture has always a negative overall contribution. Fig. 5.20 highlights also a positive part in the fast region as found in the β_{eff} sensitivity results, however, this phenomena is different. It is straightforward that an increase of the capture cross section (in the fast region) enhances the number of neutrons captured in the system. This phenomenon increases the time that neutrons take to induce fissions because they are at lower energies and therefore lower velocity.

The negative profile of Fig. 5.20 can be explained with the predominance effect of l_{eff} sensitivity. In fact increasing the capture cross section (at that low energies) would decrease the time that neutrons take to be removed from the system, leading to a strong negative sensitivity profile for l_{eff} leading to the same effect for Λ_{eff}. In addition, even the capture k_{eff} sensitivity in that region is almost null, as can be seen in Fig 5.5.

The contribution of inelastic scattering reactions is always positive, because they are extending neutrons lifetime l_{eff} and at the same time they have a negative effect on the multiplication factor for a fast system. Fig. 5.21 shows the Λ_{eff} sensitivity profile to the inelastic scattering of ^{238}U with relatively low statistical error.

From the beginning, the aim of this study was to demonstrate the SERPENT2 sensitivity capabilities and not to find very high accurate results. For this reason, unacceptable statistical errors can be found in Table 5.12 related to elastic scattering reactions. It can be concluded that the elastic scattering ISC values of Table 5.12 are not reliable and a larger number of simulated neutron histories are needed to make the statistical error decrease.

The decision taken for this analysis was to investigate the Λ_{eff} sensitivity to fuel nuclides. However, a previous study [72] has already shown that the major contributors to Λ_{eff} sensitivity are nuclides such as ^{56}Fe, ^{16}O, ^{209}Bi, ^{206}Pb with their relevant scattering reactions.

Sensitivity to PNFS largely depends on the nuclides and are very different for thermal and fast reactor systems [64]. As can be seen from Fig 5.22, their Integrated Sensitivity Coefficient is always null because of the balanced positive and negative profile. From the discussions made before and the MYRRHA fast spectrum, it is straightforward that they should have the positive part at lower energies.

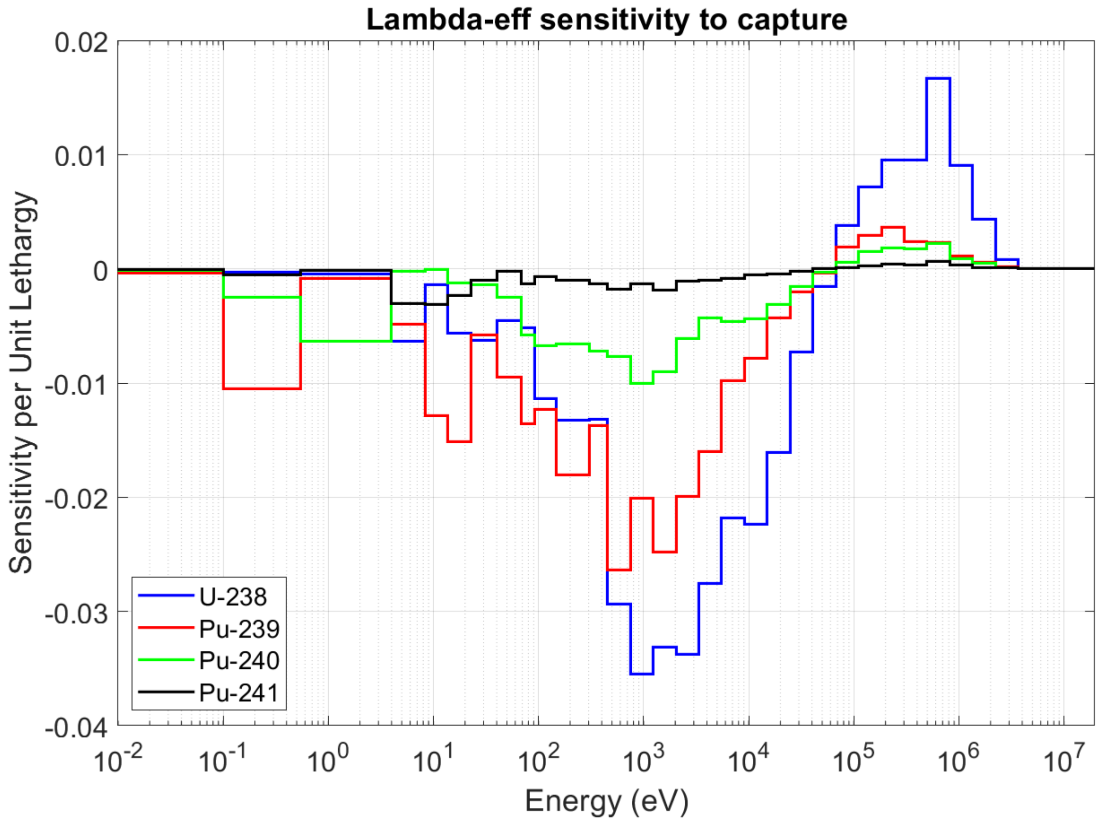

Figure 5.20: MYRRHA 1.6: Λ_{eff} sensitivity with respect to capture.

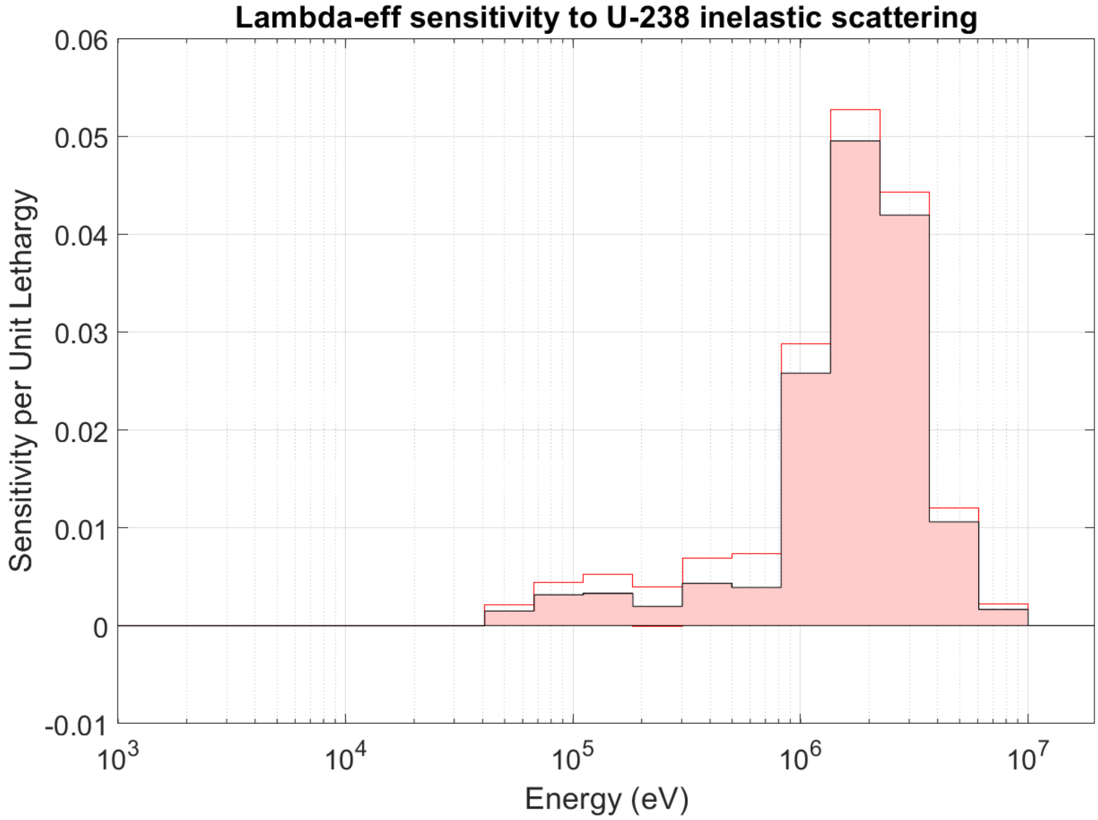

Figure 5.21: MYRRHA 1.6: Λ_{eff} sensitivity with respect to ^{238}U inelastic scattering.

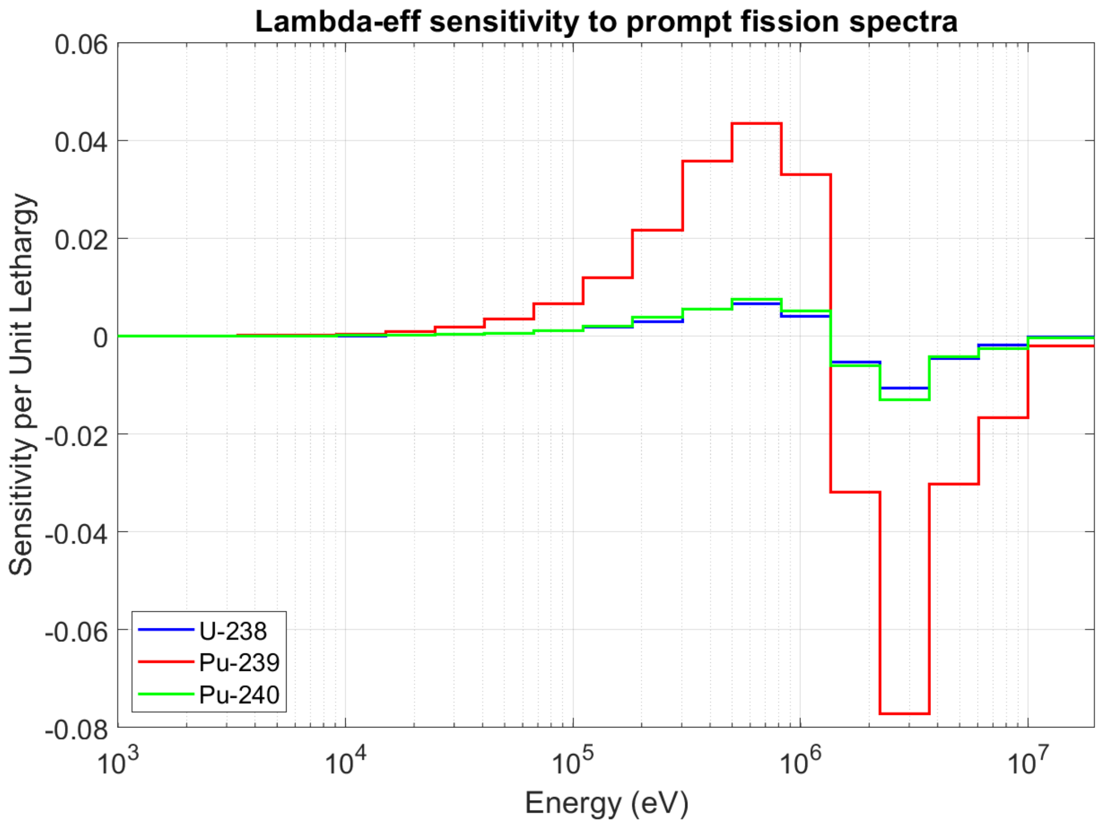

Figure 5.22: MYRRHA 1.6: Λ_{eff} sensitivity with respect to prompt fission neutron spectra.

5.3 Void coefficient α_{coolant}

As stated in Section 2.3.2.4, with a k_{eff} sensitivity analysis is also possible to directly calculate the value of the reactivity coefficient α_{coolant}. This calculation has been done in order to further integrate all the results obtained from the different void injection scenarios conducted in Chapter 4. The results are summarized in Fig. 5.23.

It can be concluded that different void analyses have been performed using three distinct methods.

- *Decreasing Coolant Density*: this method consists in decreasing the 0-1-5-20-50-100 % of the coolant density in the so called "Black Zone" defined in Section 4.1.1.2. The void formation with this technique is homogeneous and it is indicated by the red circles in Fig. 5.23.

- *Sensitivity* analysis discussed in Section 2.3.2.4: it calculates the value of α_{coolant} expressed as the variation in reactivity caused by the 1 % of volume void in the "Black Zone". Represented with the green point.

- *Voiding the core* heterogeneously, starting from the coolant around the central IPS, going up to the second ring with an axially height of 34 cm that defines the "Worst Zone". The results from this analysis are the one explained in Section 4.1.1.2. They are represented by the blue color in Fig. 5.23.

The first point on the abscissa corresponds to the nominal case (the no void condition) and it is signed by the colors red and blue since it can be reproduced in both analyses. The same can be done with the calculation of the full void case, corresponding to the 100 % of void.

Fig. 5.23 shows that a linear correlation is a good approximation for the *Decreasing Coolant Density* method. It is stressed that these results are valid only in the "Black Zone". Therefore, performing such analysis on the total volume of LBE present in MYRRHA should led to different results, since the volume of LBE in the fuel active zone corresponds only to the 1 % of the total volume of LBE. An advantage of this method is the possibility to run only 1 simulation and to deduct all the results corresponding to other percentage of voided volumes with a linear correlation.

From the zoom presented in Fig. 5.23, it is possible to compare the results from two different methods that can calculate the reactivity insertion caused by the 1% of void volume scenario. Different calculation methods bring to the exact value (α_{coolant}). It derives from the fact that in both calculations this condition has the same meaning. Therefore, even if it is calculated with different methods, respectively *Decreasing Coolant Density* and the *Sensitivity* approach led to the same result (within the statistical error σ).

For what concerns the *Voiding the core* method, Fig. 5.23 shows that it leads to higher estimations of reactivity because the void injection starts from the center (where the neutron flux is higher) and propagates radially outwards. In fact, it can be seen from Fig. 5.23 that at the 20 % of void volume condition, the *Decreasing Coolant Density* and *Voiding the core* method lead to different results, because the first methods accounts for a homogeneous void of 20 % in the "Worst Zone", while in the second technique the 20 % of void volume is located in the center of the "Black Zone".

As Fig. 5.23 pointed out, three different methods bring to similar results. It can be concluded that in a first rough analysis, just one calculation is needed and all the other behaviors can be deducted from this.

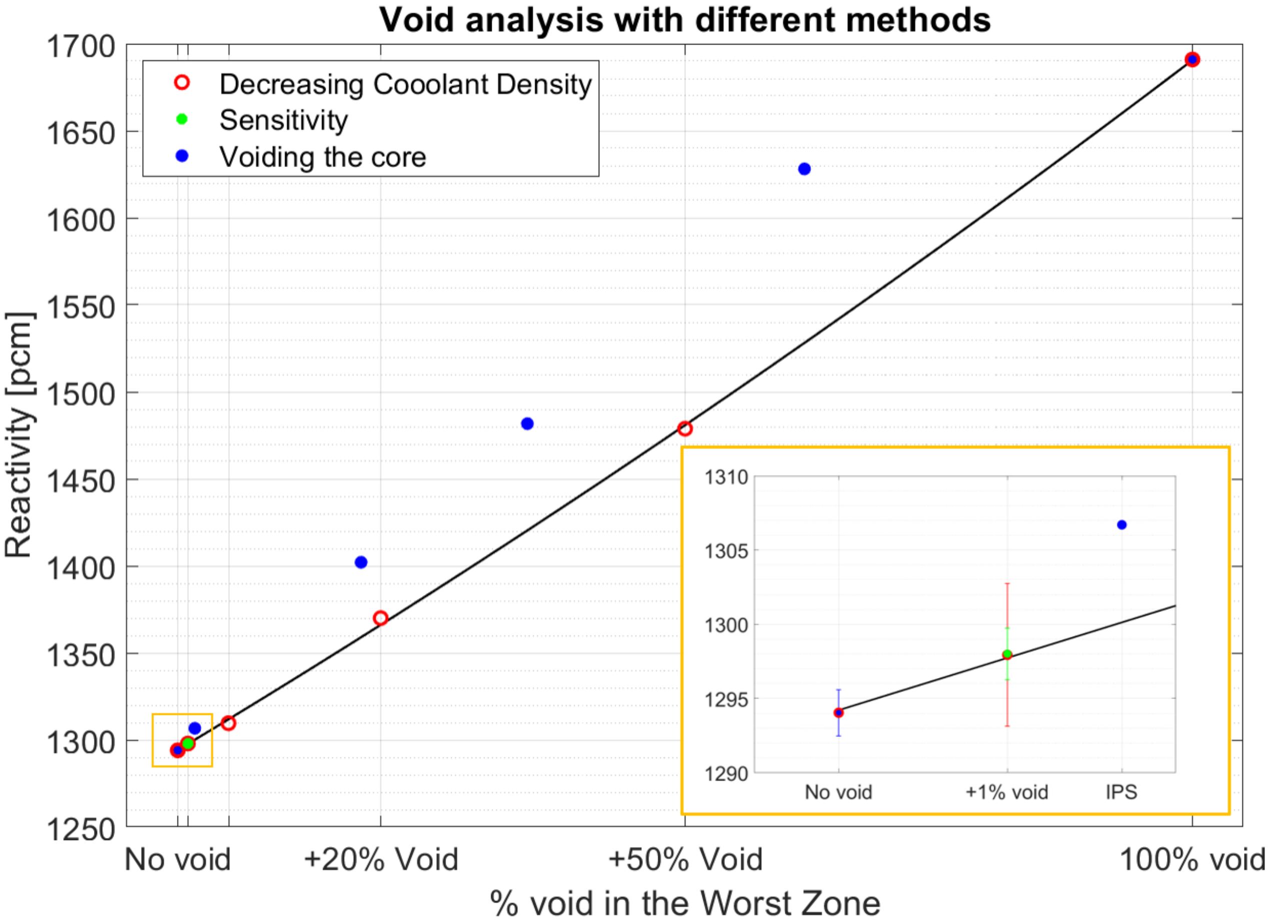

Figure 5.23: MYRRHA 1.6: effects of different void analyses.

5.4 Doppler coefficient α_{Doppler}

Same discussion can be done for the second reactivity coefficient α_{Doppler}. A k_{eff} sensitivity calculation was performed to calculate the Doppler coefficient.

The perturbed parameters of interest are three different ^{239}Pu cross sections: fission, capture and elastic scattering. The reference fuel operational temperature used in this study is 1300 K. These cross sections were broadened at three different temperatures: 1301 K, 1320 K, 1350 K in order to investigate how the Doppler coefficient evolves when the temperature continues to increase.

The Integrated Sensitivity Coefficients coming from the k_{eff} sensitivity analysis are listed in Table 5.13. A quite linear behavior profile have been found, but this should be caused by the XGPT implementation. Because it relies on first-order (linear) perturbation theory, while the temperature effect on the cross section is quite non linear, more precisely logarithmic as discussed in section 2.1.5. In Table 5.13 the Doppler coefficients related to these perturbations are calculated from Eq. 2.39.

Fig. 5.24 shows the behavior of the reactivity variation as function of the ^{239}Pu temperature. The two different effects discussed in section 2.1.5 can be distinguished: a first effect is the increase in neutron capture by fuel nuclides leading to a negative reactivity contribution. The second one is the enhancement in neutron production from fissile nuclides that brings to a positive reactivity insertion.

Table 5.13 highlights higher statistical errors when elastic scattering reactions are accounted, an ordinary situation in all the analyses conducted. This analysis was carried out with 1.5e5 particles and 1e3 active cycles leading to a smaller numbers of simulated neutron histories respect to other analyses, mainly because in this type of calculations the required memory and the computing time are much higher.

Table 5.13: MYRRHA 1.6: k_{eff} ISC for $1K$ temperature perturbation and relative Doppler coefficients.

Isotope	Reaction	Sensitivity Coeff. (%/%)	Std. dev. (2σ)	α_{Doppler} $[pcm]$
^{239}Pu	(n, f)	$+2.41\,e^{-6}$	$\pm1\,e^{-8}$	$+318$
^{239}Pu	(n, γ)	$-1.35\,e^{-6}$	$\pm2\,e^{-8}$	-178
^{239}Pu	(n, n)	$-1.72\,e^{-6}$	$\pm3.8\,e^{-7}$	-226

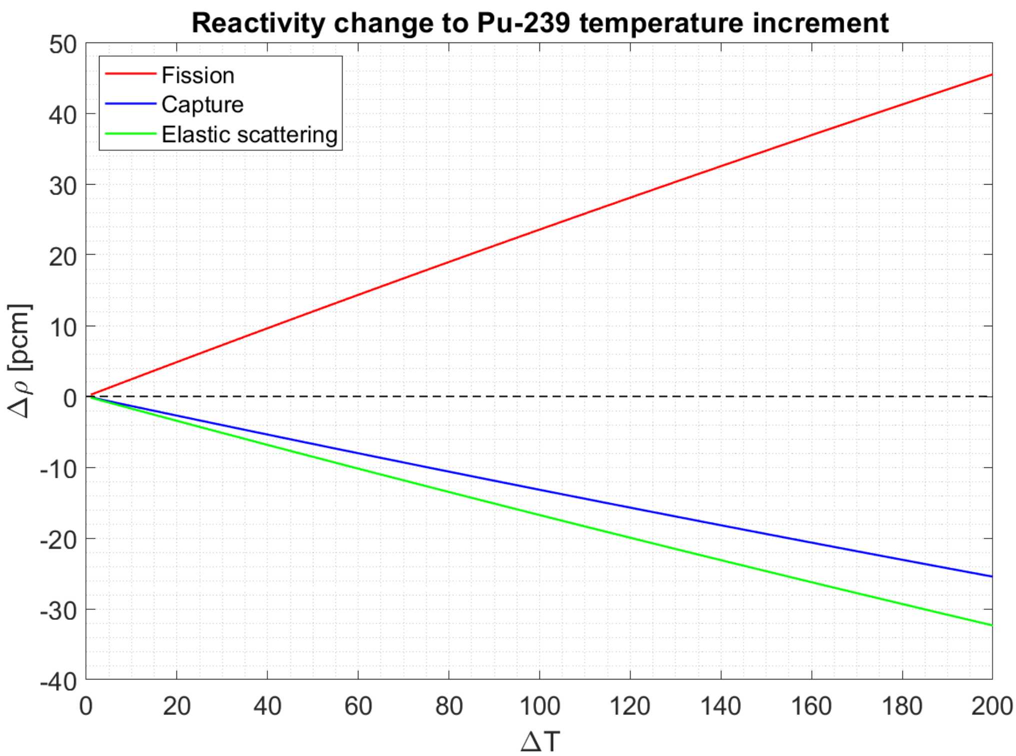

Figure 5.24: MYRRHA 1.6: Doppler effect to different temperature perturbation.

5.5 Worst condition

The sensitivity analysis can be used to rank which nuclear parameter data has the greatest impact on the selected response functions. Moreover, sensitivity analysis can also be used to estimate the main contributors of a reactivity insertion due to e.g. accidental scenario. In the present study, this feature is used to rank the contribution of different nuclear parameters to the positive reactivity insertion related to the *worst condition* respect to the MYRRHA reference scenario. Since the worst condition discussed in Section 4.1.1.2 is an accidental condition linked to a void injection in the core, this enables the opportunity of performing sensitivity analysis to nuclear data on the reactivity effects due to void presence in LBE.

In Table 5.14, the column *nominal* and *worst* indicate the k_{eff} Integrated Sensitivity Coefficients respectively for the nominal case (without void injection) and the worst condition (when the void substitutes LBE up to the second ring, with a total height of 34 cm formed symmetrically from the center of the core).

The Rel. Diff. column indicates the relative difference calculated from Eq. 5.1, taking as reference value the nominal condition:

$$\text{Rel. Diff.} = \frac{S_{worst} - S_{nominal}}{S_{nominal}} \times 100 \tag{5.1}$$

from this definition it derives that a parameter with a positive Rel. Diff. when the void injection occurs increased its relevance. Therefore a positive perturbation of such parameter causes a higher growth (or lower reduction) in k_{eff} in the worst condition than in the reference one. On the opposite, a negative Rel. Diff. value indicates that if the parameter is positively perturbed it causes a lower growth (or higher reduction) in k_{eff} in the worst condition respect to the one created in the reference one.

As stated in Section 4, the void injection in the worst condition causes a positive insertion of reactivity up to +398 pcm respect to the reference system. Combining the results from the k_{eff} sensitivity analysis conducted on the nominal and on the worst condition it is possible to attribute a contribution (in pcm) of this reactivity insertion to each nuclide and reaction. A more detailed discussion can be found in [72].

In the following, the mathematical derivation of that study has been reported. $\rho_{1\to2}$ represents the change in reactivity associated to the change in the system from state 1 (the nominal case) to state 2 (the worst condition):

$$\rho_{1\to2} = \rho_2 - \rho_1 = \frac{1}{k_1} - \frac{1}{k_2} \tag{5.2}$$

where k is the multiplication factor. It derives that $S_{\rho_{1\to2},\alpha}$ is the sensitivity coefficient of the reactivity related to the perturbation $\partial\alpha$:

$$S_{\rho_{1\to2},\alpha} = \frac{\partial\rho_{1\to2}}{\rho_{1\to2}}\frac{\alpha}{\partial\alpha} = \frac{\alpha}{\rho_{1\to2}}\left(\frac{\partial(1/k_1)}{\partial\alpha} - \frac{\partial(1/k_2)}{\partial\alpha}\right) = \frac{\frac{1}{k_1}S_{1,\alpha} - \frac{1}{k_2}S_{2,\alpha}}{\rho_{1\to2}} \tag{5.3}$$

since the sensitivity coefficient is defined in term of relative changes, to calculate the reactivity contribution for each nuclide and reaction normalized on the perturbation $\partial\alpha$, their sensitivity coefficients have been multiplied to the total change in reactivity:

$$\Delta\rho = S_{\rho_{1\to2},\alpha}\,\rho_{1\to2} = \left(\frac{1}{k_1}S_{1,\alpha} - \frac{1}{k_2}S_{2,\alpha}\right)10^5 \quad [pcm] \tag{5.4}$$

this value is present in the last column of Table 5.14 and the different reactions are ranked based on the absolute $\Delta\rho$ value. The meaning of $\Delta\rho$ can be better understand assuming the condition in which all sensitivity coefficient for all nuclides and reactions are known for the nominal and worst conditions. It derives that the sum of all the different reactivity contributions $\Delta\rho$ would lead to $\rho_{1\to2}$.

Table 5.14 shows the results of the sensitivity analyses and the reactivity contributions to the total increase of 398 pcm. The signs and the magnitude of the results are consistent with the reaction rate ones presented in Section 4.1.1.1. E.g. the prompt nubar and fission cross section of all the analyzed fissile nuclides have a negative contribution (because of the hardest flux in the core central region where the loss of LBE severely reduces the neutron moderation), while a positive trend can be found in fissionable nuclides for the same reactions. The absence of elastic scattering reactions from Table 5.14 is justified by their too high statistical error values on ISC, higher than the absolute difference between the two sensitivities.

Table 5.14: MYRRHA 1.6: reactivity contribution ranking table.

Isotope	Reaction	ISC Nominal	ISC Worst	Rel. Diff. [%]	$\Delta\rho$ [pcm]
^{239}Pu	$\bar{\nu_p}$	+0.68081	+0.67638	−0.65	−706
^{239}Pu	(n,f)	+0.48347	+0.47993	−0.73	−540
^{238}U	(n,γ)	−0.11652	−0.11430	+1.91	+264
^{241}Pu	$\bar{\nu_p}$	+0.08988	+0.08887	−1.12	−135
^{240}Pu	$\bar{\nu_p}$	+0.08798	+0.08935	+1.56	+100
^{238}U	$\bar{\nu_p}$	+0.07254	+0.07628	+5.16	+339
^{241}Pu	(n,f)	+0.06482	+0.06403	−1.22	−103
^{240}Pu	(n,f)	+0.06077	+0.06162	+1.40	+59
^{239}Pu	(n,γ)	−0.04557	−0.04461	+2.11	+112
^{238}U	(n,f)	+0.04530	+0.04756	+4.99	+204
^{238}U	(n,n')	−0.02479	−0.02605	−5.08	−114
^{240}Pu	(n,γ)	−0.02262	−0.02223	+1.72	+47
^{235}U	$\bar{\nu_p}$	+0.01993	+0.01972	−1.05	−29
^{235}U	(n,f)	+0.01292	+0.01277	−1.16	−29
^{209}Bi	(n,n')	−0.00681	−0.00503	+26.14	+178
^{241}Pu	(n,γ)	−0.00456	−0.00449	+1.54	+9
^{209}Bi	(n,γ)	−0.00301	−0.00251	+16.61	+50
^{206}Pb	(n,n')	−0.00281	−0.00209	+25.62	+72
^{239}Pu	(n,n')	−0.00214	−0.00232	−8.41	−17
^{206}Pb	(n,γ)	−0.00161	−0.00133	+17.39	+28

The following graphs show the behavior of such sensitivity profiles, where the worst condition (red) is compared to the nominal one (blue). Fig. 5.25 shows that fission of ^{239}Pu becomes more relevant at higher energies (the void leads to high energy neutrons, therefore more fast fissions). This effect is counterbalance with higher magnitude by the reduction of relevance at lower energies, leading to an overall negative $\Delta\rho$.

The opposite behavior can be seen in Fig. 5.26, since ^{238}U presents a fission energy threshold. It is subjected by the same consideration as ^{239}Pu, but ^{238}U is not affected to the negative contribution at lower energies, leading to an overall positive $\Delta\rho$.

For what concern lead and bismuth, their volumetric reduction caused by the void injection brings to a lower relevance for their sensitivity point of views. It can be seen in Fig. 5.27 and 5.28, where the blue lines are higher (in absolute term) respect to the red ones at each energies. However, since a reduction of capture reactions has a positive effects to the multiplication factor, these reactions has an overall positive reactivity contribution $\Delta\rho$.

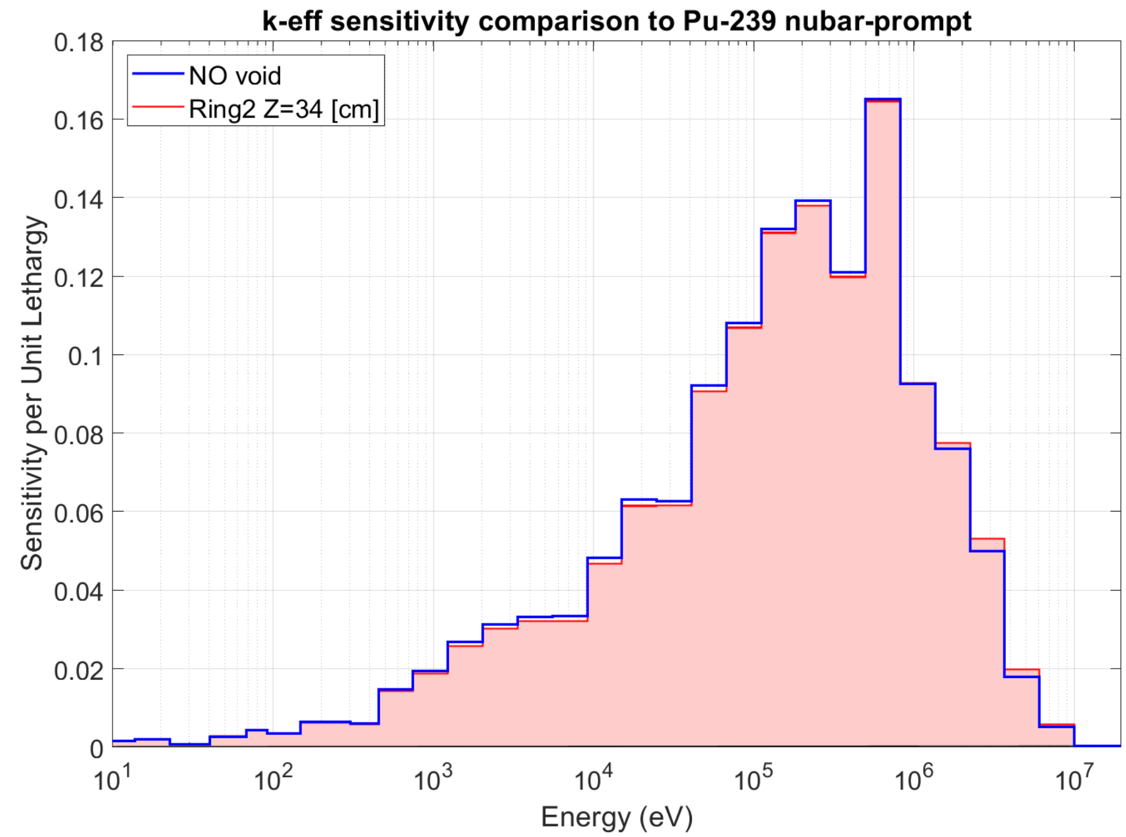

Figure 5.25: MYRRHA 1.6: k_{eff} sensitivities comparison with respect to ^{239}Pu nubar prompt.

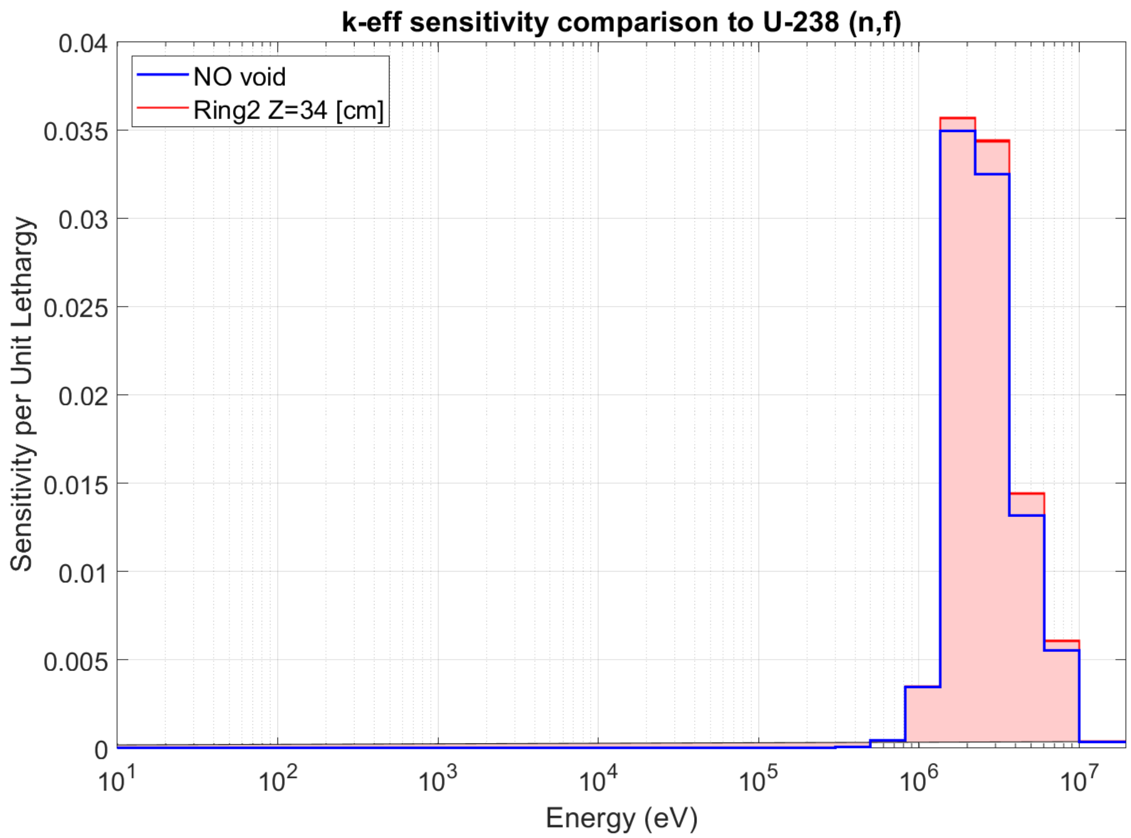

Figure 5.26: MYRRHA 1.6: k_{eff} sensitivities comparison with respect to ^{238}U fission.

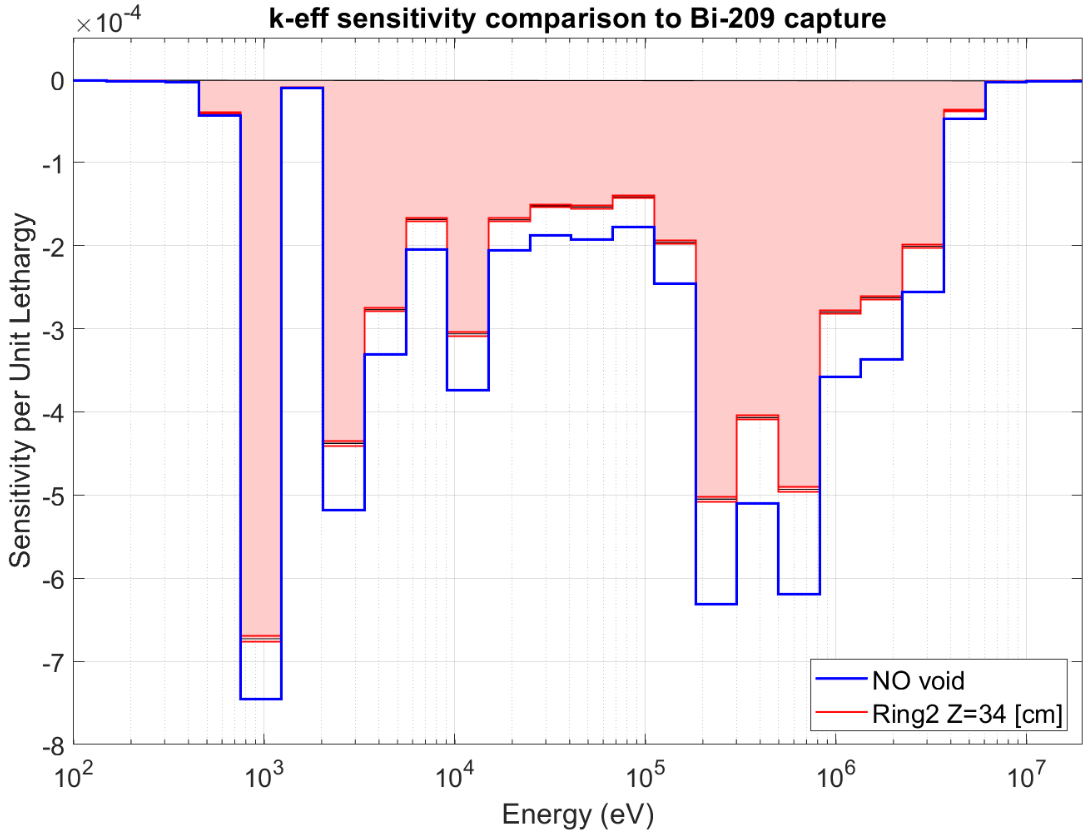

Figure 5.27: MYRRHA 1.6: k_{eff} sensitivities comparison with respect to ^{209}Bi capture.

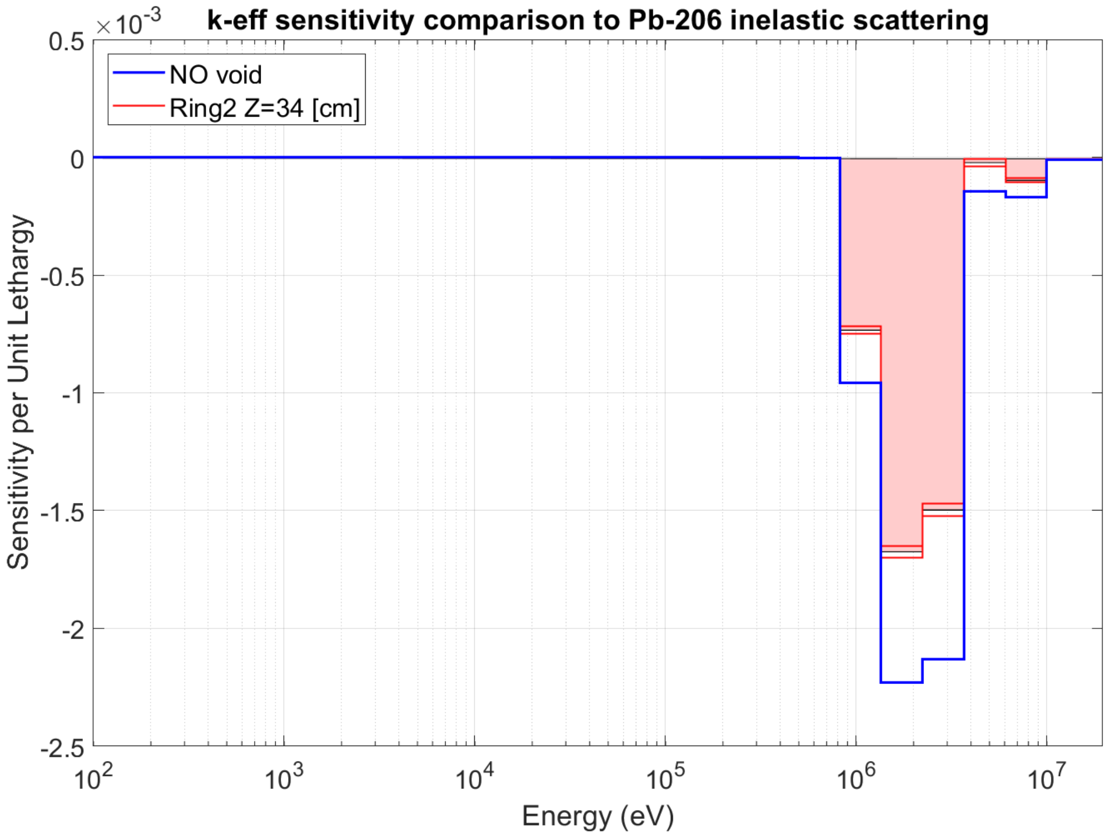

Figure 5.28: MYRRHA 1.6: k_{eff} sensitivities comparison with respect to ^{206}Pb inelastic scattering.

Chapter 6

Conclusions

This Master's thesis presents the study on different applications of the SERPENT2 Monte Carlo code to the new concept pool-type hybrid reactor MYRRHA 1.6 core. The aim of the work is to determine some important safety neutronic parameters for the critical mode of MYRRHA and their dependences and behaviors. Two main analyses were conducted: the void injection analyses due to different accidental scenarios, and several sensitivity calculations on different response functions, as the multiplication factor and kinetic parameters.

In the first analysis the objective was to evaluate the effective multiplication behavior as a function of a volumetric void-growing along the LBE in the core. The maximum reactivity difference of 421 pcm was found out between the reference and the worst case scenario, which occurred when the rings are voided radially and up to the half of the second ring and at an axial height of 34 cm. This is an important result for safety reasons since such configuration leads to a positive reactivity insertion greater than the effective delayed neutron fraction of the system. The major reason of such result is the spectral change produced by the void that positively influences fission reactions in fissionable nuclides, while the opposite effect has been found in fissile ones. Regarding the other localized void injections, such as the one due to pin failure in a single fuel assembly, it was found that the effect of the released gas on the reactivity of the system is negligible.

An independent sensitivity analysis was conducted on the reference core to assess which neutron-induced reaction (and from which nuclide) has the greatest effect in such parameters. The main result of this analysis is that the ^{239}Pu influences more the global reactor parameters than other nuclides. For k_{eff} and Λ_{eff} sensitivities, fission and prompt-nubar have shown to be the most relevant nuclear data perturbations to influence such response functions. Regarding β_{eff} sensitivity, even the delayed nubar has a great relevance. In the end, the sensitivity capabilities were also applied to further understand which nuclides and reactions contribute positively or negatively to the 421 pcm of reactivity difference between the reference and the worst condition. The same sign and magnitude behavior has been found with the previous tallies calculations on fissile and fissionable nuclides. The sensitivity calculation can be also used to obtain reactivity parameters as the Doppler coefficient and the void coefficient.

The SERPENT2 capabilities used in this work have been compared with other codes, either deterministic and probabilistic. The results are consistent with previous studies, proving that this Monte Carlo code can be used for such analyses and extremely precise results can be obtained taking advantage of its Monte Carlo nature.

The present calculations can be used in the existing research as an addition to previous safety and sensitivity results obtained with other codes for the same MYRRHA model. At the same time, they can be used for future MYRRHA models since this thesis has proven their reliability and consistency.

The void analyses results presented in this Master's thesis, can be obtained during criticality calculations with the possibility to model several accidental scenarios easily, thanks to the SERPENT2 geometry routine. The sensitivity analyses results, even if simulations are very memory and time consuming to obtain, have proven the SERPENT2 capabilities of attaining accurate outcomes. Especially on kinetic parameters, without the need for spatial core homogenization and application of deterministic-based tools. This feature opens the doors to a new efficient way to obtain such important sensitivity profiles.

Bibliography

[1] *SCKCEN*. 2020. URL: https://www.sckcen.be/en/projects/myrrha.

[2] *International Conference on Fast Reactors and Related Fuel Cycles: Next Generation Nuclear Systems for Sustainable Development*. 2017. URL: https://www.iaea.org/newscenter/pressreleases/top-nuclear-scientists-discuss-fast-reactors-and-related-fuel-cycles-at-iaea-international-conference.

[3] CEA. "4th Generation sodium-cooled fast reactors: the ASTRID technological demonstrator". In: (2012), p. 96.

[4] *Reuters, France drops plans to build sodium-cooled nuclear reactor*. 2019. URL: https://www.reuters.com/article/us-france-nuclearpower-astrid/france-drops-plans-to-build-sodium-cooled-nuclear-reactor-idUSKCN1VK0MC.

[5] *World nuclear news*. 2019. URL: https://world-nuclear-news.org/Articles/Nuclearelectrica-to-cooperate-in-development-of-AL.

[6] Judith F. Briesmeister. "MCNPTM – A General Monte Carlo N-Particle Transport Code". In: *Los Alamos National Laboratory* (2000), p. 790.

[7] Weston Stacey and Noel Corngold. *Nuclear Reactor Physics*. Vol. 55. May 2002, pp. 60–. DOI: 10.1063/1.1485589.

[8] Jakko Leppanen. "PSG2 / Serpent – a Continuous-energy Monte Carlo Reactor Physics Burnup Calculation Code". In: (2008).

[9] Jaakko Leppänen. *Development of a new Monte Carlo reactor physics code*. 2007, pp. 3–228. ISBN: 9513870189.

[10] J.Duderstadt_J.Hamilton. *Nuclear Reactor Analysis*. Vol. 62. 1977, pp. 347–347. ISBN: 0471223638. DOI: 10.13182/nse77-a26972.

[11] Andrej Trkov. *From basic nuclear data to applications*. 2001. URL: http://users.ictp.it/%7B~%7Dpub%7B%5C_%7Doff/lectures/lns005/Number%7B%5C_%7D1/Trkov%7B%5C_%7D1.pdf.

[12] Paul K. Romano et al. "OpenMC: A state-of-the-art Monte Carlo code for research and development". In: *Annals of Nuclear Energy* 82 (2015). Joint International Conference on Supercomputing in Nuclear Applications and Monte Carlo 2013, SNA + MC 2013. Pluri- and Trans-disciplinarity, Towards New Modeling and Numerical Simulation Paradigms, pp. 90–97. ISSN: 0306-4549. DOI: https://doi.org/10.1016/j.anucene.2014.07.048. URL: http://www.sciencedirect.com/science/article/pii/S030645491400379X.

[13] *MYRRHA, fusion reactor research*. 2020. URL: https://myrrha.be/science-and-myrrha/fusion-reactor-research/.

[14] Hamid Aït Abderrahim et al. "MYRRHA Technical Description". In: (2011). URL: https://ecm.sckcen.be/OTCS/llisapi.dll/Overview/21854976.

[15] Paul Schuurmans and Myrrha Team. "The MYRRHA ADS project". In: (2013).

[16] Paul Ageron. "Swimming pool reactor". In: (1966).

[17] Gustavo Rubio Anton and MYRRHA team. "The MYRRHA Reactor : Approach to Nuclear Safety". In: (2017).

[18] E. Malambu and A. Stankovskiy. "Revised Core Design for MYRRHA - Rev 1.6." In: (2014).

[19] V.M. Pavlovych V.O. Babenko, V.I. Gulik. “The Transmutation of Nuclear Waste in the Two-Zone Subcritical System Driven by High-Intensity Neutron Generator”. In: *Proceeding of Waste Management Conference (WM2012)* (2012), pp. 1–8.

[20] Gert Van den Eynde et al. “An updated core design for the multi-purpose irradiation facility MYRRHA”. In: *Journal of Nuclear Science and Technology* 52 (Apr. 2015), pp. 1–5. DOI: 10.1080/00223131.2015.1026860.

[21] IAEA. “Basic Principles Objectives IAEA Nuclear Energy Series Liquid Metal Coolants for Fast Reactors Cooled By Sodium, Lead, and Lead-Bismuth Eutectic”. In: (2012), pp. 31–35. ISSN: 1995-7807. URL: http://www.iaea.org/Publications/index.html.

[22] Paul Demkowicz. “Lead Coolant Test Facility Development Workshop”. In: (July 2005).

[23] Luca Fiorito et al. “Nuclear data uncertainty analysis for the Po-210 production in MYRRHA”. In: *EPJ Nuclear Sciences & Technologies* 4 (2018), p. 48. ISSN: 2491-9292. DOI: 10.1051/epjn/2018044.

[24] P. Romojaro et al. “Nuclear data sensitivity and uncertainty analysis of effective neutron multiplication factor in various MYRRHA core configurations”. In: *Annals of Nuclear Energy* 101 (2017), pp. 330–338. ISSN: 18732100. DOI: 10.1016/j.anucene.2016.11.027.

[25] A Gersten. “On the expansion of the scattering amplitude in functions interpolating legendre polynomials”. In: *Annals of Physics* 44.1 (1967), pp. 112–125. ISSN: 0003-4916. DOI: https://doi.org/10.1016/0003-4916(67)90268-0. URL: http://www.sciencedirect.com/science/article/pii/0003491667902680.

[26] George I. Bell and Samuel Glasstone. *Nuclear Reactor theory*. 1970.

[27] Allan F. Henry. *Nuclear-reactor analysis*. 1975, p. 560.

[28] John R. Lamarsh. *Introduction to Nuclear Reactor*.

[29] *Delayed neutron example*. 2020. URL: https://www.framatome.com/customer/liblocal/docs/KUNDENPORTAL/PRODUKTBROSCHUEREN/Brosch%C3%BCren%20nach%20Nummer/PS-G-1272-ENG-201901-Severe%20Accident%20Training.pdf.

[30] J. Svany. “Information about the new 8-group delayed neutron set preparation”. In: ().

[31] P. Saracco, S. Dulla, and P. Ravetto. “The adjoint neutron transport equation and the statistical approach for its solution”. In: *European Physical Journal Plus* 131 (2016), pp. 0–23. ISSN: 21905444. DOI: 10.1140/epjp/i2016-16412-0. arXiv: 1609.08315.

[32] *Nuclear-power.net*. 2020. URL: https://www.nuclear-power.net/nuclear-power/fission/delayed-neutrons/.

[33] A. A. Balygin and A. V. Krayushkin. “Change of RBMK reactivity and power during measurements of the steam coefficient of reactivity”. In: *Atomic Energy* 100 (2006), pp. 169–171. ISSN: 10634258. DOI: 10.1007/s10512-006-0068-6.

[34] Mukhtar Ahmed Rana. “Remembering the Chernobyl Nuclear Reactor Accident (26 April 1986)”. In: (2019). DOI: 10.13140/RG.2.2.16285.26088.

[35] Bjorn Becker. “On the influence of the resonance scattering treatment in Monte Carlo codes on high temperature reactor characteristics”. PhD thesis. 2010.

[36] *Doppler Effect*. 2020. URL: https://www.nuclear-power.net/glossary/doppler-broadening/.

[37] E A P- et al. “Calculation of Doppler Coefficient and Other Safety Parameters For a Large Fast Oxide Reactor”. In: (1961).

[38] E Woodcock et al. “Techniques used in the GEM code for Monte Carlo neutronics calculations in reactors and other systems of complex geometry”. In: *Proc. Conf. Applications of Computing Methods to Reactors, ANL-7050* (1965), pp. 557–579.

[39] Ivan A. Kodeli. “Beta-effective sensitivity and uncertainty analysis of MYRRHA reactor for possible use in nuclear data validation and improvement”. In: *Annals of Nuclear Energy* 113 (2018), pp. 425–435. ISSN: 18732100. DOI: 10.1016/j.anucene.2017.11.039. URL: https://doi.org/10.1016/j.anucene.2017.11.039.

[40] Ji Ma et al. "Perturbation Theory-Based Whole-Core Eigenvalue Sensitivity and Uncertainty (SU) Analysis via a 2D/1D Transport Code". In: *Science and Technology of Nuclear Installations* (2020). ISSN: 16876083. DOI: 10.1155/2020/9428580.

[41] Manuele Aufiero et al. "A collision history-based approach to sensitivity/perturbation calculations in the continuous energy Monte Carlo code SERPENT". In: *Annals of Nuclear Energy* 85 (2015), pp. 245–258. ISSN: 18732100. DOI: 10.1016/j.anucene.2015.05.008. URL: http://dx.doi.org/10.1016/j.anucene.2015.05.008.

[42] Brian C. Kiedrowski, Forrest B. Brown, and Paul P.H. Wilson. "Adjoint-weighted tallies for k-eigenvalue calculations with continuous-energy Monte Carlo". In: *Nuclear Science and Engineering* 168 (2011), pp. 226–241. ISSN: 00295639. DOI: 10.13182/NSE10-22.

[43] Yasushi Nauchi and Takanori Kameyama. "Development of calculation technique for iterated fission probability and reactor kinetic parameters using continuous-energy monte carlo method". In: *Journal of Nuclear Science and Technology* 47 (2010), pp. 977–990. ISSN: 00223131. DOI: 10.1080/18811248.2010.9711662.

[44] Guillaume Truchet et al. "Computing adjoint-weighted kinetics parameters in TRIPOLI-4® by the Iterated Fission Probability method". In: *Annals of Nuclear Energy* 85 (2015), pp. 17–26. ISSN: 18732100. DOI: 10.1016/j.anucene.2015.04.025. URL: http://dx.doi.org/10.1016/j.anucene.2015.04.025.

[45] Energy Monte, Brian Kiedrowski, and Forrest Brown. "Adjoint-Weighting for Critical Systems". In: 836 (2009).

[46] Ivan A. Kodeli and Slavko Slavič. "SUSD3D Computer Code as Part of the XSUN-2017 Windows Interface Environment for Deterministic Radiation Transport and Cross-Section Sensitivity-Uncertainty Analysis". In: *Science and Technology of Nuclear Installations* (2017). ISSN: 16876083. DOI: 10.1155/2017/1264736.

[47] B. T. Rearden and M. A. Jessee. *SCALE Code System*. March. 2017. ISBN: 1800553684.

[48] A. Gandini, G. Palmiotti, and M. Salvatores. "Equivalent generalized perturbation theory (EGPT)". In: *Annals of Nuclear Energy* 13.3 (1986), pp. 109–114. ISSN: 0306-4549. DOI: https://doi.org/10.1016/0306-4549(86)90001-0. URL: http://www.sciencedirect.com/science/article/pii/0306454986900010.

[49] J. M. Ruggieri et al. "ERANOS 2.1: International code system for GEN IV fast reactor analysis". In: *Proceedings of the 2006 International Congress on Advances in Nuclear Power Plants, ICAPP'06* 2006 (2006), pp. 2432–2439.

[50] E. Brun et al. "Tripoli-4®, CEA, EDF and AREVA reference Monte Carlo code". In: *Annals of Nuclear Energy* 82 (2015), pp. 151–160. ISSN: 18732100. DOI: 10.1016/j.anucene.2014.07.053. URL: http://dx.doi.org/10.1016/j.anucene.2014.07.053.

[51] K. Yokoyama et al. "MARBLE: A next generation neutronics analysis code system for fast reactors". In: *International Conference on the Physics of Reactors 2008, PHYSOR 08* 3 (Jan. 2008), pp. 2315–2322.

[52] B. Davison and J. B. Sykes. *Neutron Transport Theory*. 1958.

[53] M.M. Bretscher. "Evaluation of reactor kinetic parameters without the need for perturbation codes". In: (1997).

[54] *SERPENT Forum*. 2020. URL: https://ttuki.vtt.fi/serpent/viewtopic.php?f=25&t=2611&p=7898&hilit=void+coefficient#p7898.

[55] *Janis - OECD*. 2020. URL: https://www.oecd-nea.org/janis/.

[56] Augusto Hernandez Solis. *Reactivity studies of the MYRRHA 1 . 6 core under void conditions*. 2020.

[57] A.E. Waltar, D.R. Todd, and Pavel Tsvetkov. *Fast Spectrum Reactors*. Oct. 2012, pp. 1–720. DOI: 10.1007/978-1-4419-9572-8.

[58] Naoto Kasahara. *Fast Reactor System Design*. Vol. 8. Jan. 2017. ISBN: 978-981-10-2820-5. DOI: 10.1007/978-981-10-2821-2.

[59] X. N. Chen et al. “Safety studies for the MYRRHA critical core with the SIMMER-III code”. In: *Annals of Nuclear Energy* 110 (2017), pp. 1030–1042. ISSN: 18732100. DOI: 10.1016/j.anucene.2017.08.021.

[60] *ECCO 33 multi-group energy grid.* 2020. URL: http://www.oecd-nea.org/tools/abstract/detail/nea-1344/.

[61] *JEFF-3.1.2 nuclear data library.* 2020. URL: https://www.oecd-nea.org/dbforms/data/eva/evatapes/jeff_31/JEFF312/.

[62] Hiroki Iwamoto et al. “ Sensitivity and uncertainty analysis of β eff for MYRRHA using a Monte Carlo technique ”. In: *EPJ Nuclear Sciences & Technologies* 4 (2018), p. 42. ISSN: 2491-9292. DOI: 10.1051/epjn/2018023.

[63] Ivan A. Kodeli and Slavko Slavič. “SUSD3D Computer Code as Part of the XSUN-2017 Windows Interface Environment for Deterministic Radiation Transport and Cross-Section Sensitivity-Uncertainty Analysis”. In: *Science and Technology of Nuclear Installations* (2017). ISSN: 16876083. DOI: 10.1155/2017/1264736.

[64] Ivan Kodeli et al. “Evaluation and use of the prompt fission neutron spectrum and spectra covariance matrices in criticality and shielding”. In: *Nuclear Instruments and Methods in Physics Research, Section A: Accelerators, Spectrometers, Detectors and Associated Equipment* 610 (2009), pp. 540–552. ISSN: 01689002. DOI: 10.1016/j.nima.2009.08.076. URL: http://dx.doi.org/10.1016/j.nima.2009.08.076.

[65] A Hogenbirk. “The JEZEBEL benchmark Results of MCNP4A calculations”. In: (1995).

[66] Dalton Ellery Girão Barroso. “Equation of State of Uranium and Plutonium”. In: (2015). arXiv: 1502.00497. URL: http://arxiv.org/abs/1502.00497.

[67] A Jeffrey. “Jezebel : Reconstructing a Critical Experiment from 60 Years Ago”. In: (2017).

[68] I. Kodeli and W. Zwermann. “Evaluation of uncertainties in βeff by means of deterministic and monte carlo methods”. In: *Nuclear Data Sheets* 118 (2014), pp. 370–373. ISSN: 00903752. DOI: 10.1016/j.nds.2014.04.083. URL: http://dx.doi.org/10.1016/j.nds.2014.04.083.

[69] Spaider Enciso; Julian Aponte. “Los Alamos Critical Assemblies Facility”. In: (2015), p. 1.

[70] *Flattop.* 2020. URL: https://en.wikipedia.org/wiki/Flattop_(critical_assembly).

[71] Ivan Alexander Kodeli. “Sensitivity and uncertainty in the effective delayed neutron fraction (βeff)”. In: *Nuclear Instruments and Methods in Physics Research, Section A: Accelerators, Spectrometers, Detectors and Associated Equipment* 715 (2013), pp. 70–78. ISSN: 01689002. DOI: 10.1016/j.nima.2013.03.020. URL: http://dx.doi.org/10.1016/j.nima.2013.03.020.

[72] Pablo Romojaro, Francisco Álvarez-Velarde, and Nuria García-Herranz. “Nuclear data analyses for improving the safety of advanced lead-cooled reactors”. In: *EPJ Web of Conferences* 211 (2019), p. 05002. DOI: 10.1051/epjconf/201921105002.